NTIA Report 93-293

Wideband HF Noise/Interference Modeling Part II: Higher-Order Statistics

John J. Lemmon
Christopher J. Behm

U.S. DEPARTMENT OF COMMERCE
Barbara Hackman Franklin, Secretary

Gregory F. Chapados, Assistant Secretary
for Communications and Information

January 1993

CONTENTS

LIST OF FIGURES

List of Figures (cont.)

List of Figures (cont.)

List of Figures (cont.)

Page

LIST OF TABLES

WIDEBAND HF NOISE/INTERFERENCE MODELING PART II: HIGHER ORDER STATISTICS

John J. Lemmon and Christopher J. Behm*

This report is the second in a series of reports which describe the development of a wideband HF noise/interference model. The model is based on measured data and is suitable for implementation in a wideband HF channel simulator. The measured data, analyses of the first-order statistics of the data, and a proposed noise/interference model based upon those analyses were discussed in Part I of this series. The present report, Part II of the series, describes analyses of selected higher-order statistics of the data: the autocorrelation function and pulse width and pulse spacing distributions. Examples of these quantities generated from the model are compared with measured data, and refinements of the model based upon analyses of the higher-order statistics are discussed.

Key words: channel simulator; noise/interference; wideband HF

1. INTRODUCTION

1.1 Background

During the past several years interest in HF communication systems over wide bandwidths (on the order of 1 MHz or more) has been revitalized. This resurgence of interest in wideband HF has been motivated by the application of spread spectrum technology to HF systems and the development of digital signal processing techniques which enable the development of HF systems having far better performance than HF systems of only a few years ago.

In view of the numerous uncertainties concerning the performance of new communication systems which have not been fielded and tested extensively, channel simulation is an attractive approach for the evaluation of communication system performance. Channel simulation enables the laboratory performance evaluation of communication systems without the cost and time of building hardware and running extensive field tests. Other advantages of channel simulation, including accuracy, repeatability, stationarity, availability, and parameter variation, have been discussed by Hoffmeyer and Vogler (1987).

---

*The authors are with the Institute for Telecommunication Sciences, National Telecommunications and Information Administration, U.S. Department of Commerce, Boulder, CO 80303-3328.

For a number of years, laboratory performance evaluations of narrowband HF communication systems have been conducted using the channel model and channel simulation techniques developed by Watterson et al. Although this narrowband model and its implementation in channel simulators has been widely reported in the literature (Watterson, 1981 and 1982; Watterson and Coon, 1962; Watterson et al., 1962 and 1970; CCIR, 1974; Ehrman et al., 1982; Mooney, 1985; Girault et al., 1988; McRae and Perkins, 1988; LeRoux et al., 1987), the model has only been validated for narrowband (less than 12 kHz) stable channels.

Motivated by the need for a wideband HF channel simulator, the Institute for Telecommunication Sciences has undertaken the development of a wideband HF channel model. The model is to be accurate over wide bandwidths (on the order of 1 MHz or more), validated with measured data, and suitable for implementation in a wideband HF channel simulator. The model is to include noise and interference, which can be quite severe in the HF band, as well as a model of ionospheric skywave propagation.

The wideband propagation model and the implementation of the propagation and noise/interference models in a real-time channel simulator have been discussed elsewhere (Vogler et al., 1988; Vogler and Hoffmeyer, 1988 and 1990; Hoffmeyer and Vogler, 1990; Hoffmeyer et al., 1991; Mastrangelo et al., 1991). The purpose of the present series of reports is to discuss the development of a wideband HF noise/interference model.

1.2 Noise/Interference Model

In Part I of this series (Lemmon and Behm, 1991) a wideband HF noise/interference model based on measured data was presented. It was pointed out that, in contrast to previously developed models which attempt to describe statistical characteristics of the noise/interference, the present model describes the noise/interference waveform itself, which is essential if the model is to be used to simulate that waveform.

The measured data were obtained by the Mitre Corporation as part of its experimental wideband HF communications program. The equipment used in the experiments was described briefly in Part I and in more detail by Perry and Rifkin (1989). The data consist of 42 one-second records of the digitized (sampled at 1.024 MHz), baseband, in-phase (I) and quadrature (Q) components of the received noise/interference over an equivalent rf bandwidth of 800 kHz.

The data were collected in March, 1989 in Bedford, MA at various times of day and at various frequencies in the HF band (3-30 MHz). The times, dates, center frequencies of the data, and the values of the variable attenuation used in the front-end of the receiver are listed in Table A-1 in the Appendix.

To analyze these data, software was developed to generate the following quantities:

- plots of raw data (I and Q)
- probability density function (pdf) of raw data
- pdf of voltage envelope ($\sqrt{(I^2+Q^2)}$)
- pdf of power envelope (I^2+Q^2)
- pdf of phase ($\tan^{-1}Q/I$)
- cumulative distribution function (cdf) of power envelope
- distribution of average level crossing rate of the voltage envelope
- power spectrum
- cdf of power in the frequency domain (sum of the squares of the real and imaginary parts of the complex Fourier transform of the raw data)
- pdf of phase in the frequency domain (phase of the complex Fourier transform of the raw data)

In addition, software was developed to perform the following functions:

- frequency domain excision of narrowband interference
- simulations of noise/interference

Using these analysis tools, a variety of case studies were conducted. Based on the results of the case studies, it was proposed that the noise/interference can be represented as a sum of three components:

- Gaussian noise
- Narrowband interferers (sine waves)

Impulsive noise (filtered delta functions)

The narrowband interference is presumably manmade, arising from numerous users of the HF band. Broadband impulsive noise can be natural (atmospheric noise) or manmade. However, as discussed in Section 3, the impulsive noise analyzed herein is assumed to be of manmade origin, because the time durations of the noise bursts and the times between bursts are not consistent with those of atmospheric noise.

If x(t) denotes the noise/interference signal at rf, and the in-phase and quadrature components of the baseband signal are denoted by I(t) and Q(t), respectively, then x(t) can be written as

$$x(t) = I(t)\cos \omega_0 t + Q(t) \sin \omega_0 t, \qquad (1)$$

where ω_0 is the carrier frequency. The proposed noise/interference model describes the complex baseband voltage,

$$z(t) = I(t) + iQ(t), \qquad (2)$$

by the expression

$$z(t) = g(t) + \sum_{i=1}^{N_i} A_i e^{-i(\Delta\omega_i t + \phi_i)} + \sum_{j=1}^{N_j} B_j \frac{\sin 2\pi B(t-t_j)}{t-t_j} e^{i\omega_0 t_j}, \qquad (3)$$

where g(t) is a complex, zero-mean, white Gaussian process, $\Delta\omega_i$ are the baseband frequencies of the sine waves ($\Delta\omega_i=\omega_i-\omega_0$), ,$\phi_i$ are random phases, B is the bandpass (in Hz) of the low-pass filter in the HF receiver, t_j are the arrival times of the (filtered) impulses, N_i is the number of narrowband interferers in the frequency band of interest, and N_j is the number of impulses in the time interval over which the noise/interference is being modeled. The frequency and phase distributions of the narrowband interferers are uniform, and in Part I the arrival times t_j were also uniformly distributed, although it will be shown in the present report that this is inadequate to

correctly model the higher-order statistics.

It remains to specify how the amplitudes A_i and B_j are distributed. In Part I it was proposed that the pdf for the amplitudes A_i be modeled by the amplitude pdf of a model developed by Hall (1966):

$$p(A) = \frac{(\theta_A - 1)\,\gamma_A^{\theta_A - 1}\,A}{(A^2 + \gamma_A^2)^{(\theta_A + 1)/2}}, \qquad (4)$$

where θ_A and γ_A are free parameters (with the constraint that $\theta_A > 1$, so that p(A) is normalizable). It was also proposed in Part I that the amplitude distribution of the B_j be described by that of the Hall model for amplitudes which are less than some maximum value B_{max}, and that the distribution be cut off for amplitudes greater than B_{max}:

$$p(B) = \begin{cases} \dfrac{1-\theta_B}{(B_{max}^2+\gamma_B^2)^{(1-\theta_B)/2} - \gamma_B^{2(1-\theta_B)/2}} \cdot \dfrac{B}{(B^2+\gamma_B^2)^{(\theta_B+1)/2}}, & 0 \le B \le B_{max} \\ 0, & B > B_{max} \end{cases}, \qquad (5)$$

where θ_B and γ_B are free parameters (with $\theta_B > 1$). The expression in the first line of (5) differs from that in (4) because cutting off the distribution results in a different normalization constant. The techniques used to generate amplitudes distributed according to (4) and (5), and to generate the Gaussian noise, were discussed in Part I.

1.3 Scope

The model described above enables one to simulate noise/interference signals whose statistical characteristics can be compared to those of measured data. Clearly, many such characteristics could be examined. In Part I of this series, the first-order statistics were investigated. These quantities characterize the time-averaged behavior of the noise/interference. It was shown that, for appropriate values of the model parameters, the simulated noise/interference has first-order statistics that closely resemble those of the measured data.

However, a complete characterization of the noise/interference requires investigation of the higher-order statistics as well. These statistics are necessary to specify the relationships between the noise/interference process at different instants in time. For example, it was shown that the average numbers of level crossings of the voltage envelope per unit time of the simulated noise/interference are in agreement with measured data, but it remains to investigate how these envelope crossings are distributed in time.

In this report, selected higher-order statistics of the noise/interference are discussed. To keep the analysis tractable, attention has been restricted to the following three quantities:

- Autocorrelation functions
- Pulse width distributions
- Pulse spacing distributions

Autocorrelation functions are important because they define the time scales over which the noise/interference becomes decorrelated and provide information about the time scales over which the noise/interference processes vary. Pulse width and spacing distributions are useful for detailed modeling of the noise/interference waveforms, especially impulsive noise. These distributions provide information about the fine structure of the noise bursts, as well as information about the nature of the correlations of the noise bursts in time.

2. AUTOCORRELATION FUNCTIONS

2.1 Calculation of the Autocorrelation Function

The autocorrelation function is of fundamental significance in characterizing a random process because it specifies the degree to which the process is correlated at different instants in time. For a general (nonstationary) complex-valued random process z(t), the autocorrelation function $\gamma_{xx}(t_1,t_2)$ at times t_1 and t_2 is defined as (for example,see Cox and Miller, 1965):

$$\gamma_{xx}(t_1,t_2) = E\{x(t_1)x(t_2)\}, \qquad (6)$$

where E{ }, the expected value, is defined as an ensemble average, and where * denotes the complex conjugate.

For the case of a stationary process, $\gamma(t_1,t_2)$ is not a function of t_1 and t_2 separately, but is a function of the time difference $\tau=t_2-t_1$. For the case of a stationary, ergodic process, the ensemble average is equivalent to a time average so that the autocorrelation function, denoted by $R(\tau)$, can be defined as:

$$R(\tau) = \lim_{T\to\infty}\frac{1}{T}\int_0^T z^*(t)z(t+\tau)dt, \qquad (7)$$

The noise/interference data to be analyzed consist of 42 one-second records that were collected at various times of day and at various frequencies in the HF band. Thus, for a given time and frequency, only one data record is available (not an ensemble of records), so that the ensemble average in (6) cannot be computed. On the other hand, the expression in (7) cannot be evaluated, because a record of infinite length is not available, and because the computational effort would be prohibitive for arbitrarily large, but finite T. Moreover, the noise/interference is generally nonstationary, so that the definition in (7) is not applicable. For example, Abraham et al. (1989) investigated the nonstationarity of wideband (1 MHz) HF noise after interference

excision and found, using a standard statistical F-test, that average stationary time durations were only on the order of 10 ms.

These difficulties are often encountered in the calculation of autocorrelation functions. An alternative approach that is commonly used is to calculate the quantity $R(\tau,T)$, defined as

$$R(\tau,T) = \frac{1}{T}\int_0^T z^*(t)z(t+\tau)dt. \qquad (8)$$

For a stationary, ergodic process $R(\tau,T)$ approaches $\gamma(\tau)$ as T approaches infinity. However, this is not the case for a nonstationary process, and therefore $R(\tau,T)$ is not a true autocorrelation function in the strict sense, even as T approaches infinity. Nevertheless, $R(\tau,T)$ is a useful measure of the degree to which a random process is correlated with itself at different instants of time, and this is the definition of the autocorrelation function used in this work.

An analytic expression for $R(\tau,T)$ in the proposed noise/interference model can be obtained by substituting (3) into (8). First consider R(0,T). The Gaussian noise, the narrowband interferers, and the impulsive noise are uncorrelated with one another, and the Gaussian noise and the narrowband interferers are zero-mean processes. Therefore, upon substituting (3) into (8), the integrals of the cross-terms between the Gaussian noise and the narrowband interferers, between the narrowband interferers and the impulsive noise, and between the Gaussian noise and the impulsive noise vanish. Thus, R(0,T) is simply the sum of the average power of the Gaussian noise, the narrowband interferers, and the impulsive noise. These integrals are easily performed, and were discussed in Part I. The results are:

$$P_G = 2\sigma^2 \qquad (9)$$

where σ^2 is the variance of the real and imaginary parts of g(t),

$$P_{NB} = \sum_{i=1}^{N_I} A_i^2 \qquad (10)$$

and

$$P_{IMP} = \frac{2\pi^2 B}{T} \sum_{j=1}^{N_J} B_j^2 . \qquad (11)$$

Now consider $R(\tau,T)$ for non-zero values of τ. Again, the integrals of the cross-terms between different components of the noise/interference vanish, leaving the sum of the autocorrelation functions of the individual components.

The Gaussian noise is white; hence, its power spectrum is independent of frequency, and its autocorrelation function (the inverse Fourier transform of the power spectrum) is a delta function. Therefore, the autocorrelation function of the Gaussian noise vanishes for non-zero values of τ.

The impulsive noise consists of filtered impulses which are localized, oscillatory functions of time. Therefore, the only contributions to the autocorrelation function of the impulsive noise arise at those values of τ that equal the difference of the times of arrival of two distinct impulses. Let two such impulses be labeled by a and b. Then the corresponding contribution to the autocorrelation function is:

$$\frac{2\pi^2 B}{T} B_a B_b e^{i\omega_0 (t_b - t_a)} \qquad (12)$$

where the integral from 0 to T has been approximated by the integral from $-\infty$ to $+\infty$. If the impulses arrive periodically in time, contributions of the form of (12) combine at values of τ which are integral multiples of the period. However, the arrival times of the impulses in the data analyzed herein are not precisely periodic, and therefore contributions of the form of (12) do not combine for non-zero τ. Moreover, it was shown in Part I that accurate simulation of the data containing impulsive noise required approximately 50 impulses over a duration of 4 ms. Thus, if T is on the order of or greater than 4 ms (which it is in the examples below), contributions of the form of (12) are expected to be small compared to the sum in (11). It was also shown in the aforementioned simulation in Part I that the sum in (11) is itself approximately 11 dB less than

the contribution in (10) due to the narrowband interferers. Therefore the autocorrelation function of the impulsive noise is expected to approximately vanish for non-zero τ.

Finally, the autocorrelation function of the narrowband interferers is readily evaluated. One has:

$$\sum_{i=1}^{N_I} A_i^2 e^{-i\Delta\omega_i\tau}, \tag{13}$$

where the integral over the cross-terms vanishes due to the orthogonality of sines and cosines of different frequencies.

Combining results, the complete autocorrelation function of the noise/interference model can be approximated as:

$$R(\tau,T) = (2\sigma^2+\frac{2\pi^2 B}{T}\sum_{j=1}^{N_J} B_j^2)\,\delta_{\tau,0} + \sum_{i=1}^{N_I} A_i^2 e^{-i\Delta\omega_i\tau}, \tag{14}$$

where $\delta_{\tau,0}$ is an impulse function, defined as:

$$\delta_{\tau,0} = \begin{cases} 1, & \tau=0 \\ 0, & \tau\neq 0 \end{cases}. \tag{15}$$

Thus, $R(\tau,T)$ consists of an impulse at $\tau=0$, and the periodic function in (13) at non-zero values of τ.

2.2 Comparisons of Model with Measurements

In Part I of this series, the 42 noise/interference records were examined, and five records were selected that were considered to be representative of the entire data base. Detailed case studies (consisting of analyses of the first-order statistics) were performed on these five records. The results of two of the case studies were compared with analyses of the first-order statistics of simulated noise/interference for two particular sets of model parameters. A similar program was carried out in the present work for the higher-order statistics. The times, dates, and center

frequencies for the five case studies are listed in Table 1. The autocorrelation function for each of the five case studies was computed using (8). The integration time T was chosen to be 4 ms (i.e., 4096 samples). For each case the autocorrelation function was computed for $0 \leq \tau \leq 8$ ms and 0.996 s $\leq \tau \leq$ 1.004 s, corresponding to two 8 ms windows of delay at the beginning and end of each one-second record. Because one expects an impulse in $R(\tau,T)$ at $\tau=0$, which is difficult to see on the plots, the autocorrelation functions were normalized so that $R(0,T)=1$. Finally, because $R(\tau,T)$ is complex, the absolute magnitudes of the normalized autocorrelation functions have been plotted. Thus, the quantity which has been plotted in each case is $|R(\tau,T=4 \text{ ms})/R(0,T=4 \text{ ms})|$.

To gain some insight into the nonstationarity of the noise/interference, the power (I^2+Q^2) has been plotted versus time for each of the 42 one-second records. The results are shown in the Appendix. Each plot shows the power averaged over 1,024 consecutive samples (i.e., over 1 ms) and plotted (in dB) versus time for the entire one-second record. The time scales on the horizontal axes in these plots are therefore in units of ms. Thus, the "number of 1024 samples" spans an interval of 1024, which corresponds to a time duration of 1.024 s. These plots reveal that, over time intervals of 1 second, the received power is reasonably stationary in some cases, but can be highly nonstationary in others.

Table 1. Measurement Characteristics of Wideband HF Noise/Interference Records Used in Case Studies

Case Study	Date (1989)	Time (UT)	Center Frequency (MHz)
1	10 March	09:58:11	5.936
2	28 March	22:10:40	19.29
3	28 March	10:26:48	13.666
4	29 March	02:31:34	13.666
5	15 March	19:22:32	23.862

The I-channel data, the normalized autocorrelation function, and the average power for the first case study are shown in Figures 1, 2, and 3, respectively. The time scales on the horizontal axes in Figures 1 and 2 are in units of the sample time of the data, that is, 1/1.024 MHz. Thus, the "count" in Figure 1 spans an interval of 4096 samples, which corresponds to a time duration of precisely 4 ms. Similarly, the "delay" in each of the plots in Figure 2 spans an interval of 4096 samples, which corresponds to a range of τ of precisely 4 ms.

The I-channel data in Figure 1, plotted over the first 4 ms of the record, is typical of the 42 noise/interference records. The normalized autocorrelation function in Figure 2 is as expected: a unit impulse at τ=0 followed by a periodic function of τ. By the end of the one-second record the autocorrelation function has changed slightly; this is an indication that the channel was not precisely stationary over the duration of the record, as reflected in the average power plotted in Figure 3.

Figures 4, 5, and 6 show the I-channel data, the normalized autocorrelation function, and the average power, respectively, for the second case study. As in the first case study, the autocorrelation function shows the expected behavior, but varies slightly by the end of the record, due to a small degree of nonstationarity in the channel.

The I-channel data, the normalized autocorrelation function, and the average power for the third case study are plotted in Figures 7, 8, and 9, respectively. Whereas the autocorrelation functions in the other four case studies consist of a rapidly oscillating, periodic function with a well-defined envelope, the function in Figure 8 is neither rapidly oscillating nor periodic, at least over time intervals of 8 ms or less. However, this behavior can easily be accounted for within the proposed noise/interference model.

If the sum over narrowband interferers in (13) and (14) is dominated by a single term, the magnitude of the autocorrelation function is a constant. If the channel is dominated by two narrowband interferers with equal amplitudes and closely spaced in frequency, the resulting signal (beating pattern) consists of a single carrier at the average frequency, amplitude modulated by a sine wave of half the difference frequency. It is easy to show that the magnitude of the resulting autocorrelation function is proportional to the magnitude of the autocorrelation function of the slowly varying modulating function (a sine wave). More complicated modulating functions can arise if additional pairs of narrowband interferers (with equal amplitudes) beat against one

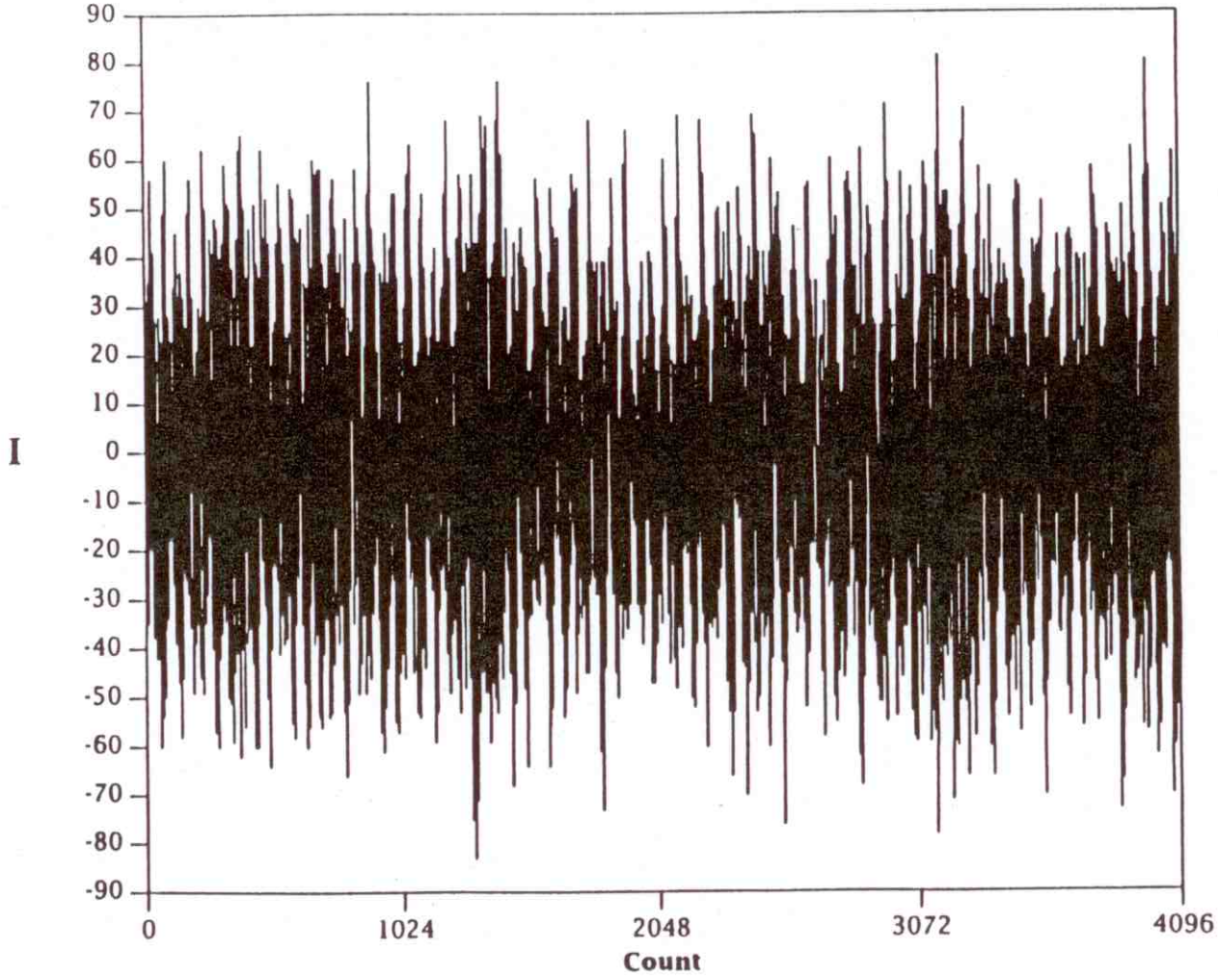

Figure 1. I-channel data at 5.936 MHz (case study 1).

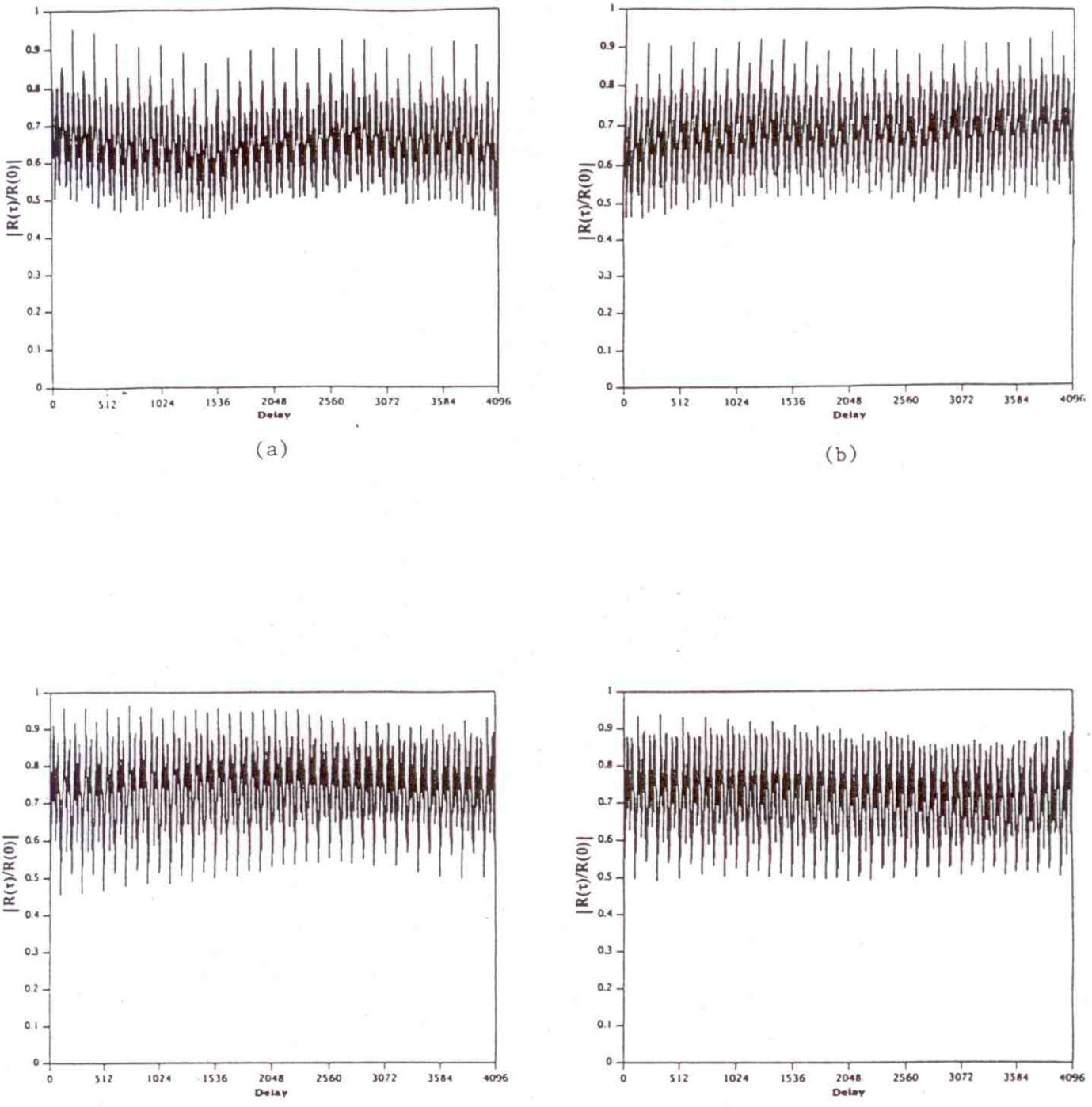

Figure 2. Normalized autocorrelation function for (a) $0 \leq \tau \leq 4$ms, (b) 4ms $\leq \tau \leq 8$ms, (c) 0.996s $\leq \tau \leq$ 1.0s, and (d) 1.0s $\leq \tau \leq$ 1.004s (case study 1).

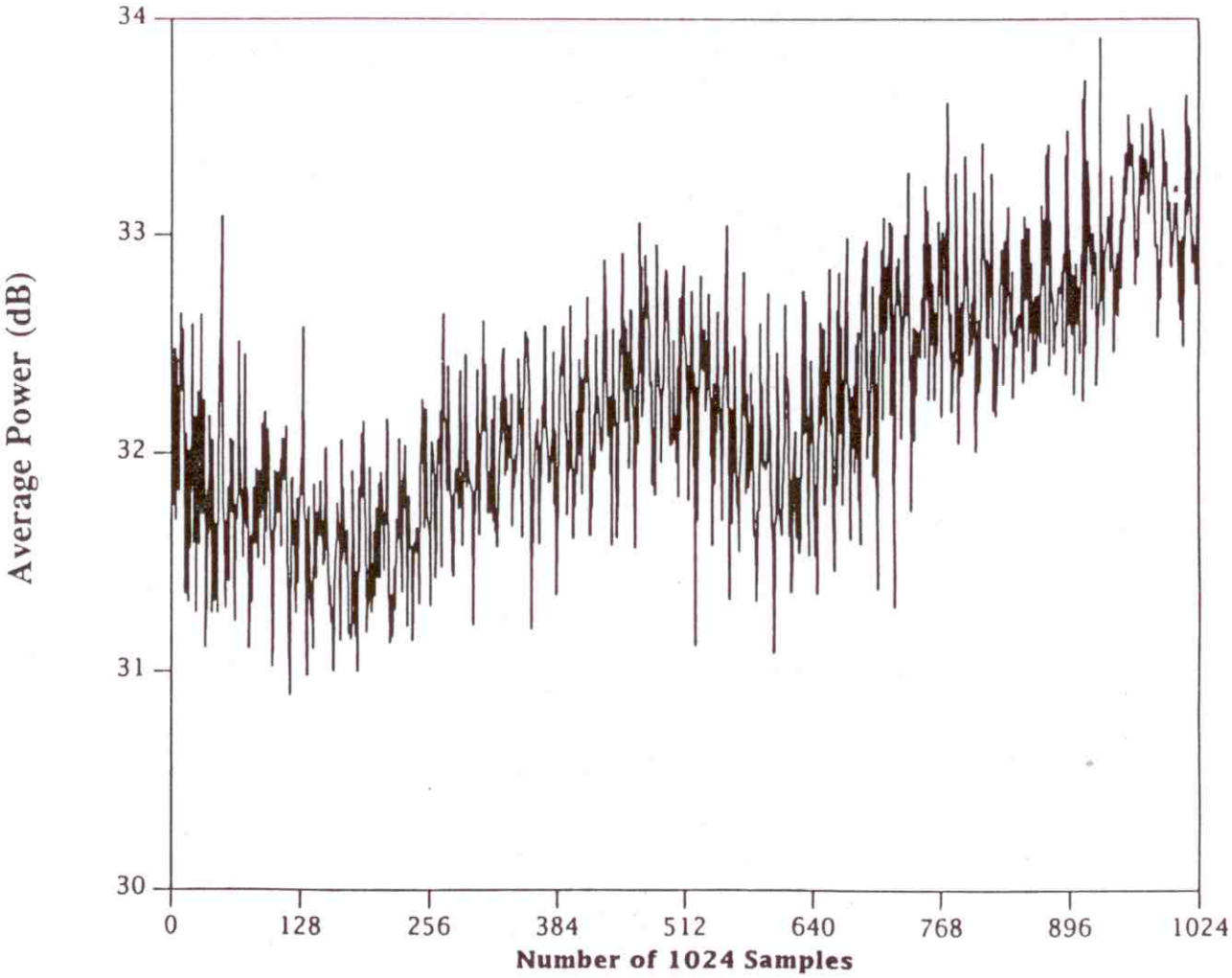

Figure 3. Average power of measured noise/interference (case study 1).

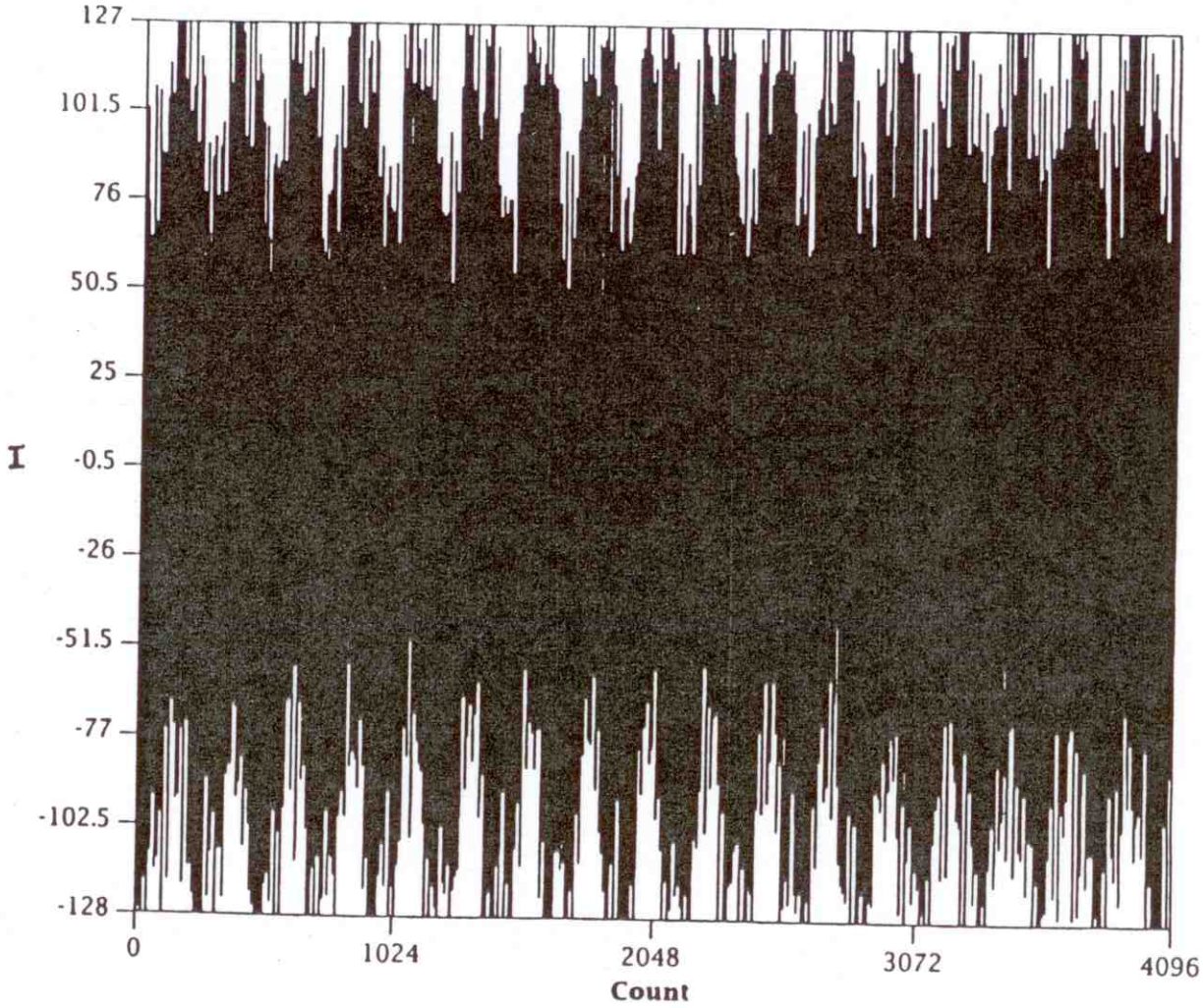

Figure 4. I-channel data at 19.29 MHz (case study 2).

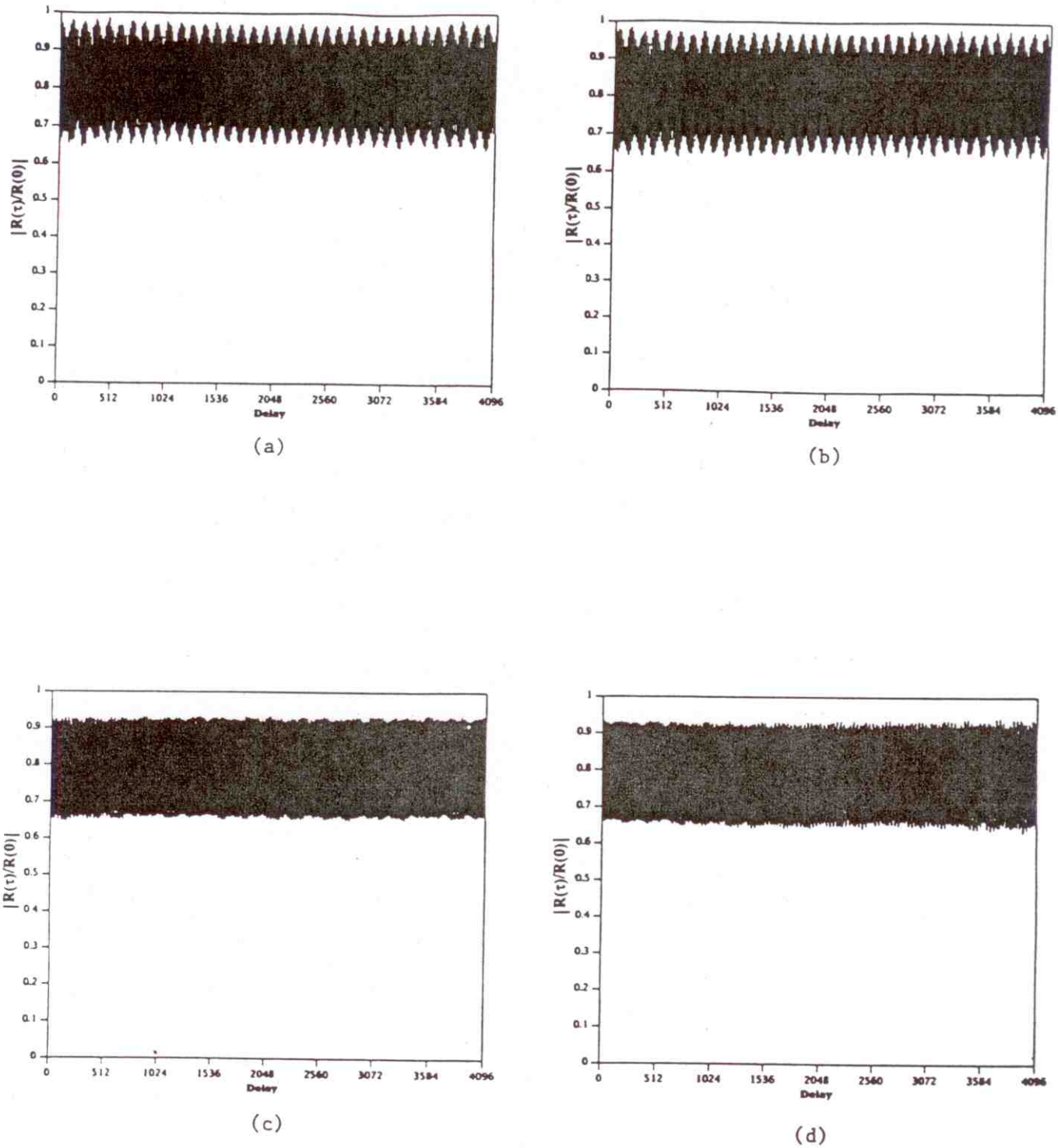

Figure 5. Normalized autocorrelation function for (a) $0 \leq \tau \leq 4$ms, (b) $4\text{ms} \leq \tau \leq 8$ms, (c) $0.996\text{s} \leq \tau \leq 1.0$s, and (d) $1.0\text{s} \leq \tau \leq 1.004$s (case study 2).

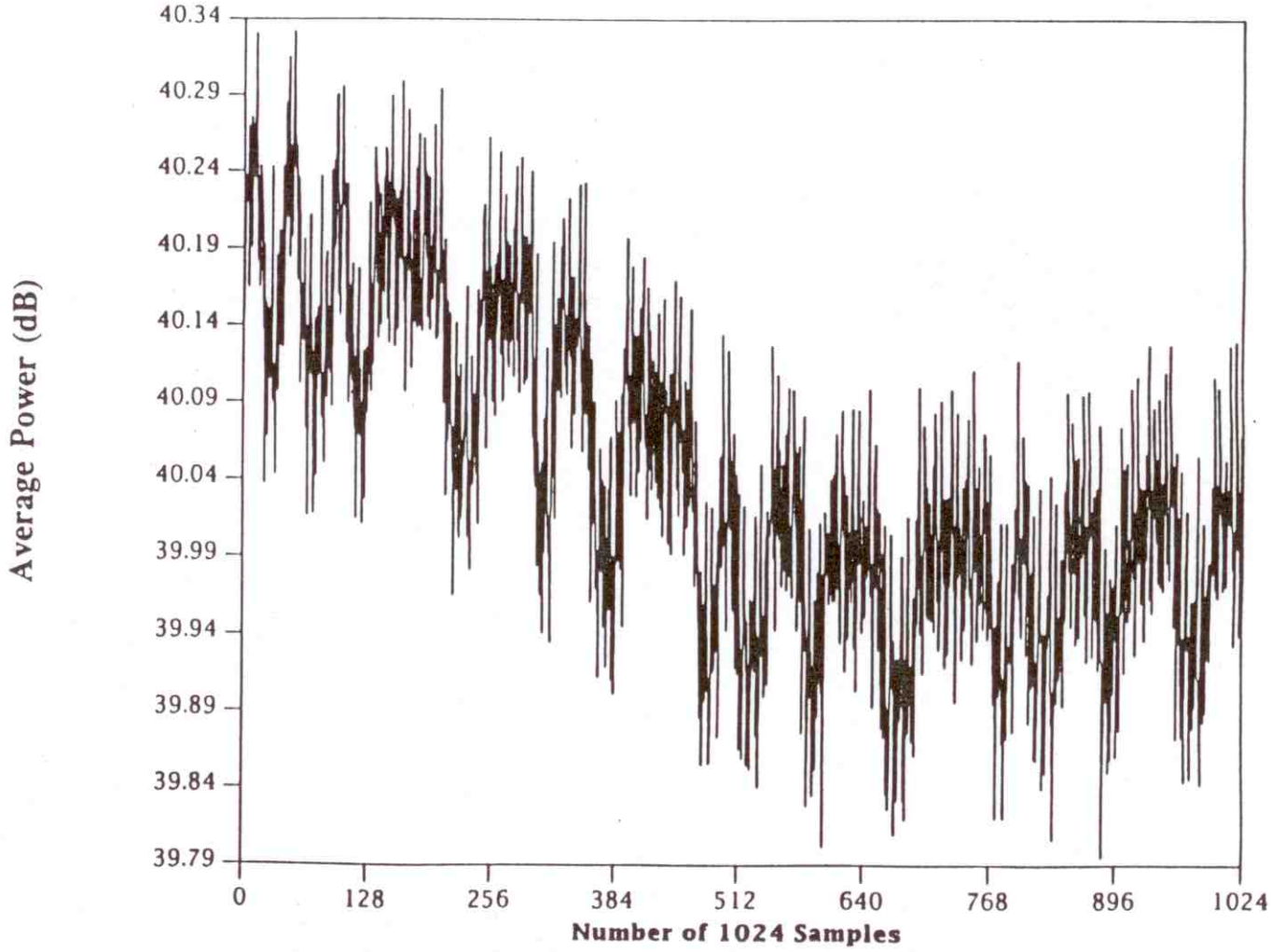

Figure 6. Average power of measured noise/interference (case study 2).

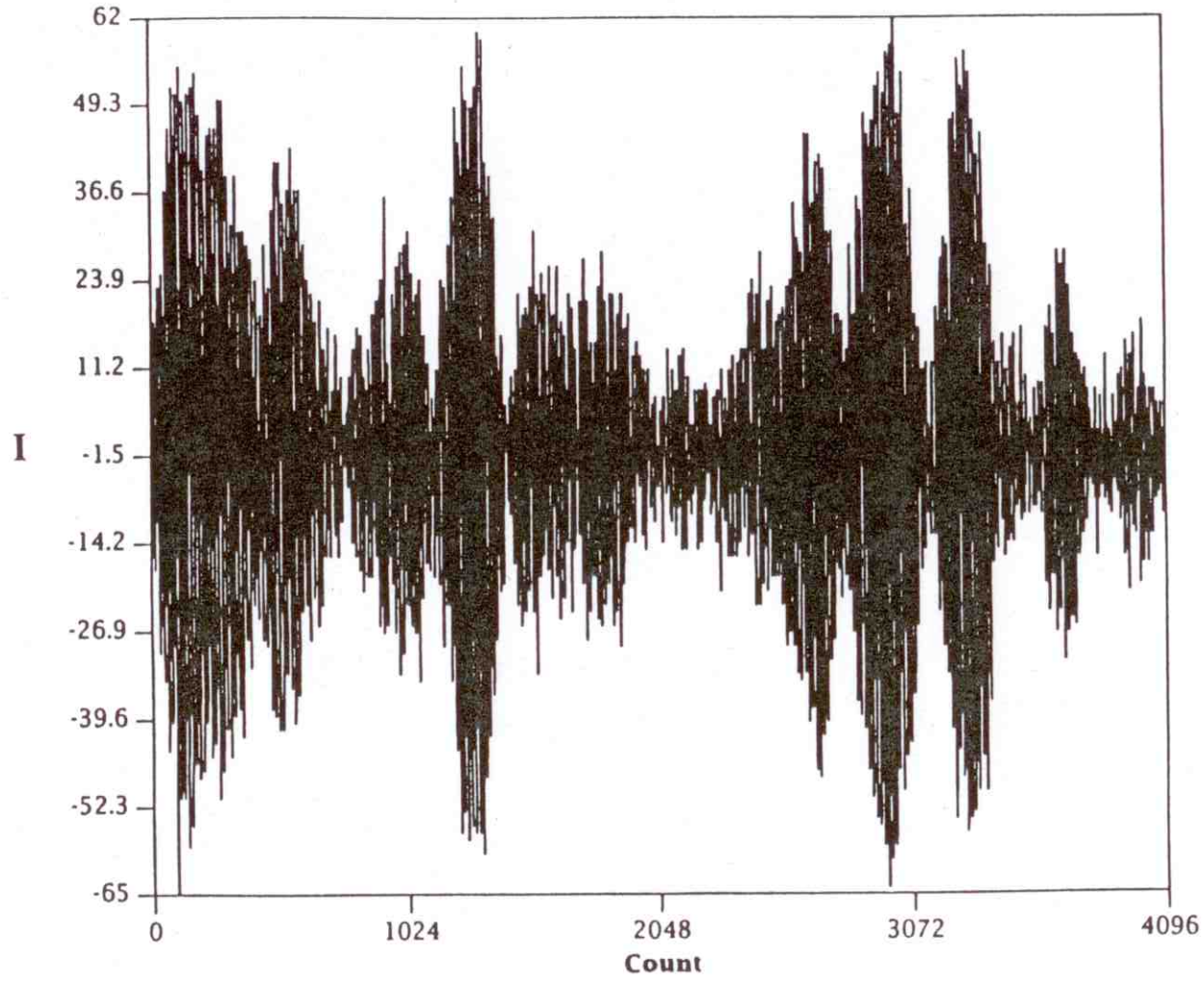

Figure 7. I-channel data at 13.666 MHz (case study 3).

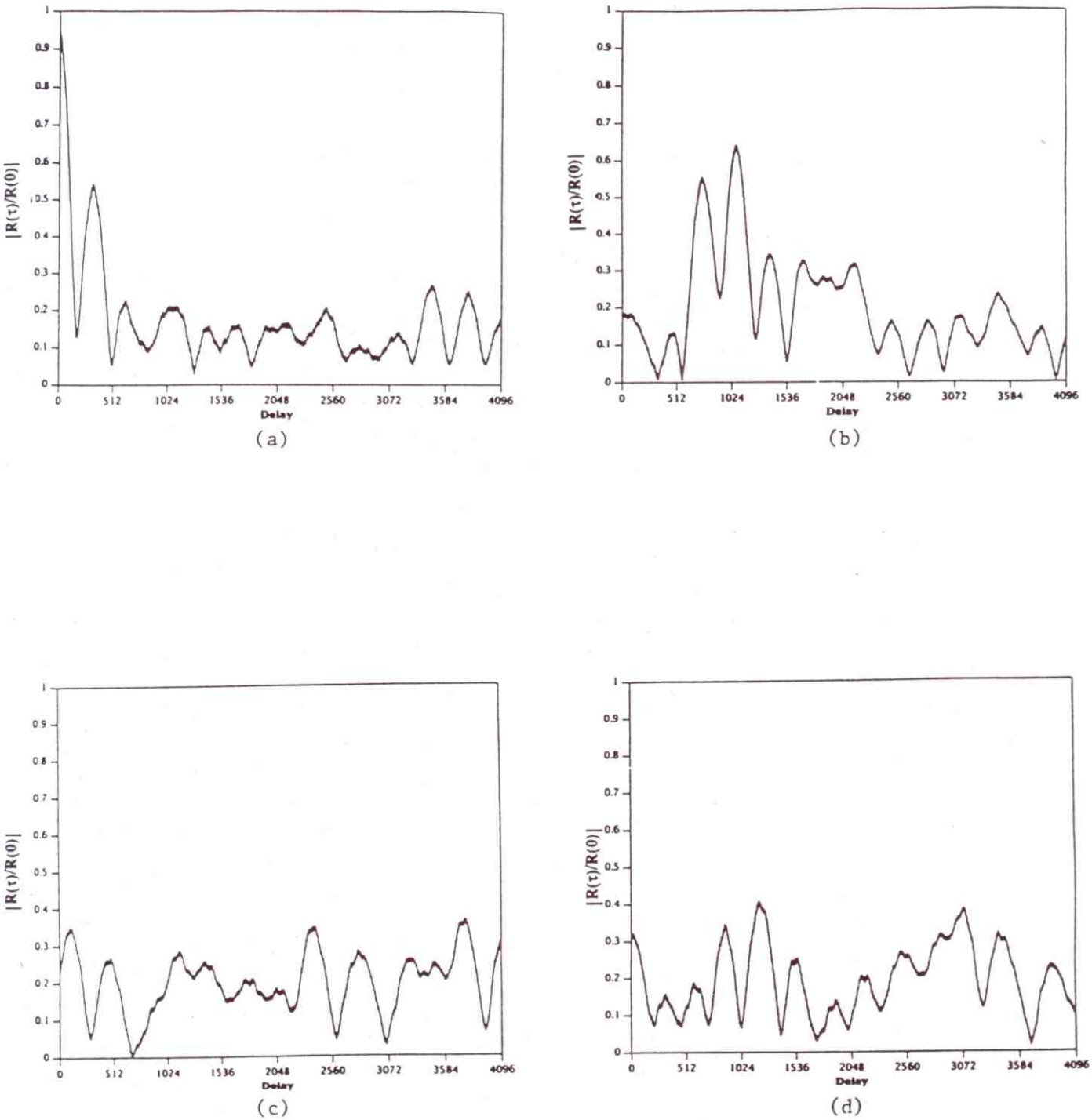

Figure 8. Normalized autocorrelation function for (a) $0 \leq \tau \leq 4$ms, (b) 4ms $\leq \tau \leq$ 8ms, (c) 0.996s $\leq \tau \leq$ 1.0s, and (d) 1.0s $\leq \tau \leq$ 1.004s (case study 3).

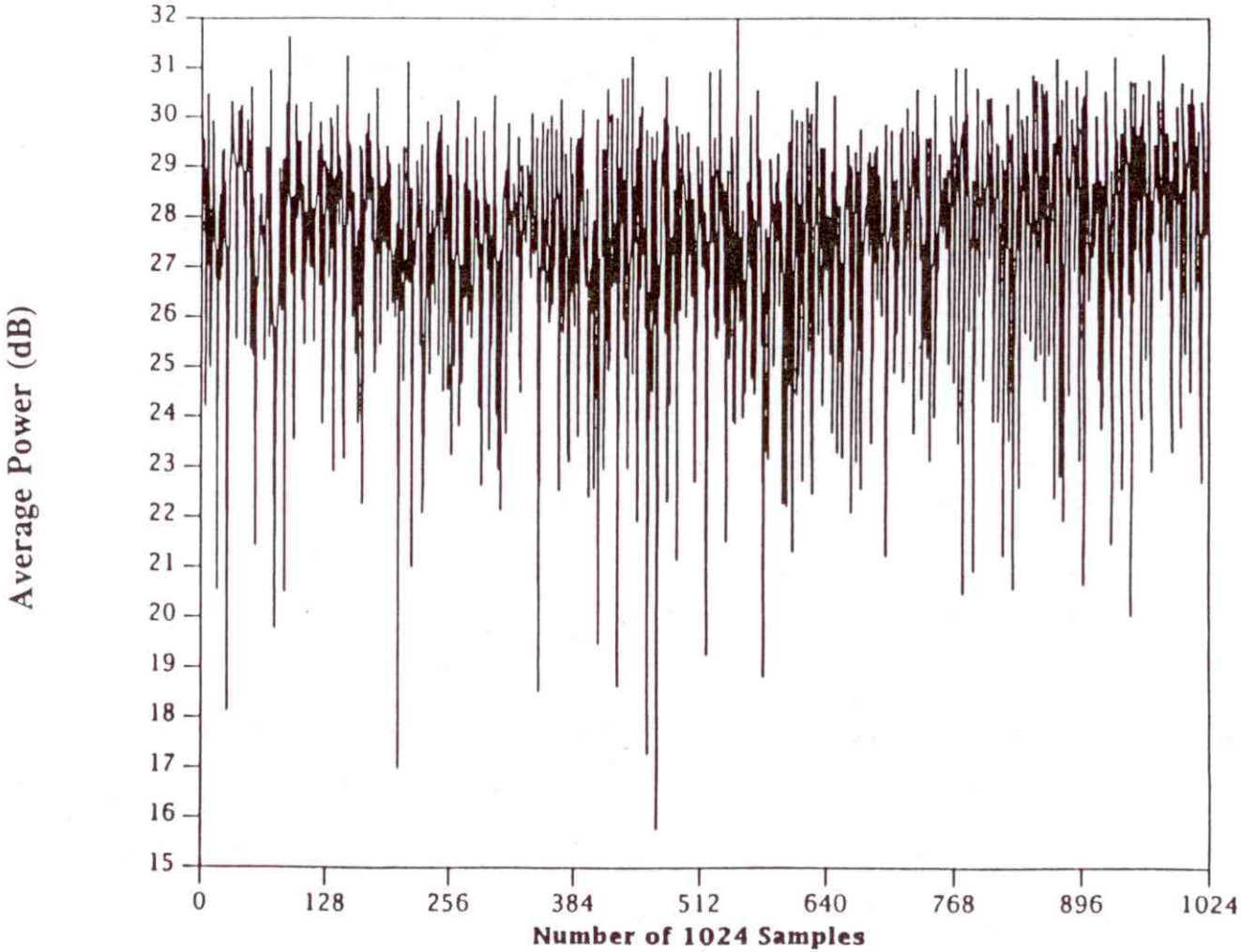

Figure 9. Average power of measured noise/interference (case study 3).

another, such that the average frequency of each pair is the same (so that the resulting signal consists of a single amplitude-modulated carrier).

To take a specific example, consider pairs of narrowband interferers with no random additive phases, distributed symmetrically in amplitude and frequency about some center frequency. The complex baseband signal can be written as:

$$z(t) = \sum_i A_i \left(e^{-i(\Delta\omega_o - \delta_i)t} + e^{-i(\Delta\omega_o + \delta_i)t}\right), \qquad (16)$$

where $\Delta\omega_0$ is the center frequency. Substituting (16) into (8) and carrying out the necessary integrations, one finds:

$$R(\tau, T) = 2e^{-i\Delta\omega_o\tau} \sum_i A_i^2 \cos\delta_i\tau. \qquad (17)$$

Although the expression in (17) is periodic, the period is large if the lowest common multiple of the periods of the cosine waves is large.

To verify that this type of scenario is applicable to the present case study, the power spectrum calculated from the first 4 ms of the data was examined. The power in the channel is indeed dominated by a cluster of narrowband interferers closely spaced in frequency and centered at approximately 65 kHz (baseband). The power spectrum is plotted on an expanded scale from 0 to 128 kHz in Figure 10. The horizontal scale is in units of 250 Hz, because the spectrum was calculated from 4 ms of data. The frequencies of the four strongest interferers appear to be distributed approximately symmetrically about the center of the cluster. It is difficult to determine whether the amplitudes of the dominant interferers are distributed symmetricaly about the center of the cluster, due to the presence of the background noise; however, the structure of the I-channel data (which resembles a single carrier with amplitude modulation) and the autocorrelation function (which is essentially devoid of rapid oscillations) strongly suggest that this is the case.

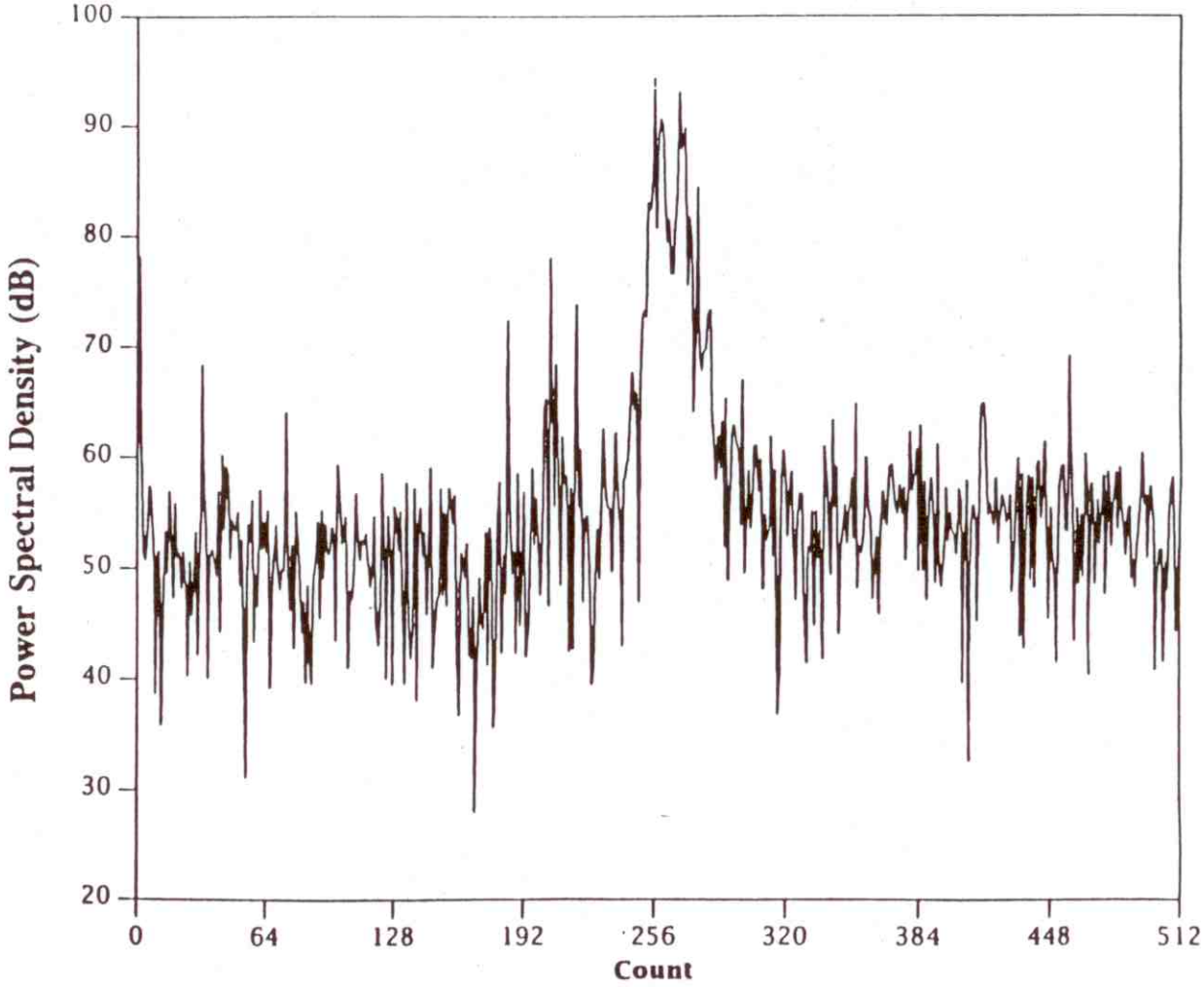

Figure 10. Power spectrum of measured noise/interference on a scale from 0 to 125 kHz (case study 3).

The I-channel data, the normalized autocorrelation function, and the average power for the fourth case study are shown in Figures 11, 12, and 13, respectively. As discussed in Part I, the noise/interference in this case is dominated by a single narrowband interferer. Thus, one expects the sum over narrowband interferers in (13) and (14) to be dominated by a single term, so that the magnitude of the autocorrelation function is approximately constant. As can be seen in Figure 12, the magnitude of the autocorrelation function is approximately constant over the first 8 ms, with small periodic oscillations. By the end of the record, the magnitude of the autocorrelation function has increased and is varying, although the structure and magnitude of the oscillations appears unchanged, indicating that the power of the dominant interferer has increased and is varying, whereas the power of the interferers responsible for the oscillations in the autocorrelation function have remained relatively stationary. Figure 13 reveals that the total power in the channel did indeed become oscillatory approximately half way through the record.

Figures 14, 15, and 16 show the I-channel data, the normalized autocorrelation function, and the average power, respectively, for the fifth case study. In this case the noise/interference includes impulsive noise in addition to narrowband interferers, as can be seen in Figure 14. However, the nature of the autocorrelation function (an impulse at $\tau=0$ followed by a periodic oscillatory function) is similar to the other case studies. This is because, as explained above, the impulses are narrow and do not arrive precisely periodically in time. The autocorrelation function in Figure 15 appears to change only slightly by the end of the record, indicating a relatively stationary channel. This is consistent with Figure 16, which shows that the fluctuations of the average power remain relatively stationary over the duration of the record, except for a noise burst approximately three fourths of the way through the record.

Based upon the case studies, it appears that the measured data have autocorrelation functions whose characteristics are well-described by (14) (with the exception of nonstationarity). Although (14) is also expected to correspond to the autocorrelation functions of the proposed noise/interference model, it remains to show that the simulated autocorrelation functions closely resemble those of the measured data. To verify this, a variety of simulations were conducted, both with and without impulsive noise.

Figure 17 shows plots of the magnitude of the normalized autocorrelation functions for simulated noise/interference consisting of Gaussian noise and narrowband interferers. As was

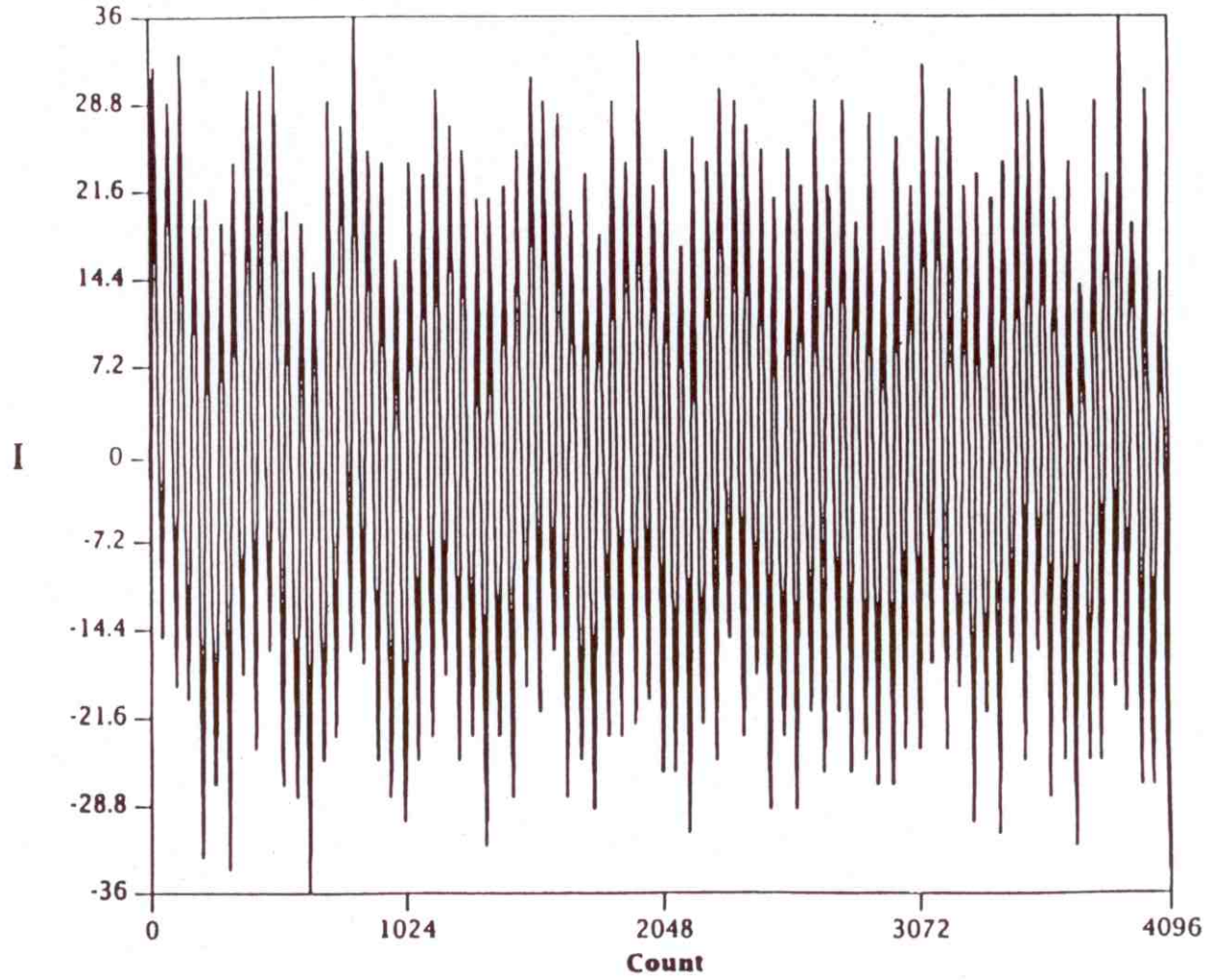

Figure 11. I-channel data at 13.666 MHz (case study 4).

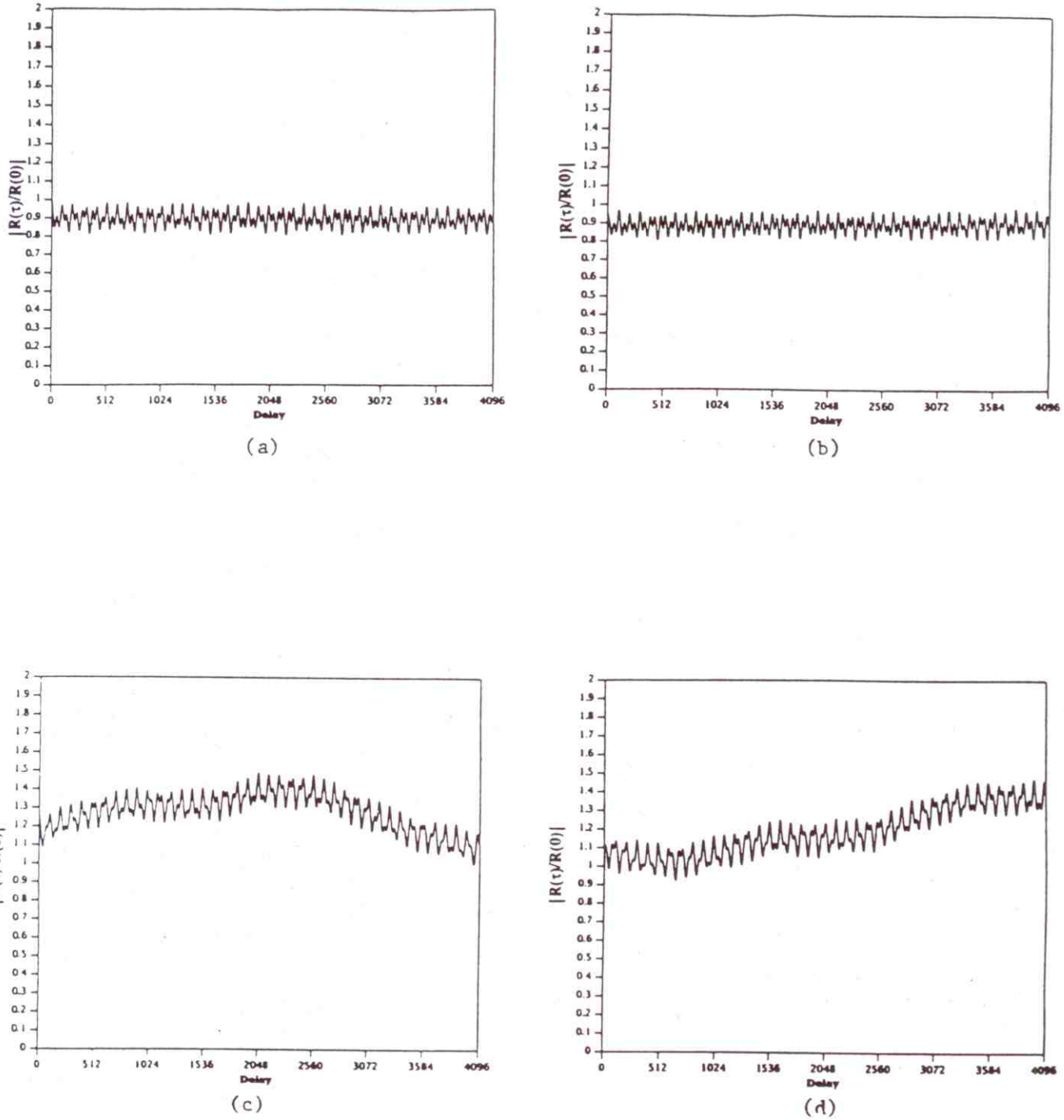

Figure 12. Normalized autocorrelation function for (a) $0 \leq \tau \leq 4$ms, (b) 4ms $\leq \tau \leq 8$ms, (c) 0.996s $\leq \tau \leq 1.0$s, and (d) 1.0s $\leq \tau \leq 1.004$s (case study 4).

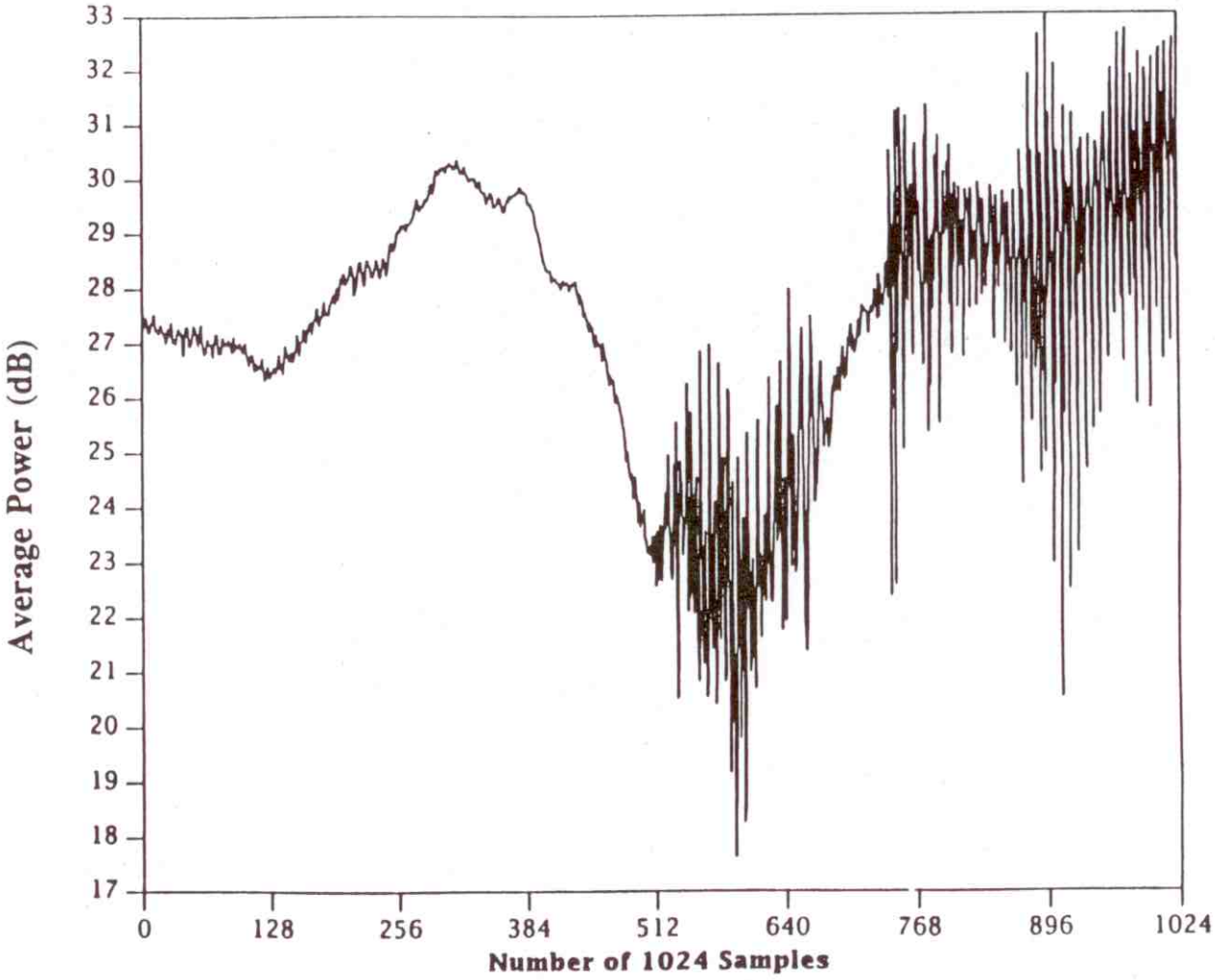

Figure 13. Average power of measured noise/interference (case study 4).

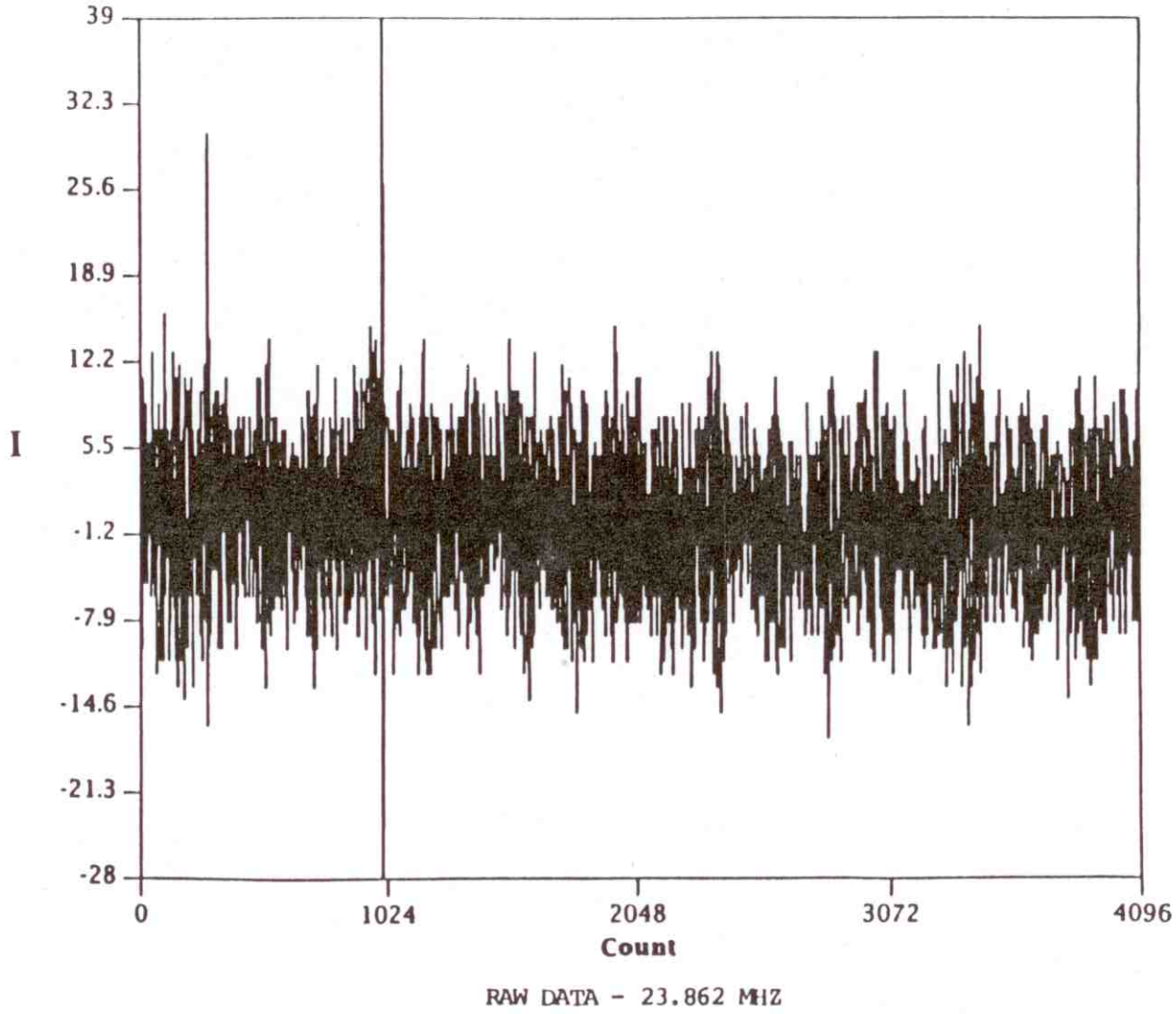

Figure 14. I-channel data at 23.862 MHz (case study 5).

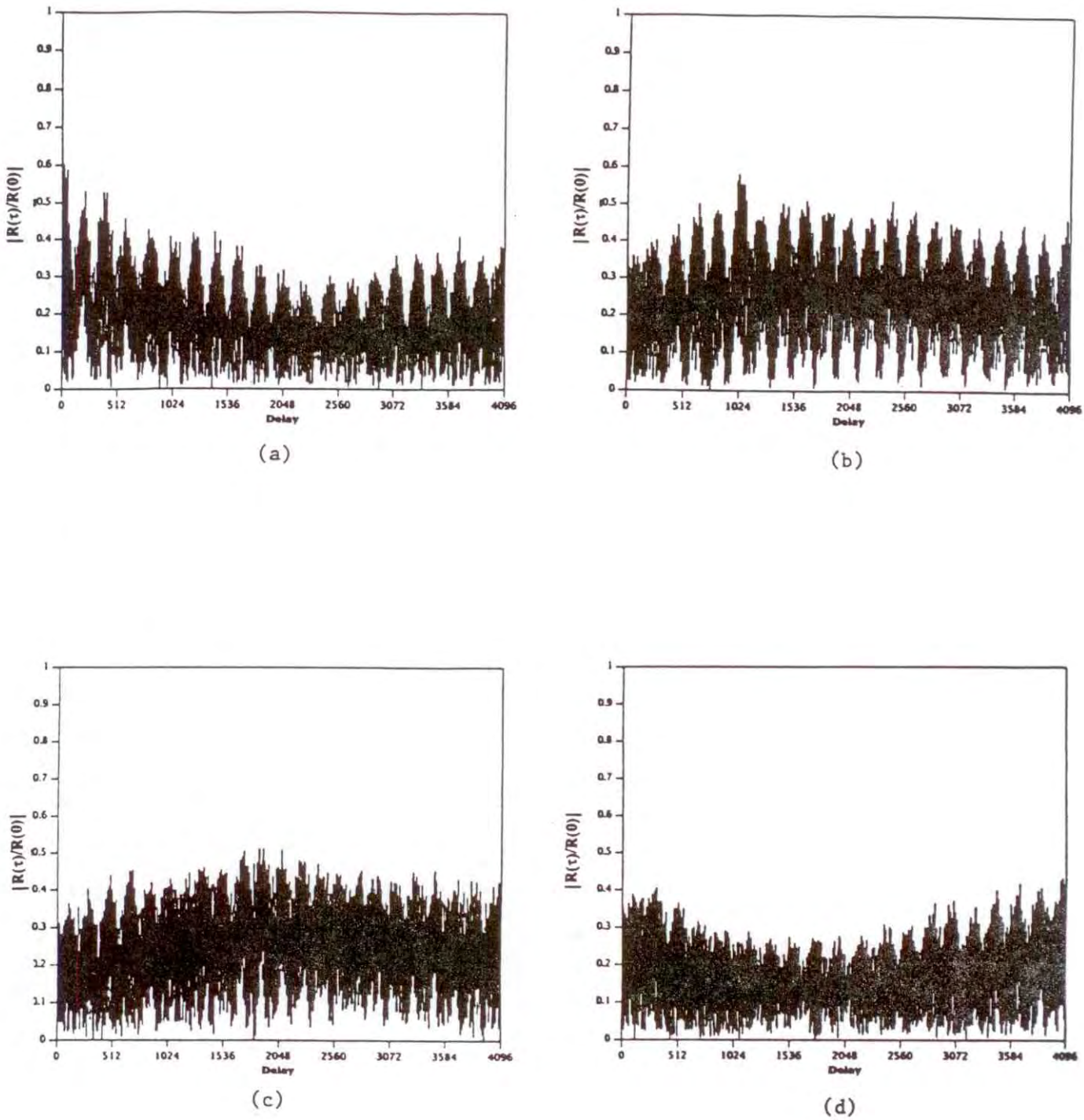

Figure 15. Normalized autocorrelation function for (a) $0 \leq \tau \leq 4$ms, (b) 4ms $\leq \tau \leq$ 8ms, (c) 0.996s $\leq \tau \leq$ 1.0s, and (d) 1.0s $\leq \tau \leq$ 1.004s (case study 5).

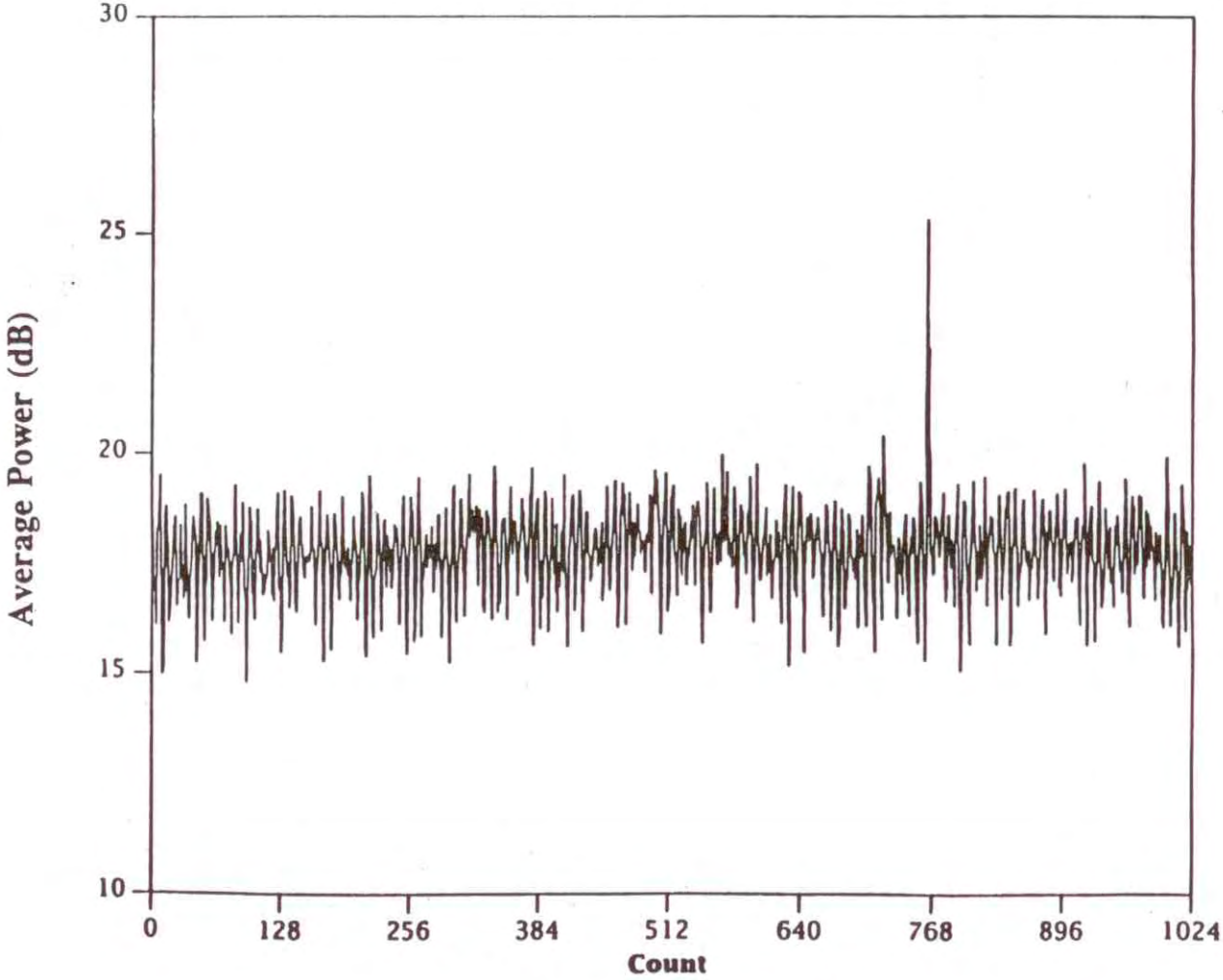

Figure 16. Average power of measured noise/interference (case study 5).

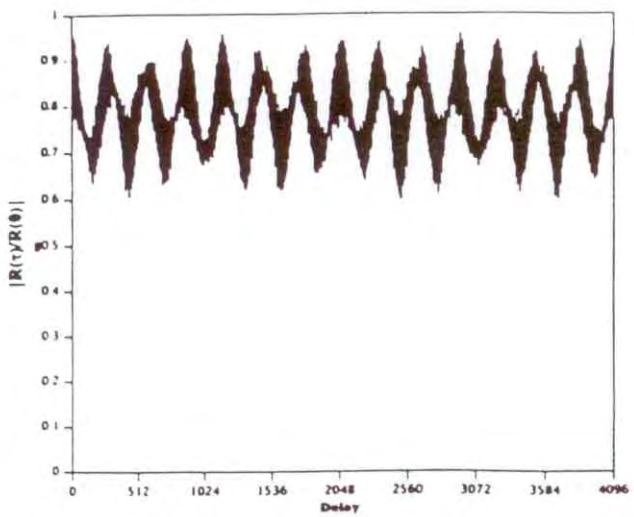

(a)

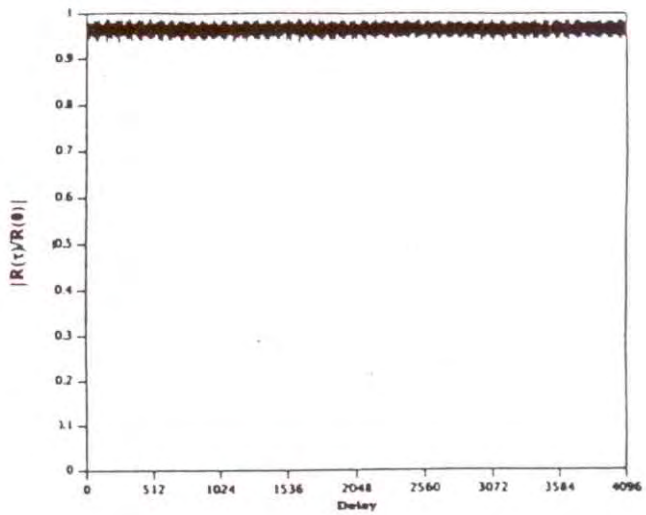

(b)

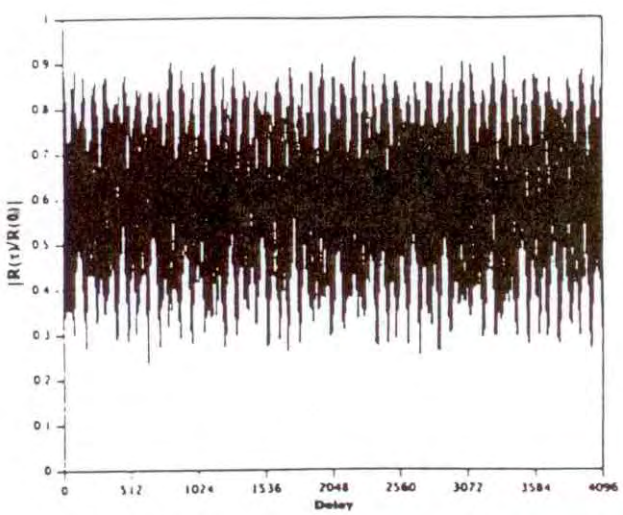

(c)

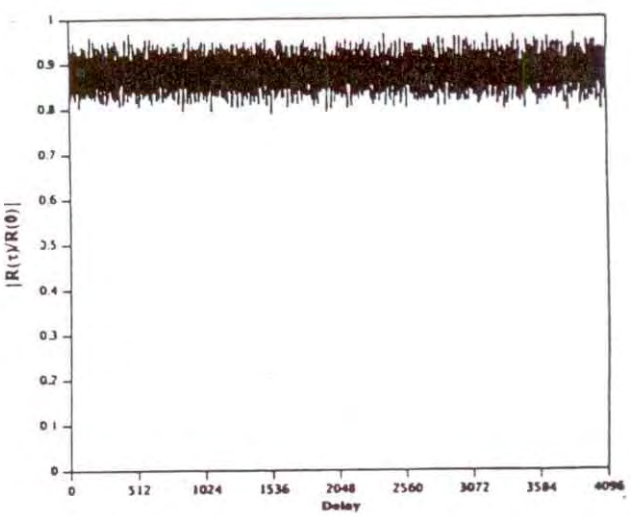

(d)

Figure 17. Normalized autocorrelation functions of simulated noise/interference (Gaussian noise and narrowband interferers).

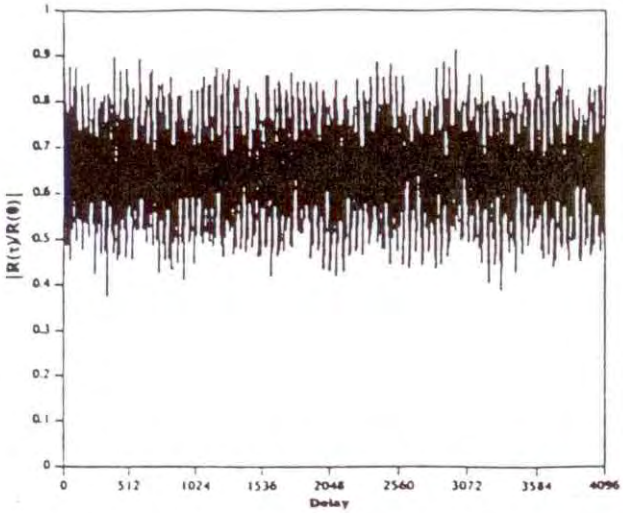

(e)

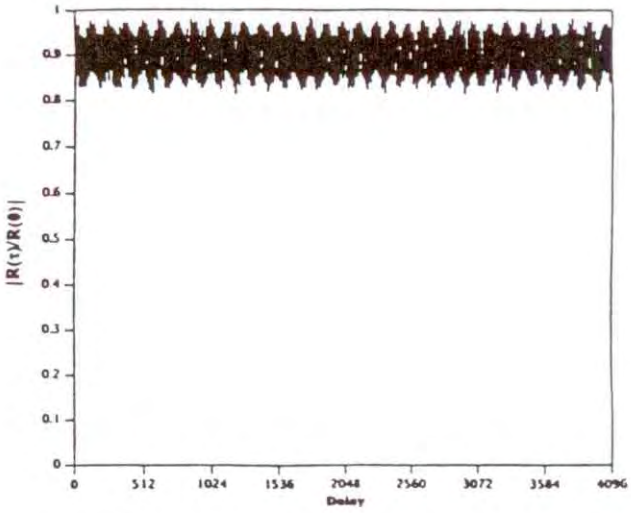

(f)

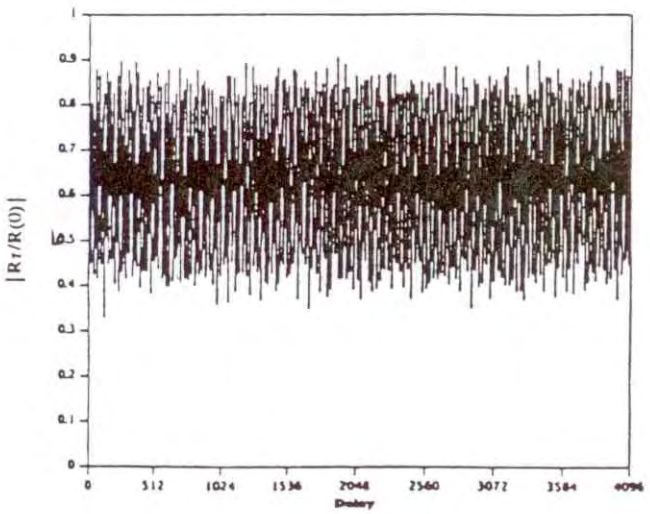

(g)

Figure 17. Normalized autocorrelation functions of simulated noise/interference. (cont.)

done for the case studies, the autocorrelation functions were computed using (8) with T=4 ms. Each plot shows an autocorrelation function for $0 \leq \tau \leq 4$ ms. The values of the model parameters are listed in Table 2, and are the same as those used in Part I to simulate noise/interference whose first-order statistics resemble those of the first case study. The examples in Figure 17 differ from one another only in the values of the random seeds used to generate the Gaussian noise and the frequencies, phases, and amplitudes of the narrowband interferers.

As expected, the normalized autocorrelation functions consist of a unit impulse at τ=0, followed by an approximately periodic function of τ. Like the autocorrelation functions of the measured data, the simulated autocorrelation functions exhibit a variety of different structures, although none of the simulated autocorrelation functions closely resembles any of the measured functions in quantitative detail. Such comparisons are admittedly qualitative, and do not constitute proof that the model can generate noise/interference waveforms which are identical (or nearly identical) to any and all of the waveforms observed in nature. The difficulty in achieving such a goal arises from the fact that one is dealing with random processes from numerous sources and environments, and therefore an infinite variety of waveforms. Thus, the purpose of the comparisons throughout this work (and in Part I as well) is not to simulate results which are identical to the measured results, but to demonstrate that, for representative examples, the model is capable of generating noise/interference whose statistical properties are similar to those of the measured data.

Table 2. Parameters Used in the Simulation Model for Figures 17 and 39 - 41

Parameter	Value
σ	0.12
N_i	39
γ_A	0.30
Θ_A	2.00

Figure 18 shows examples of autocorrelation functions for noise/interference consisting of Gaussian noise, narrowband interferers, and impulsive noise. The values of the model parameters are listed in Table 3, and are the same as those used in Part I to simulate noise/interference whose first-order statistics resemble those of the fifth case study. Again, the different examples in Figure 18 differ only in the values of the random seeds used to generate the noise/interference. As expected, the presence of impulsive noise randomly distributed in time does not appear to have any effect on the autocorrelation functions.

It remains to show that the model can generate noise/interference whose autocorrelation function resembles that of the third case study (Figure 8). To do so, noise/interference was simulated as follows. First, Gaussian noise (σ=1) was combined with 44 narrowband interferers (γ_A=0.2, θ_A=2.0). Then, the result was combined with a cluster of 5 dominant interferers whose amplitudes, phases, and frequencies are symmetrically distributed about the center of the cluster. Finally, the strongest of the original 44 interferers were excised to ensure that the cluster of 5

Table 3. Parameters Used in the Simulation Model for Figures 18 and 42 - 46

Parameter	Value
σ	0.12
N_i	39
γ_A	0.20
Θ_A	2.00
N_j	49/4 ms
γ_B	1.0×10^{-8}
Θ_B	1.20
B	400 kHz
B_{max}	2.0×10^{-5}

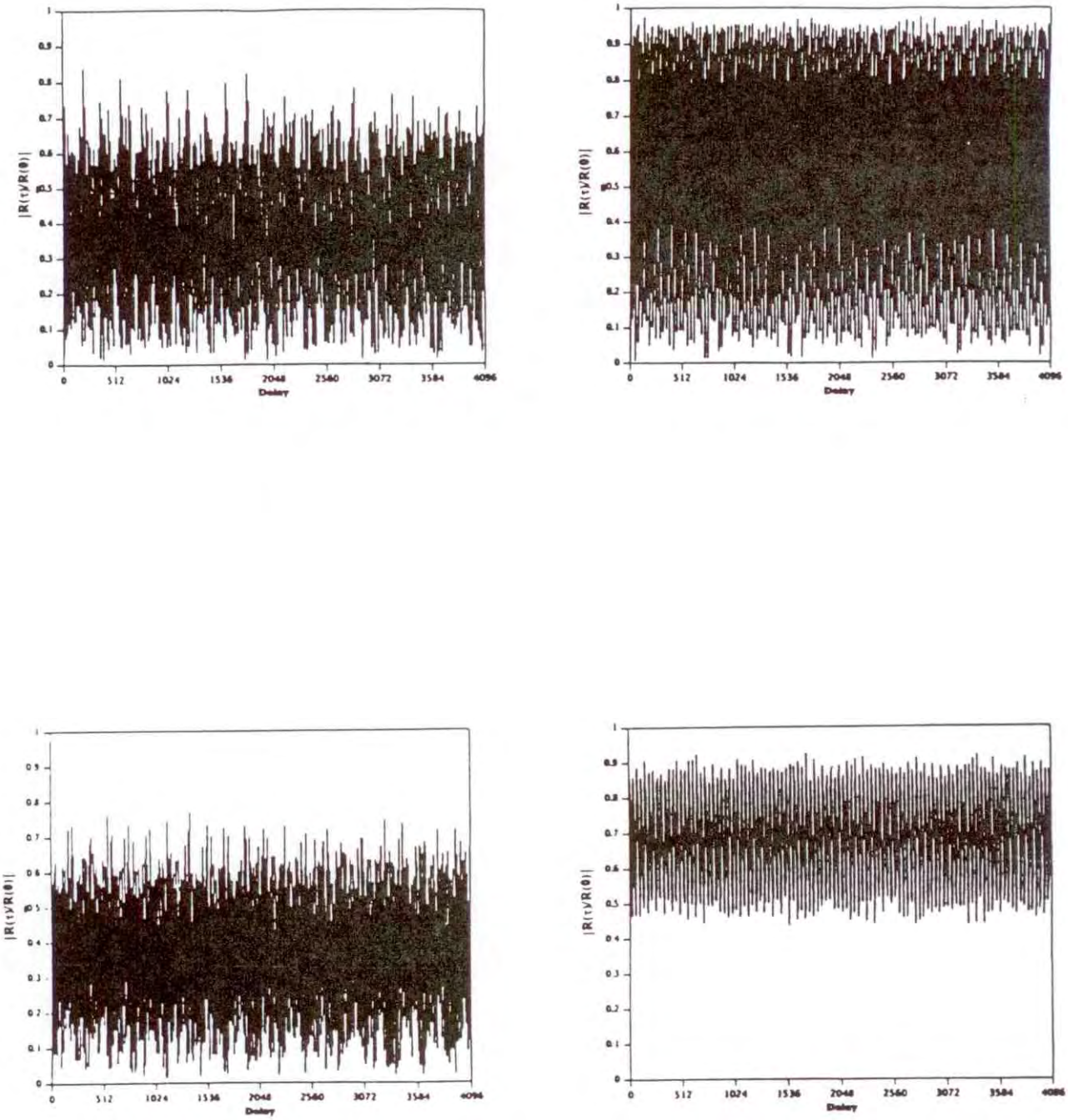

Figure 18. Normalized autocorrelation functions of simulated noise/interference (Gaussian noise, anrrowband interferers, and impulsive noise).

interferers dominates the power in the channel. The resulting power spectrum is shown in Figure 19. That portion of the power spectum containing the cluster of interferers is plotted on an expanded scale (-128 kHz to 0) in Figure 20, which resembles, but is not identical to, the spectrum in Figure 10. The first 4 ms of the simulated I-channel data are plotted in Figure 21, and resemble a single carrier with amplitude modulation, as do the data in Figure 7. The magnitude of the normalized autocorrelation function is shown in Figure 22 for $0 \leq \tau \leq 4$ ms. There are no rapid oscillations, as in the autocorrelation functions of the other simulated examples, and neither the I-channel data nor the autocorrelation function are periodic over the first 4 ms. Thus, an appropriate combination of narrowband interferers can result in an autocorrelation function similar to that in the third case study.

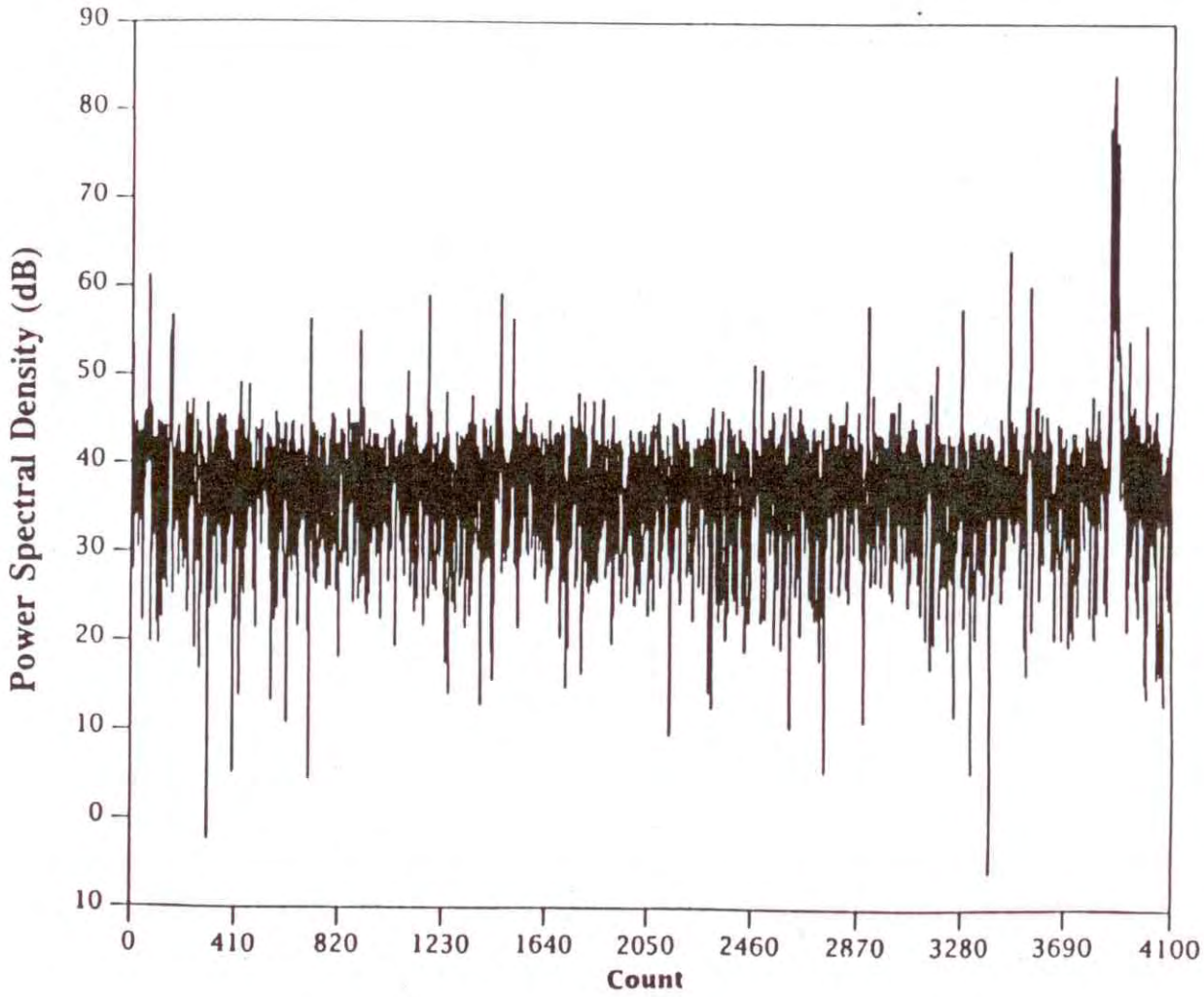

Figure 19. Power spectrum of simulated noise/interference over a bandwidth of 1.024 MHz.

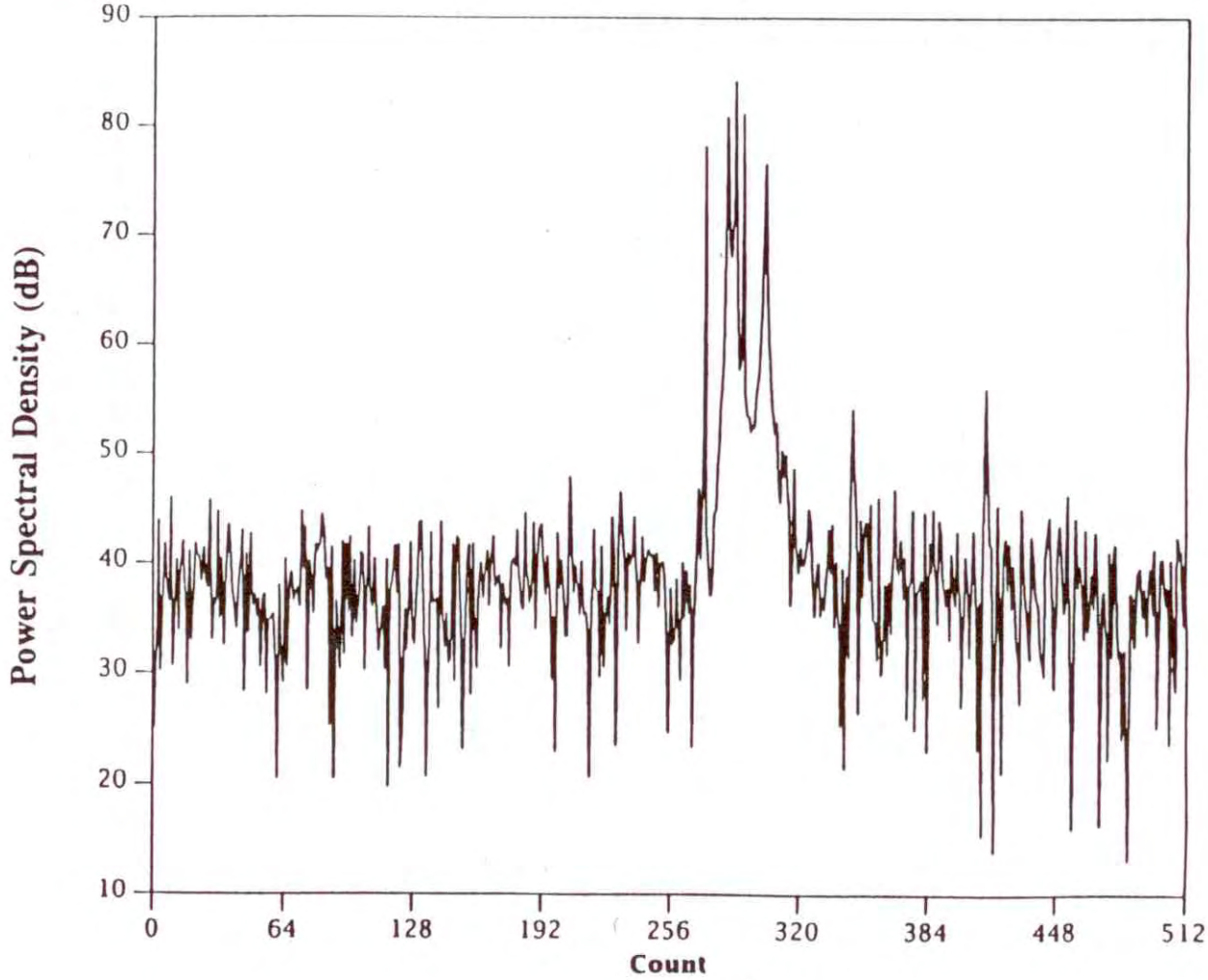

Figure 20. Power spectrum of simulated noise/interference on a scale from -125kHz to 0

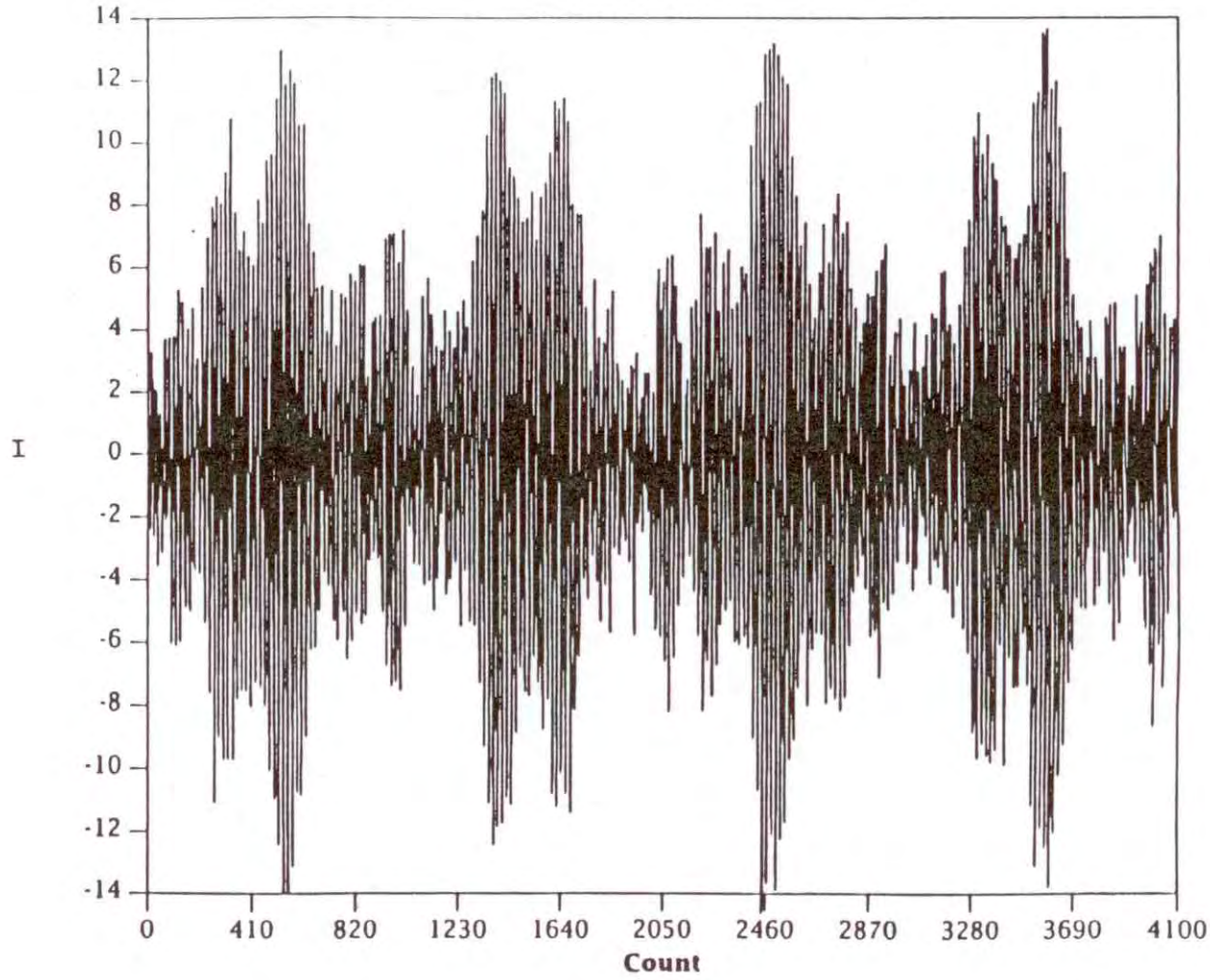

Figure 21. I-channel data of simulated noise/interference.

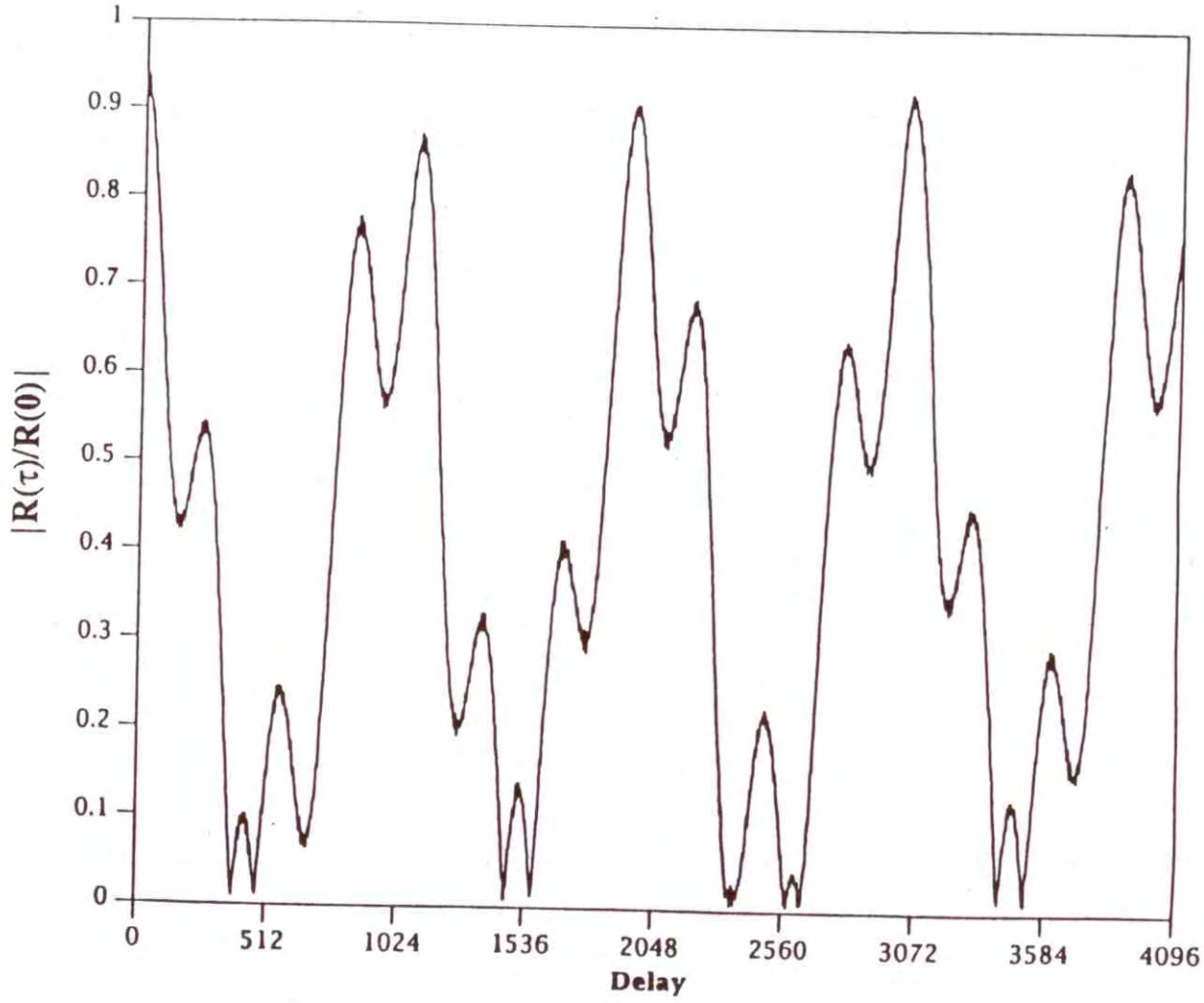

Figure 22. Normalized autocorrelation function of simulated noise/interference.

3. DISTRIBUTIONS OF ENVELOPE LEVEL CROSSINGS

The analyses of the first-order statistics of the noise/interference that were discussed in Part I, as well as the autocorrelation functions discussed above, provide support for modeling the noise/interference as a combination of Gaussian noise, narrowband interferers (sine waves), and impulsive noise (train of impulses). Comparisons of measured and simulated cumulative distributions of power in the time and frequency domains indicate that modeling the amplitude distributions of the sine waves and impulses as Hall distributions is approximately correct. The variety of time domain waveforms and power spectra suggests treating the frequencies of the sine waves as a random variable; a uniform distribution for this random variable is simple and appears to be consistent with the measured data. Furthermore, it seems reasonable to treat the phases of the sine waves as a uniformly distributed random variable, since the different sine waves presumably arise from independent sources. However, it remains to investigate the distribution of the times of arrival of the impulses.

Impulsive noise from man-made sources may be correlated in time, due to machinery which generates noise bursts in a repetitive fashion. Inspection of the time domain waveforms with impulsive noise (case study 5) reveals a tendency for the impulses to occur periodically in time. However, the impulses are not precisely periodic in time, and, as discussed above, this is corroborated by the absence of periodic impulses in the autocorrelation function. Moreover, it is well-known that the impulses in atmospheric noise are clustered in time, due to the presence of numerous individual strokes in a single lightning burst (Uman, 1987). It would therefore be incorrect to model the times of arrival of the impulses either as periodic or as a uniformly distributed random variable.

Further insight concerning the arrival times of the impulses can be gained by investigating the distributions of level crossings of the noise/interference envelope. These distributions provide information about the widths and spacings of the impulses. The calculation of these distributions is difficult, requiring numerical techniques even for the case of Gaussian processes (Rice, 1945; McFadden, 1956; Longuet-Higgins, 1962). Therefore, no attempt will be made to obtain analytic expressions for these distributions in the noise/interference model, as was done for the autocorrelation function. Instead, a purely empirical approach will be adopted, whereby the

distributions computed from the measured data will be qualitatively compared with those from the simulated data, with the goal of refining the model to make the measured and simulated distributions consistent with one another.

3.1 Pulse Width and Pulse Spacing Distributions

Pulse width is defined as the time interval between an upgoing crossing of the voltage envelope ($\sqrt{(I^2+Q^2)}$) through some threshold and the next downgoing crossing of the envelope through that same threshold. Conversely, pulse spacing is defined as the time interval between a downgoing crossing of the envelope through some threshold and the next upgoing crossing through that threshold. Thus, for a given data record, a family of distributions (corresponding to various thresholds) is required to characterize the distributions of pulse widths and pulse spacings. Accordingly, sets of distributions have been computed for each of the five case studies. As a point of reference, the first 4 ms of the voltage envelope have also been plotted for each of the case studies, so that one can make a correspondence between the values of the thresholds that were chosen and the structure of the voltage envelope.

The results are shown in Figures 23 through 37. The pulse width and spacing distributions have been presented in the form of plots in which each point corresponds to the number of occurrences of a pulse width (spacing) of a given time duration. To obtain a sufficient number of occurrences to clearly reveal the trends in the distributions, it was necessary to analyze the entire one-second record for each of the cases. The distributions corresponding to different thresholds have been plotted on separate scales for clarity; however, to facilitate comparisons, the scales of the different plots in each figure are the same. These scales were chosen to be logarithmic, due to the large ranges of values that were encountered. Thus, the logarithm of the number of occurrences of a pulse width (spacing) of a given duration has been plotted versus the logarithm of that duration in microseconds.

Although no analytical results have been derived with which to compare the measured distributions, the qualitative behavior of the distributions is in accord with intuition. For example, the voltage envelope equals zero if and only if the I- and Q-channel voltages simultaneously equal zero, which is a relatively rare event. Therefore, the voltage envelope vanishing at two or more consecutive sample times is an extremely rare event. Thus, at zero

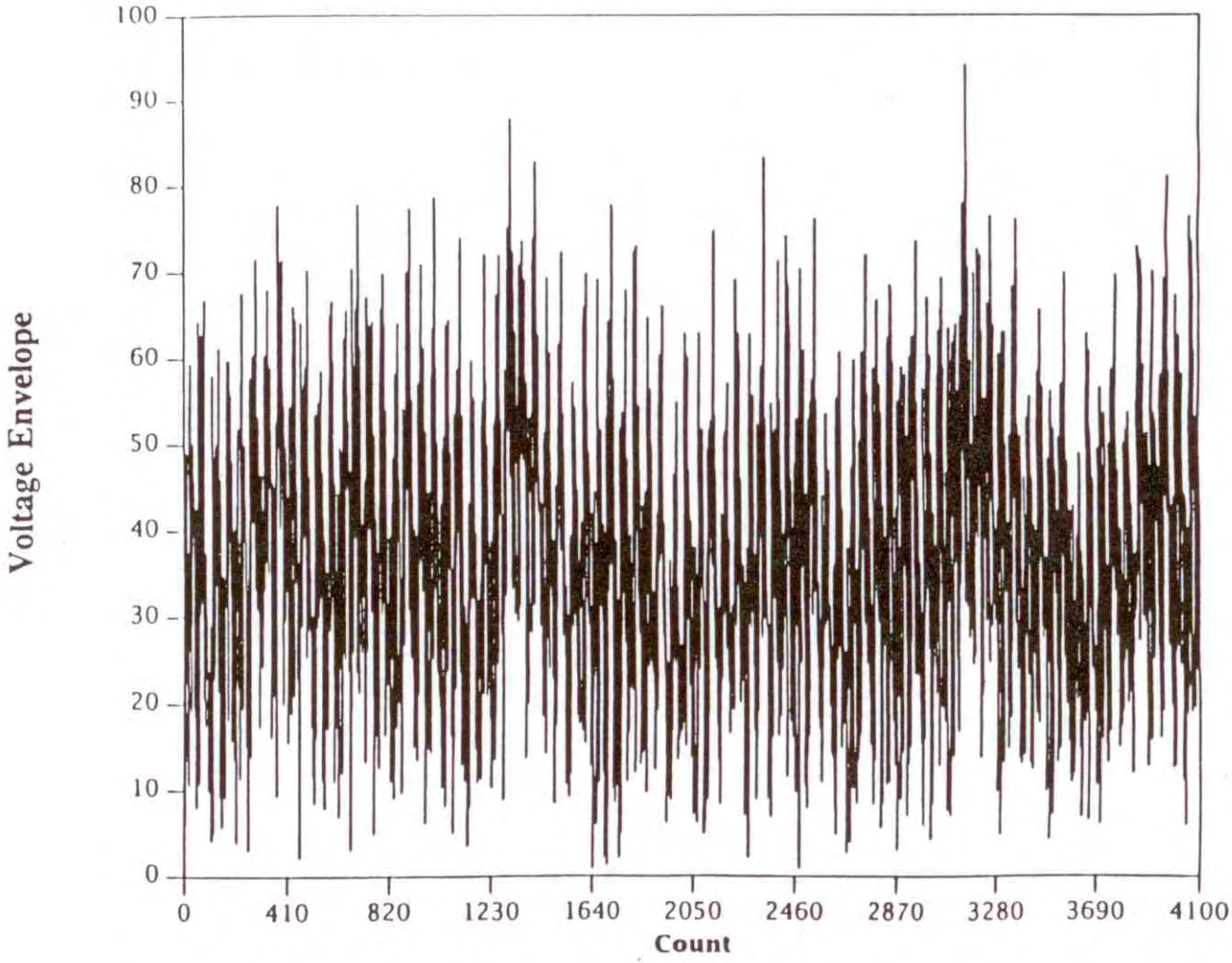

Figure 23. Voltage envelope of measured noise/interference (case study 1).

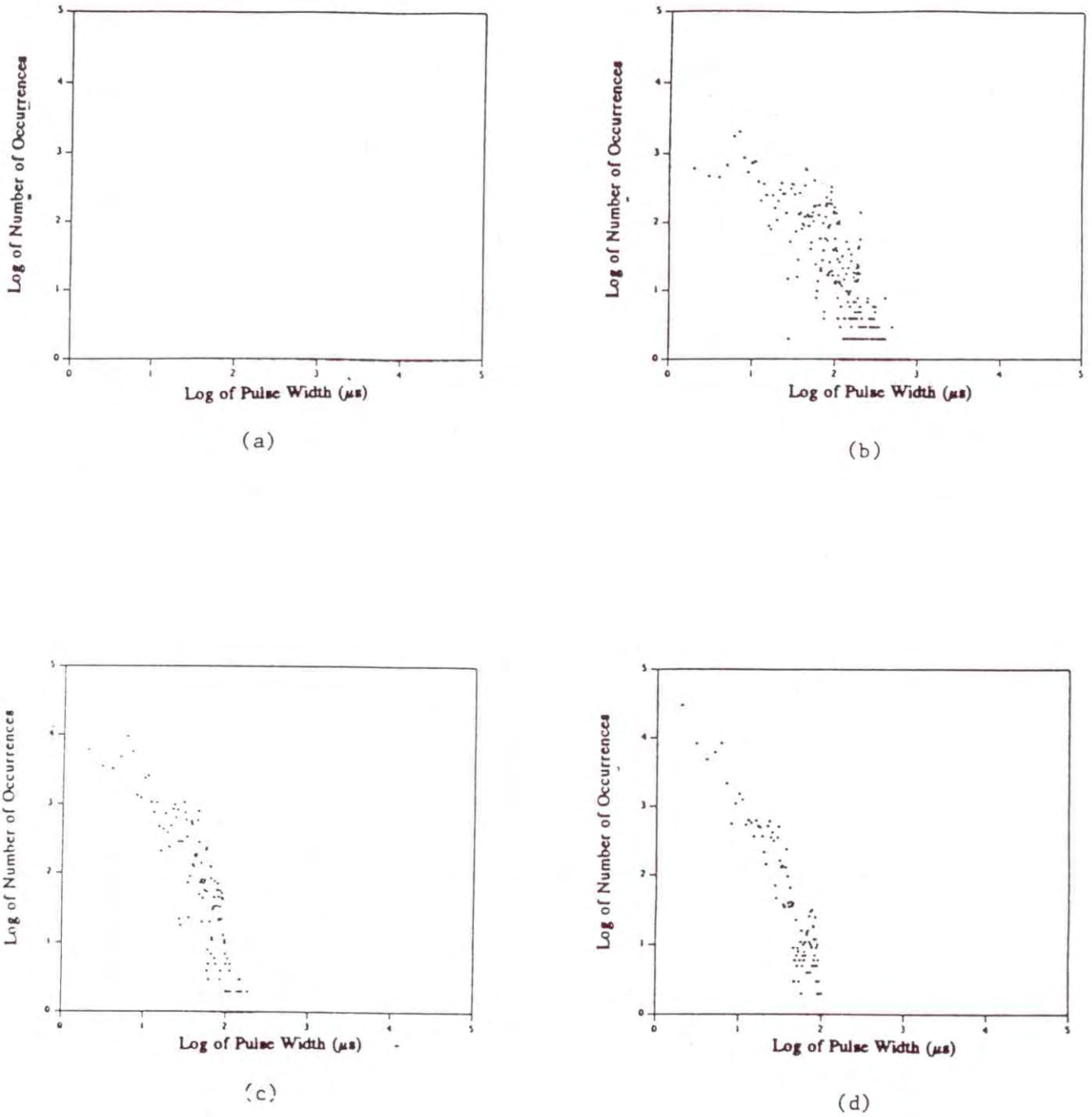

Figure 24. Pulse width distributions of measured noise/interference at thresholds of (a) 0, (b) 10, (c) 20, (d) 30, (e) 40, (f) 50, (g) 70, and (h) 90 (case study 1).

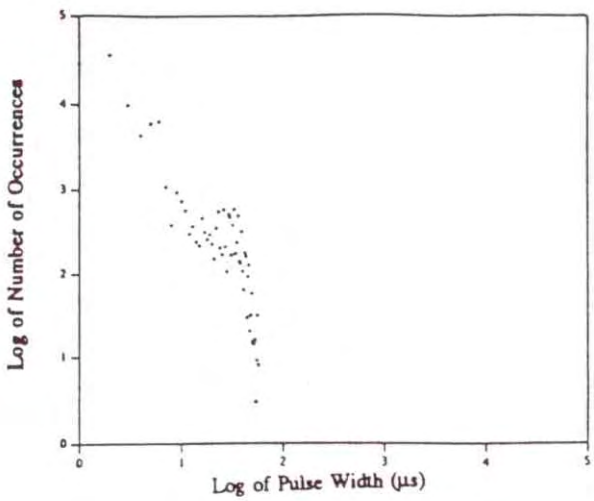

(e)

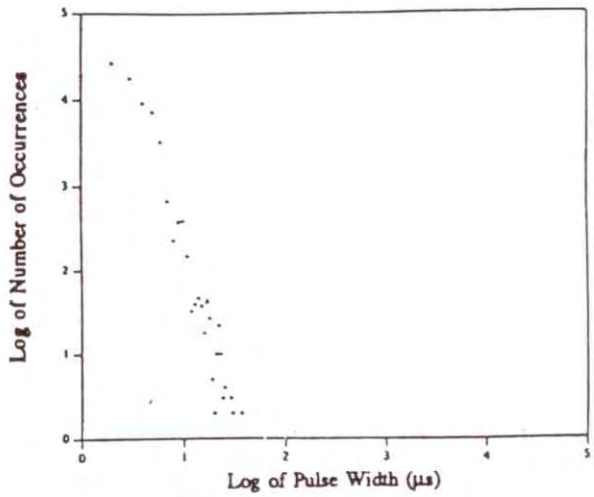

(f)

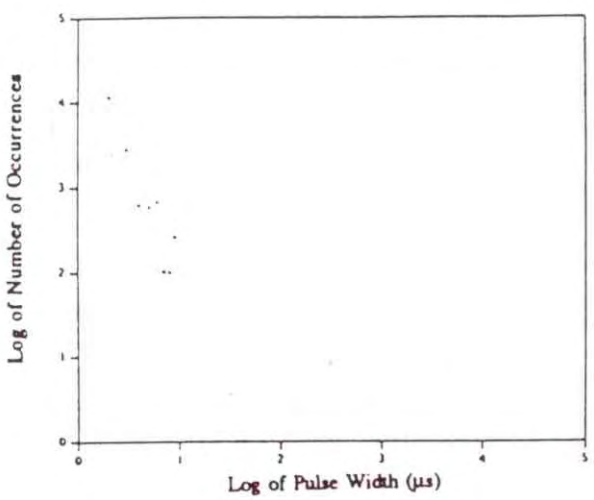

(g)

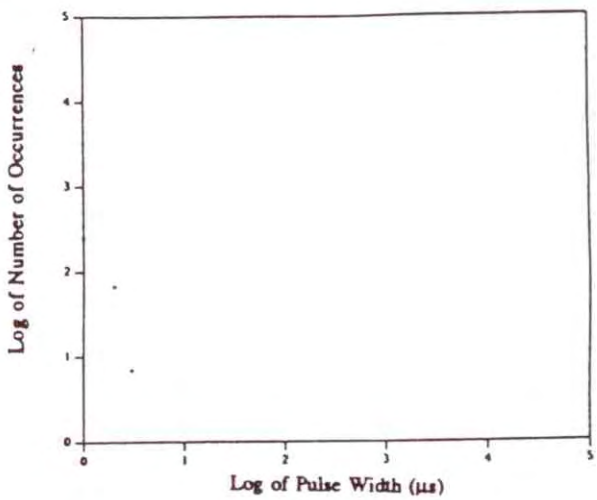

(h)

Figure 24 (cont.). Pulse width distributions of measured noise/interference at thresholds of (a) 0, (b) 10, (c) 20, (d) 30, (e) 40, (f) 50, (g) 70, and (h) 90 (case study 1).

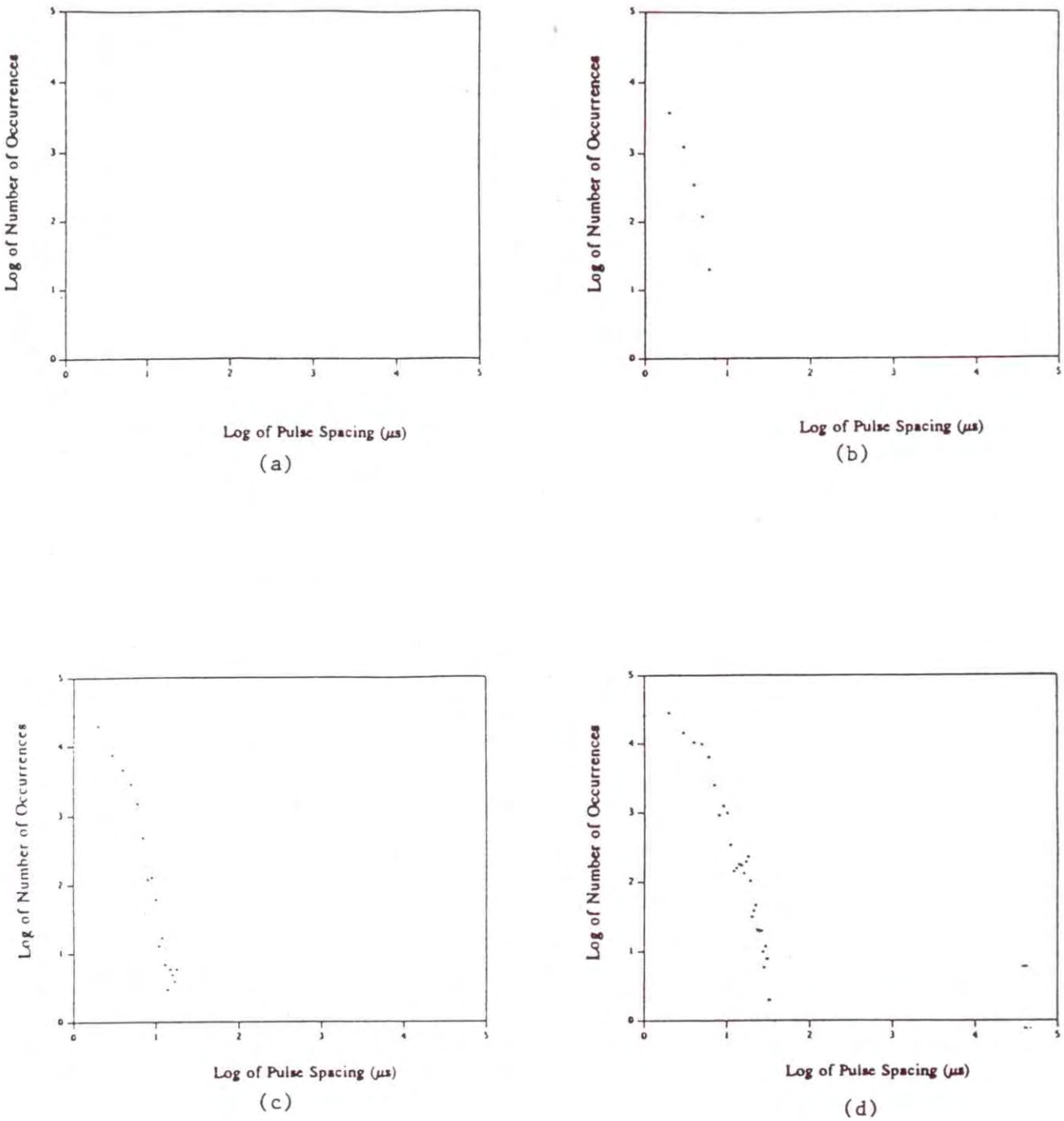

Figure 25. Pulse spacing distributions of measured noise/interference at thresholds of (a) 0, (b) 10, (c) 20, (d) 30, (e) 40, (f) 50, (g) 70, and (h) 90 (case study 1).

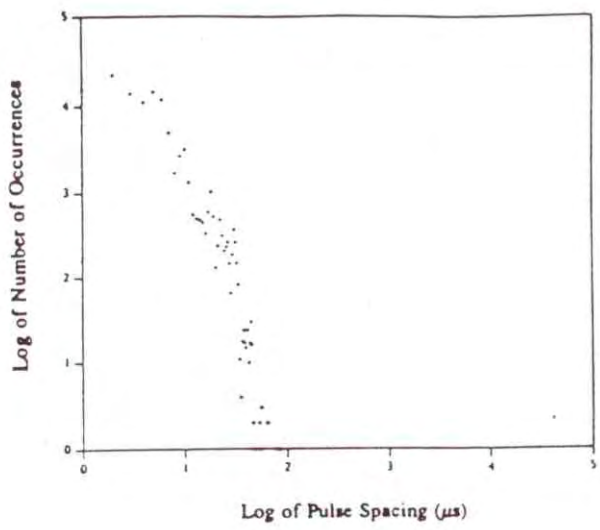

(e)

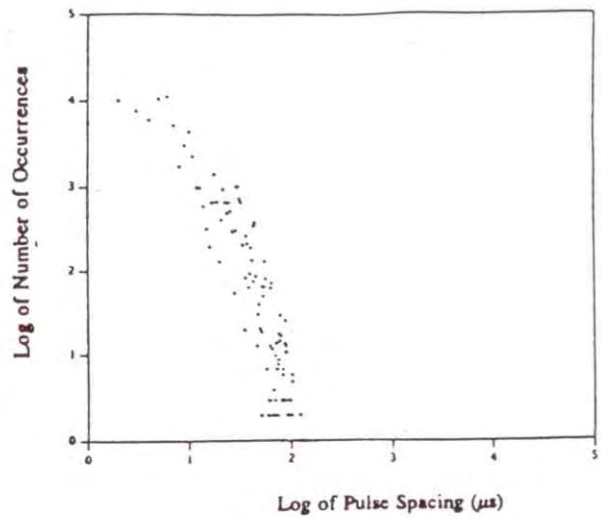

(f)

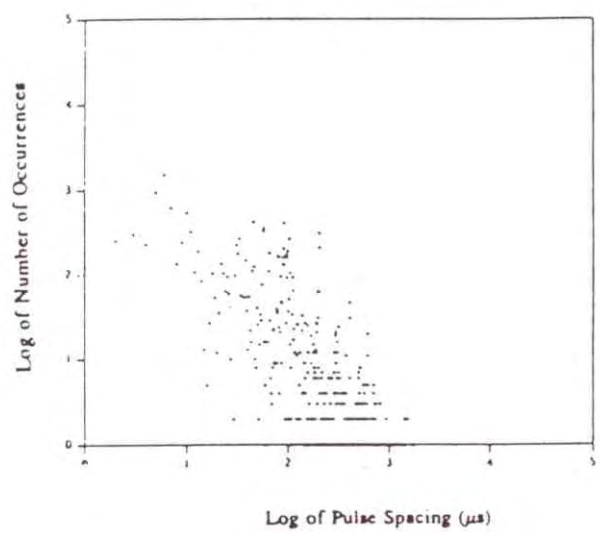

(g)

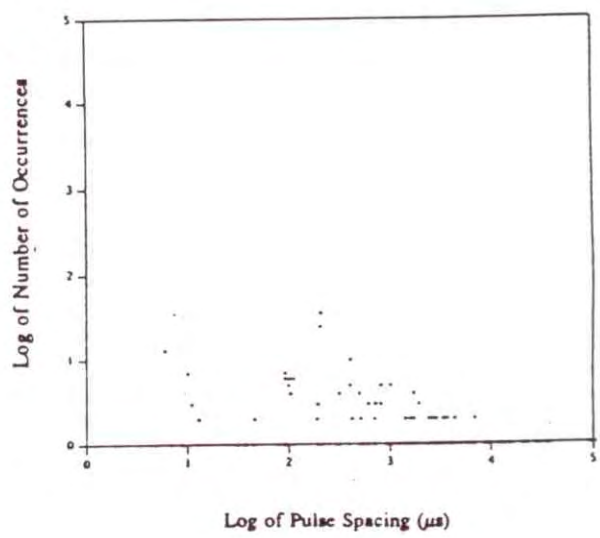

(h)

Figure 25 (cont.). Pulse spacing distributions of measured noise/interference at thresholds of (a) 0, (b) 10, (c) 20, (d) 30, (e) 40, (f) 50, (g) 70, and (h) 90 (case study 1).

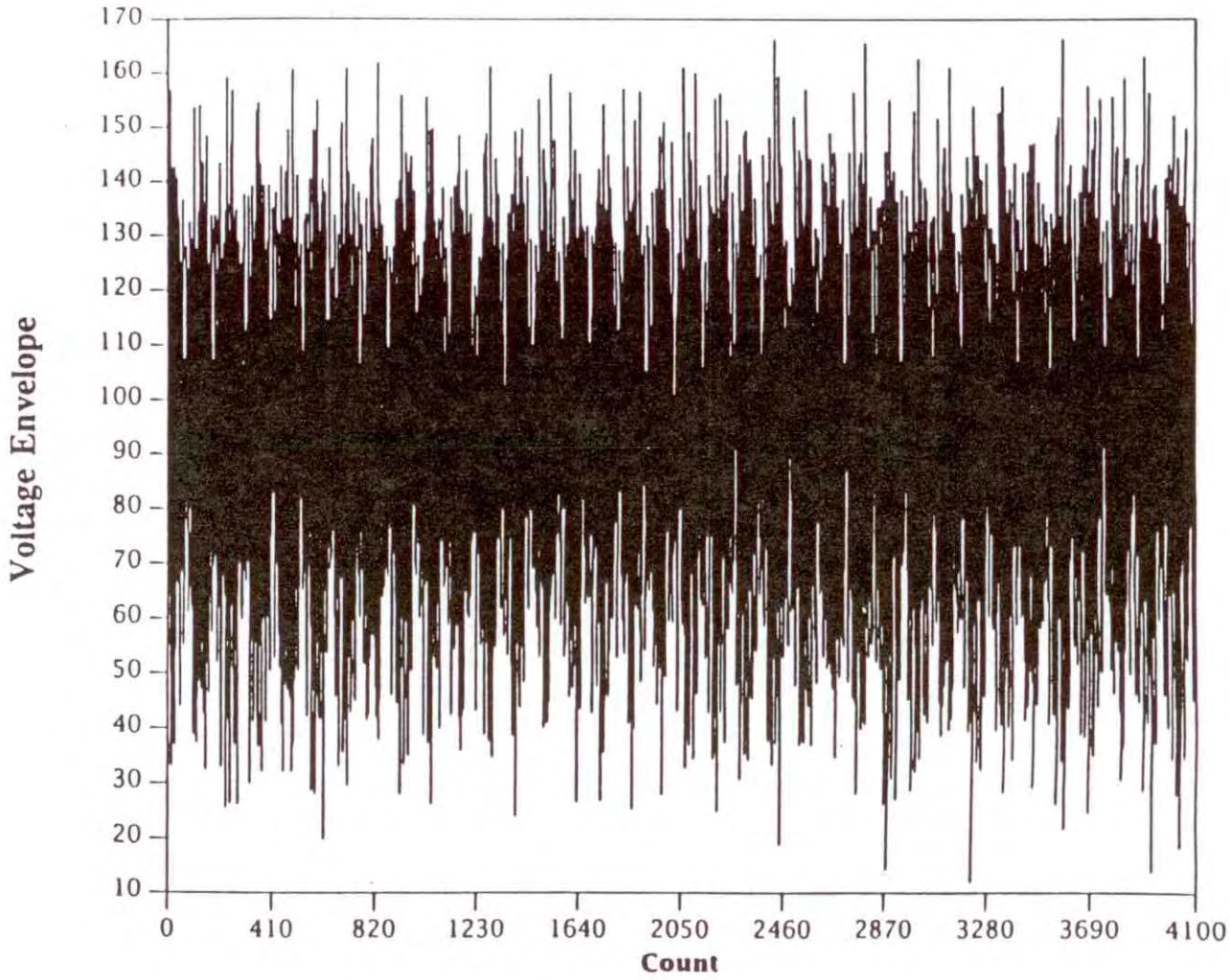

Figure 26. Voltage envelope of measured noise/interference (case study 2).

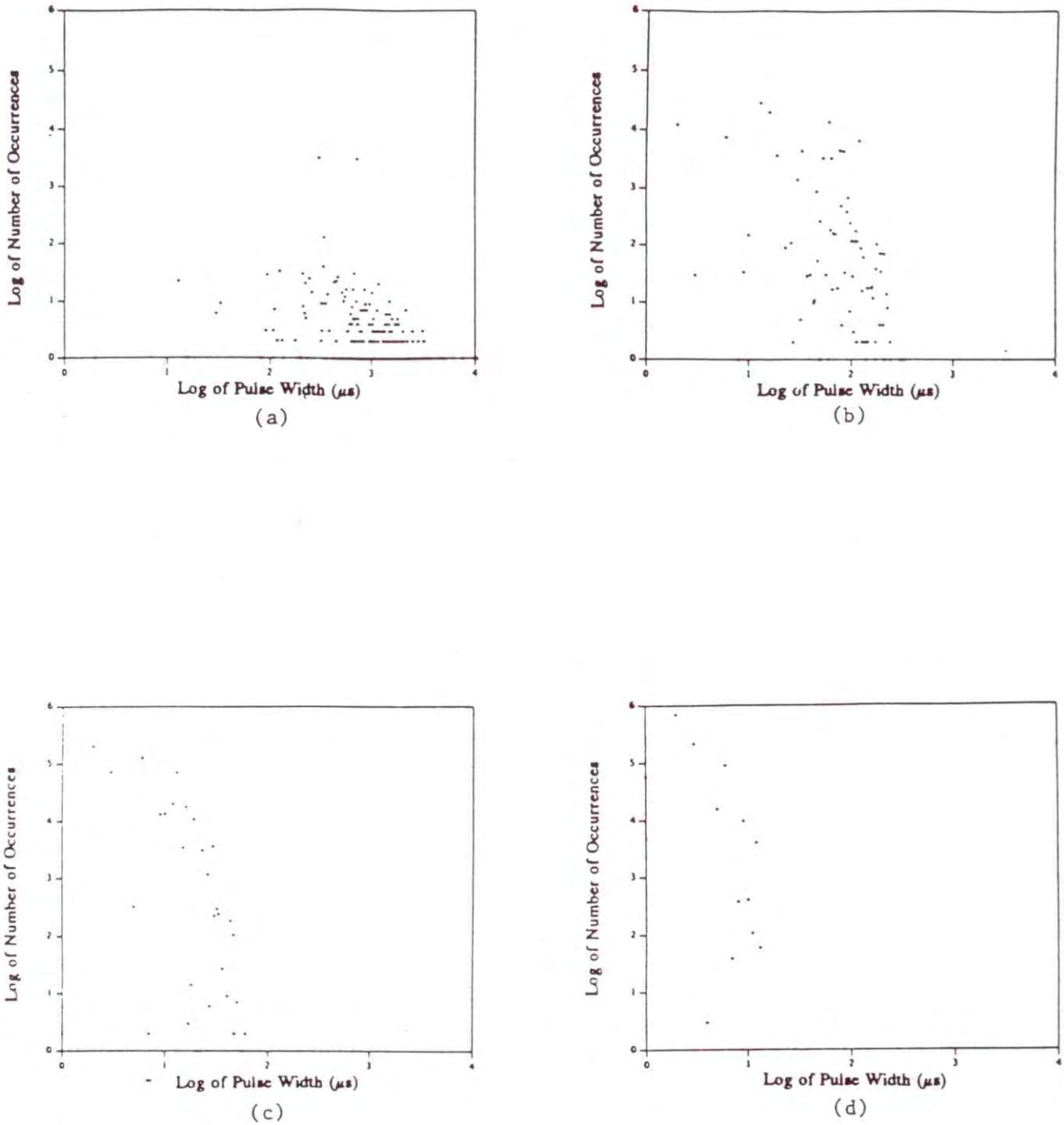

Figure 27. Pulse width distributions of measured noise/interference at thresholds of (a) 20, (b) 40, (c) 60, (d) 80, (e) 100, (f) 120, (g) 140, (h) 160 (case study 2).

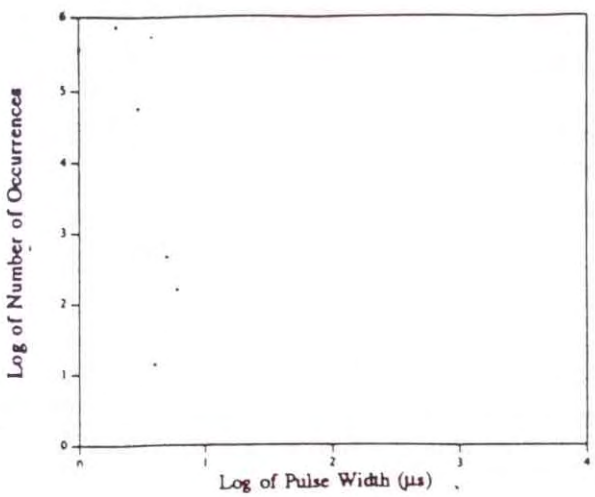

(e)

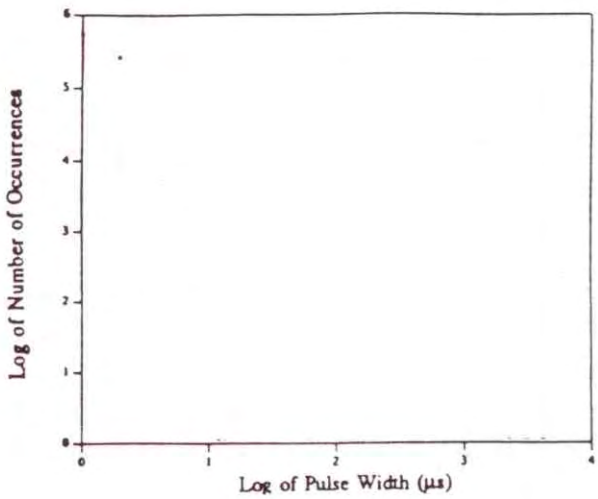

(f)

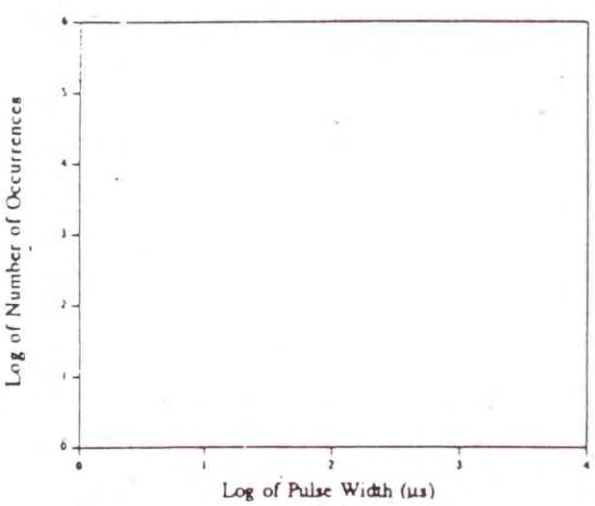

(g)

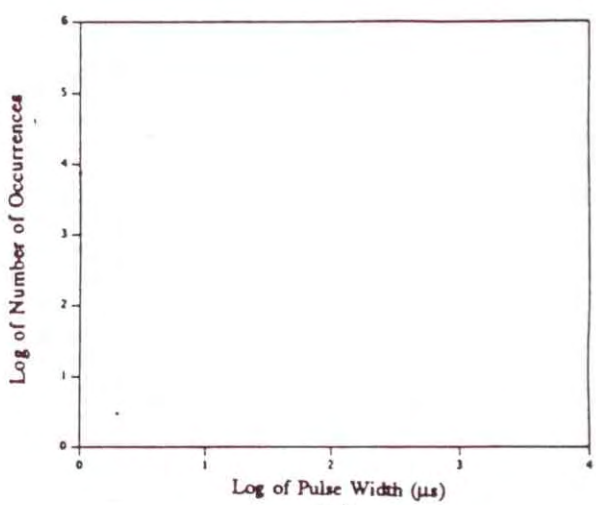

(h)

Figure 27 (cont.). Pulse width distributions of measured noise/interference at thresholds of (a) 20, (b) 40, (c) 60, (d) 80, (e) 100, (f) 120, (g) 140, (h) 160 (case study 2).

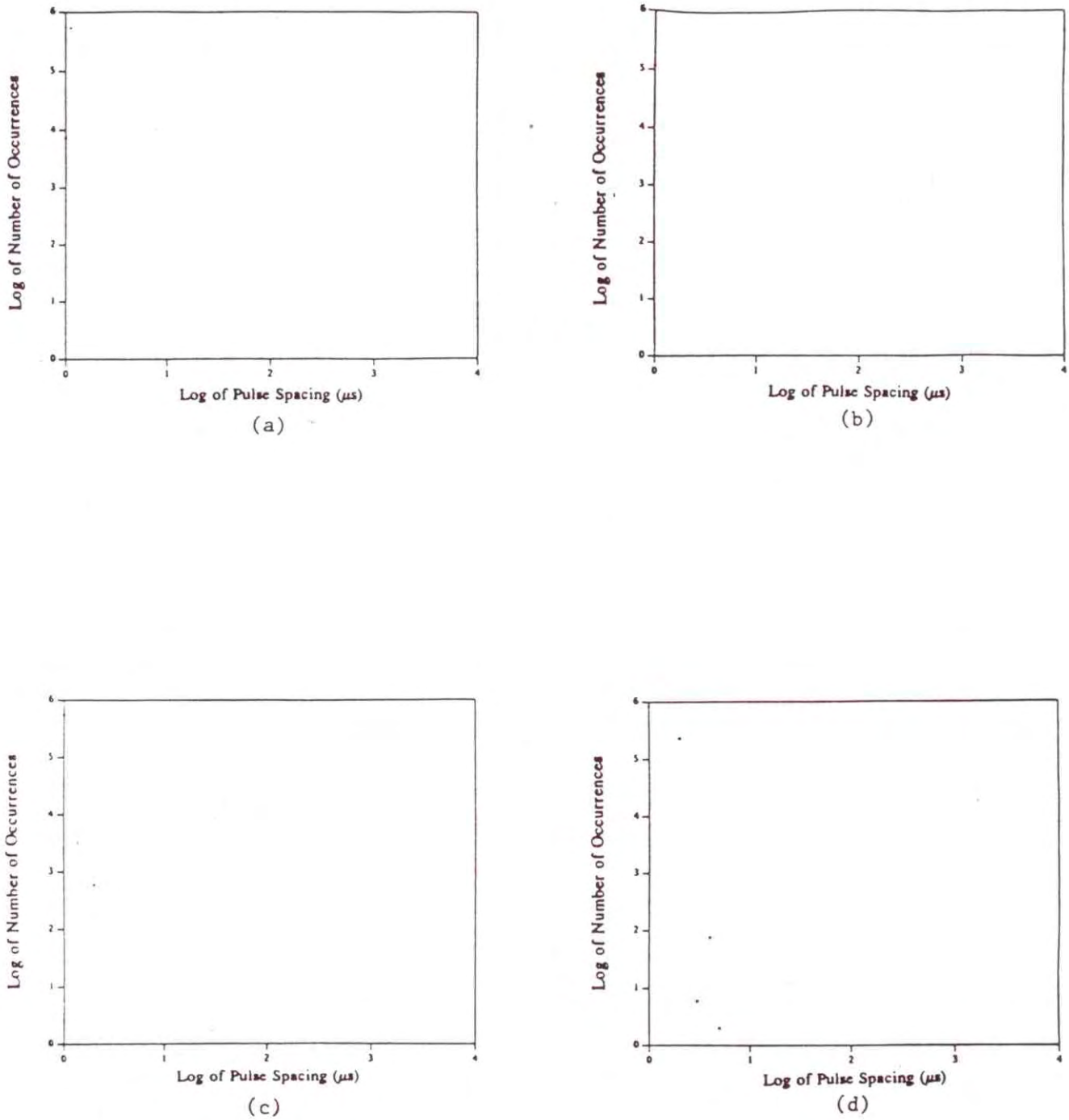

Figure 28. Pulse spacing distributions of measured noise/interference at thresholds of (a) 20, (b) 40, (c) 60, (d) 80, (e) 100, (f) 120, (g) 140, and (h) 160 (case study 2).

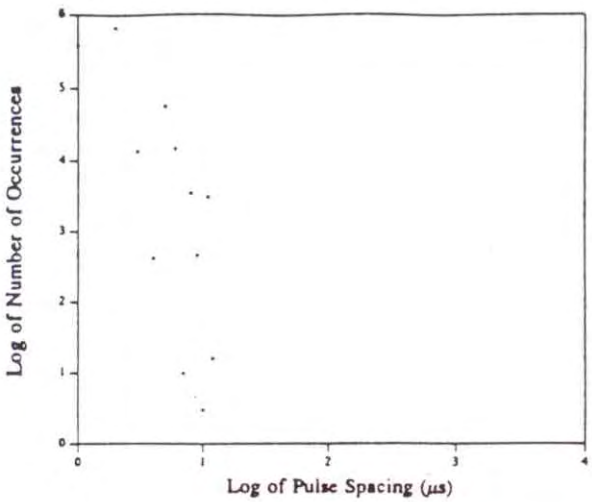

(e)

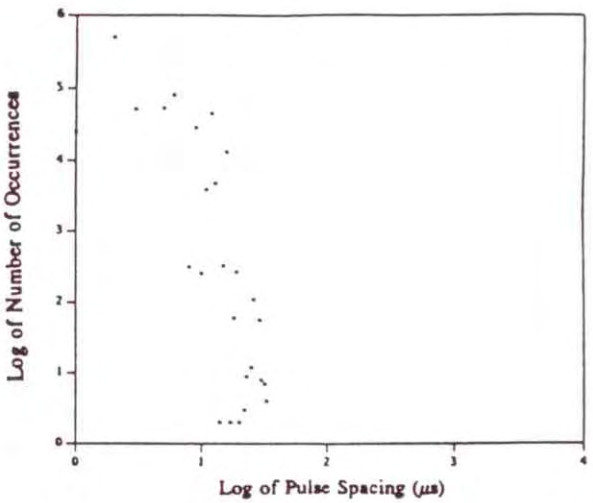

(f)

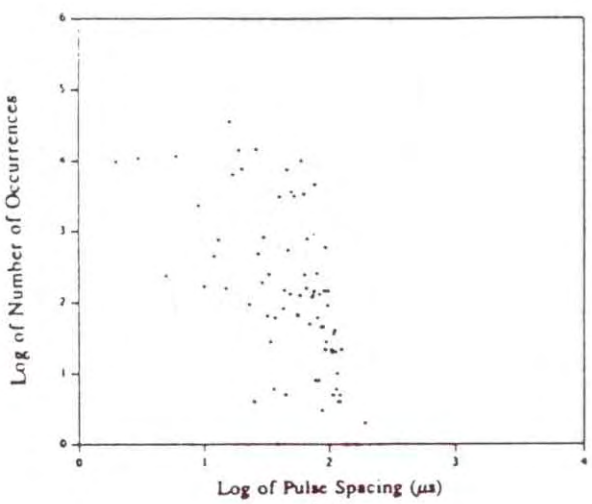

(g)

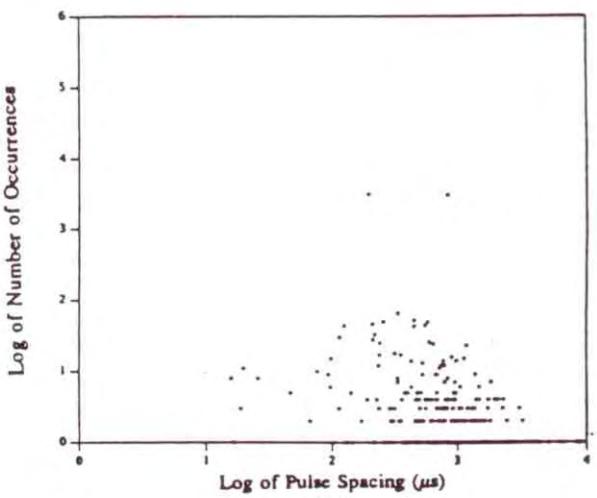

(h)

Figure 28 (cont.). Pulse spacing distributions of measured noise/interference at thresholds of (a) 20, (b) 40, (c) 60, (d) 80, (e) 100, (f) 120, (g) 140, and (h) 160 (case study 2).

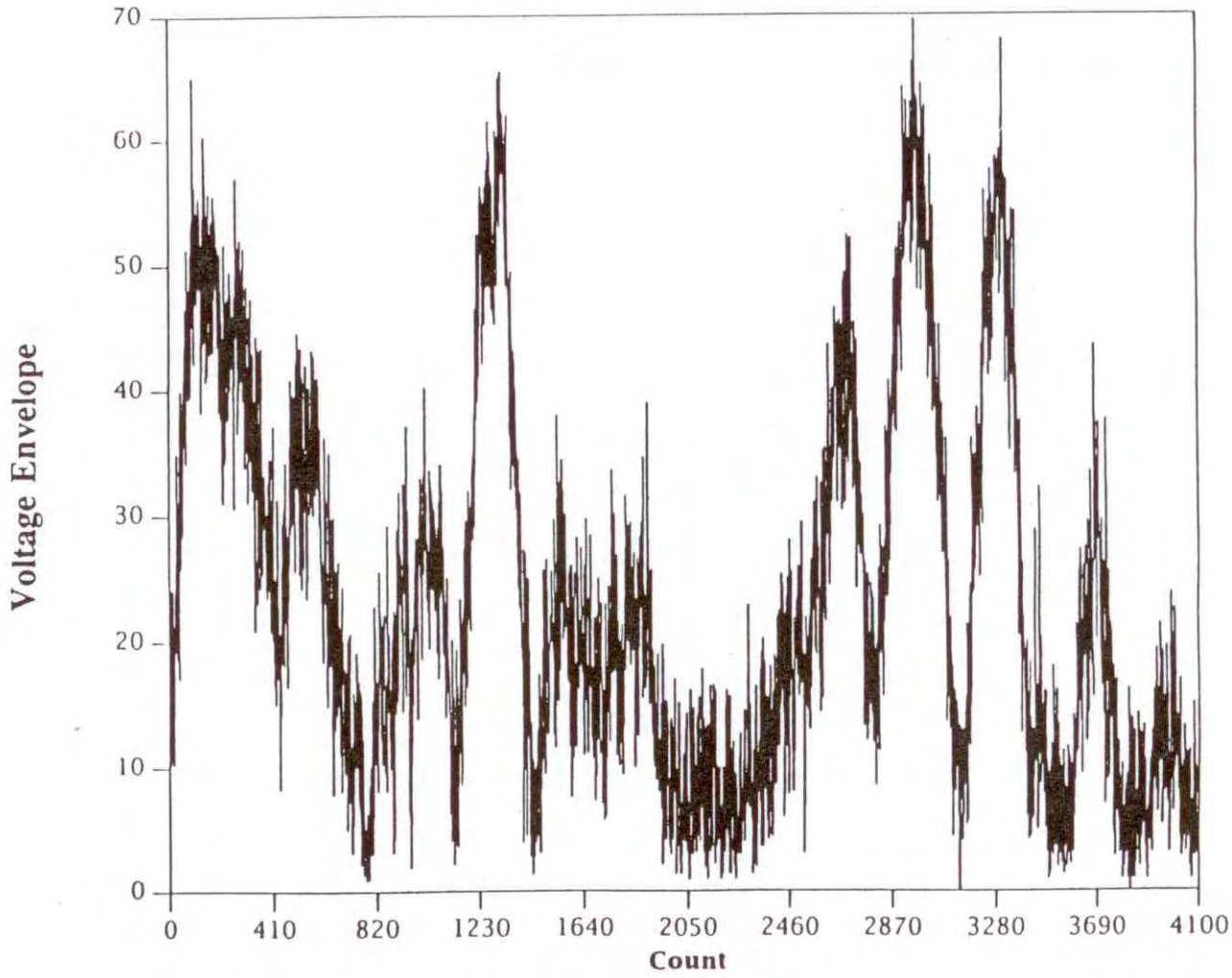

Figure 29. Voltage envelope of measured noise/interference (case study 3).

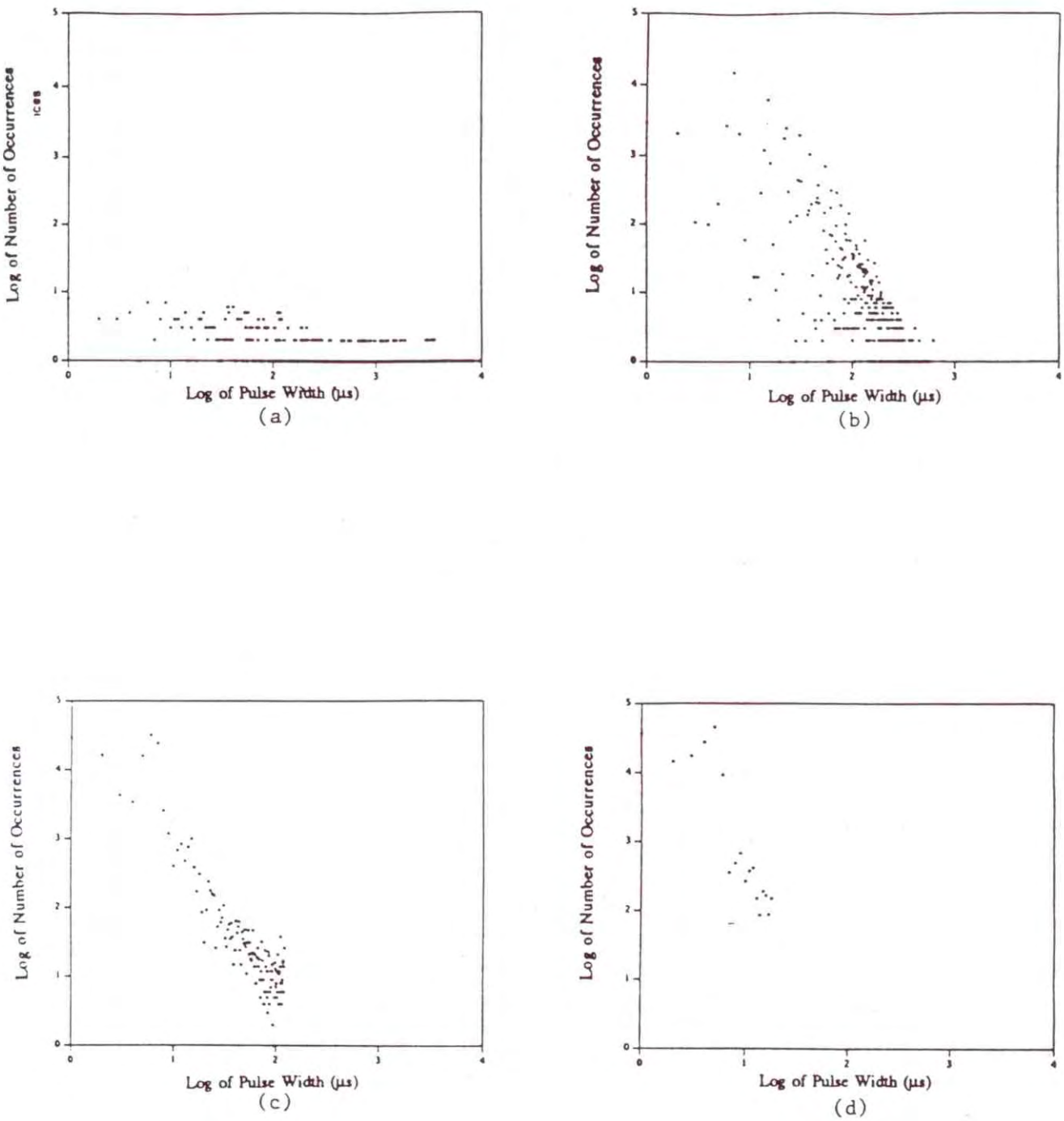

Figure 30. Pulse width distribution of measured noise/interference at thresholds of (a) 0, (b) 10, (c) 20, (d) 30, (e) 40, (f) 45 (case study 3).

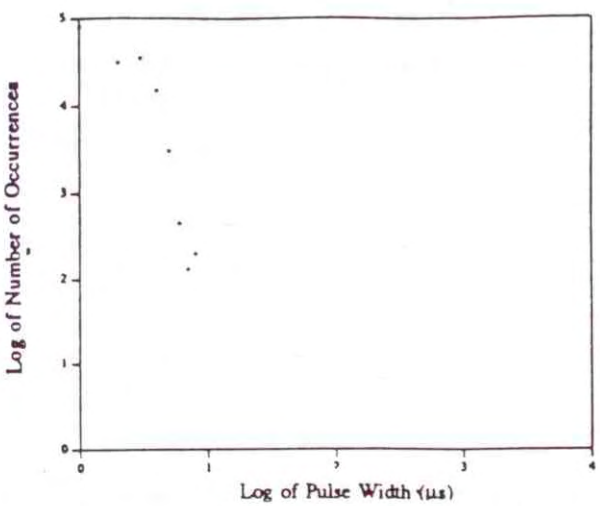

(e)

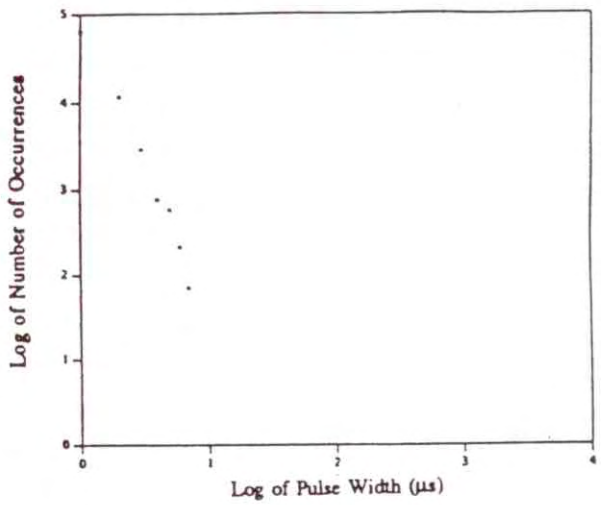

(f)

Figure 30 (cont.). Pulse width distributions of measured noise/interference at thresholds of (a) 0, (b) 10, (c) 20, (d) 30, (e) 40, (f) 45 (case study 3).

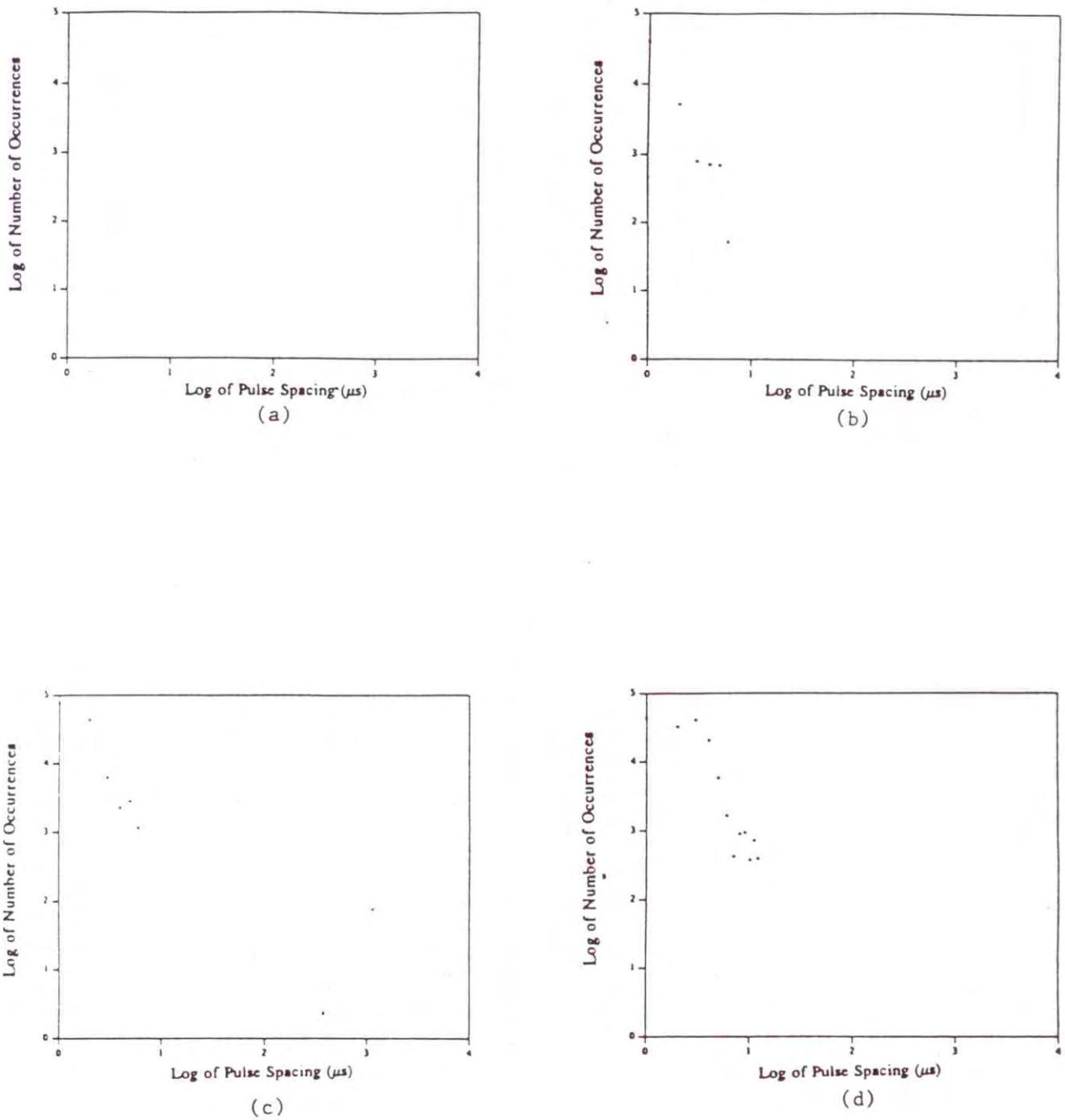

Figure 31. Pulse spacing distribution of measured noise/interference at thresholds of (a) 0, (b) 10, (c) 20, (d) 30, (e) 40, (f) 45 (case study 3).

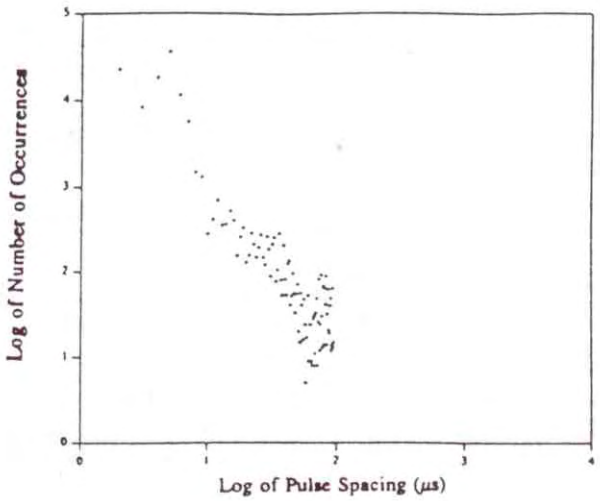

(e)

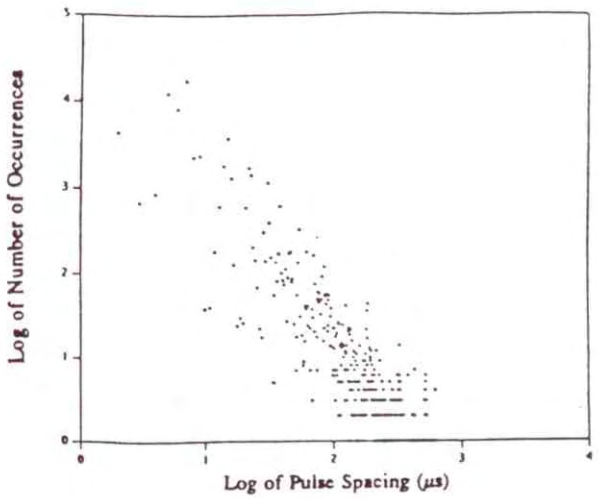

(f)

Figure 31 (cont.). Pulse spacing distribution of measured noise/interference at thresholds of (a) 0. (b) 10, (c) 20, (d) 30, (e) 40, (f) 45 (case study 3).

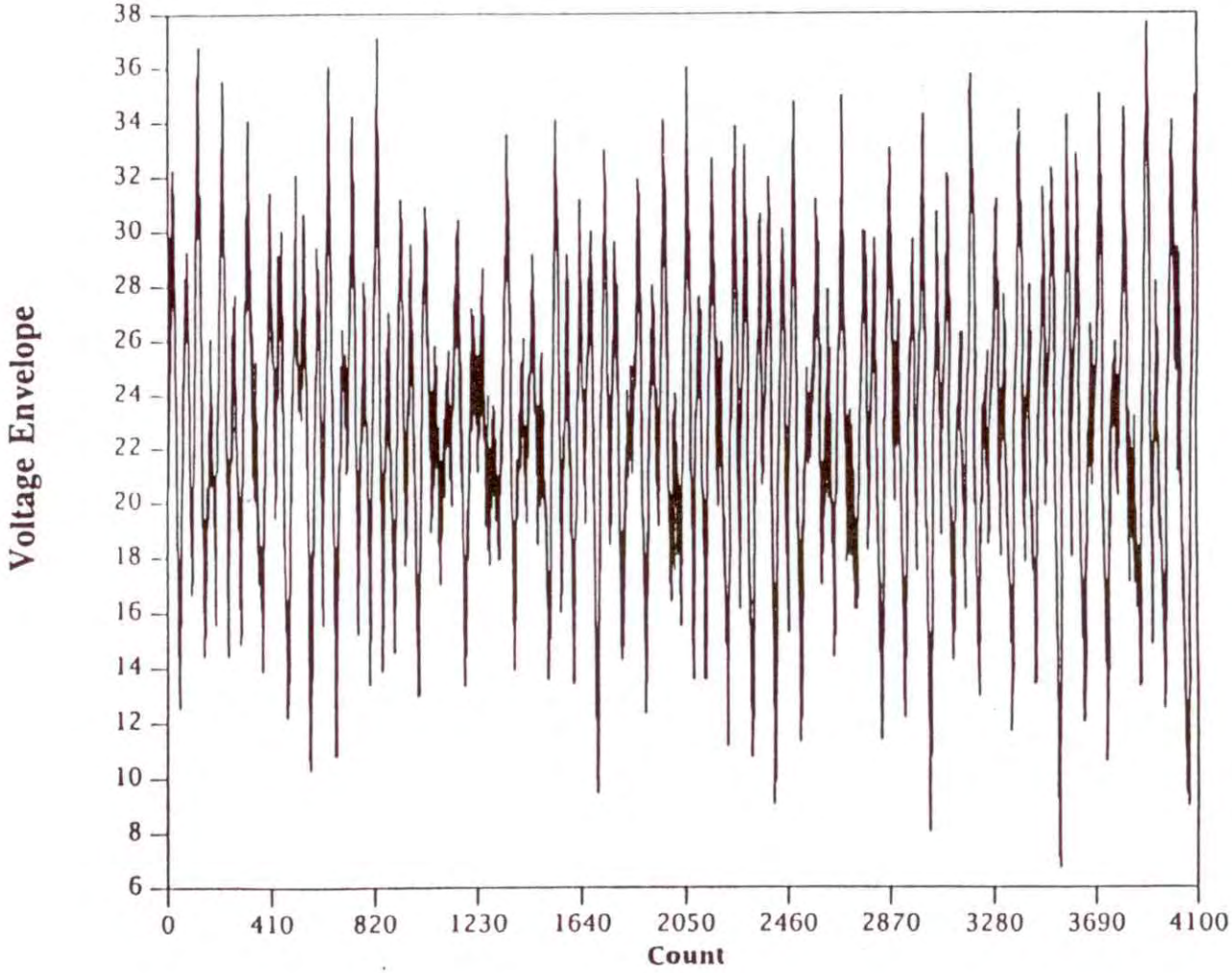

Figure 32. Voltage envelope of measured noise/interference (case study 4).

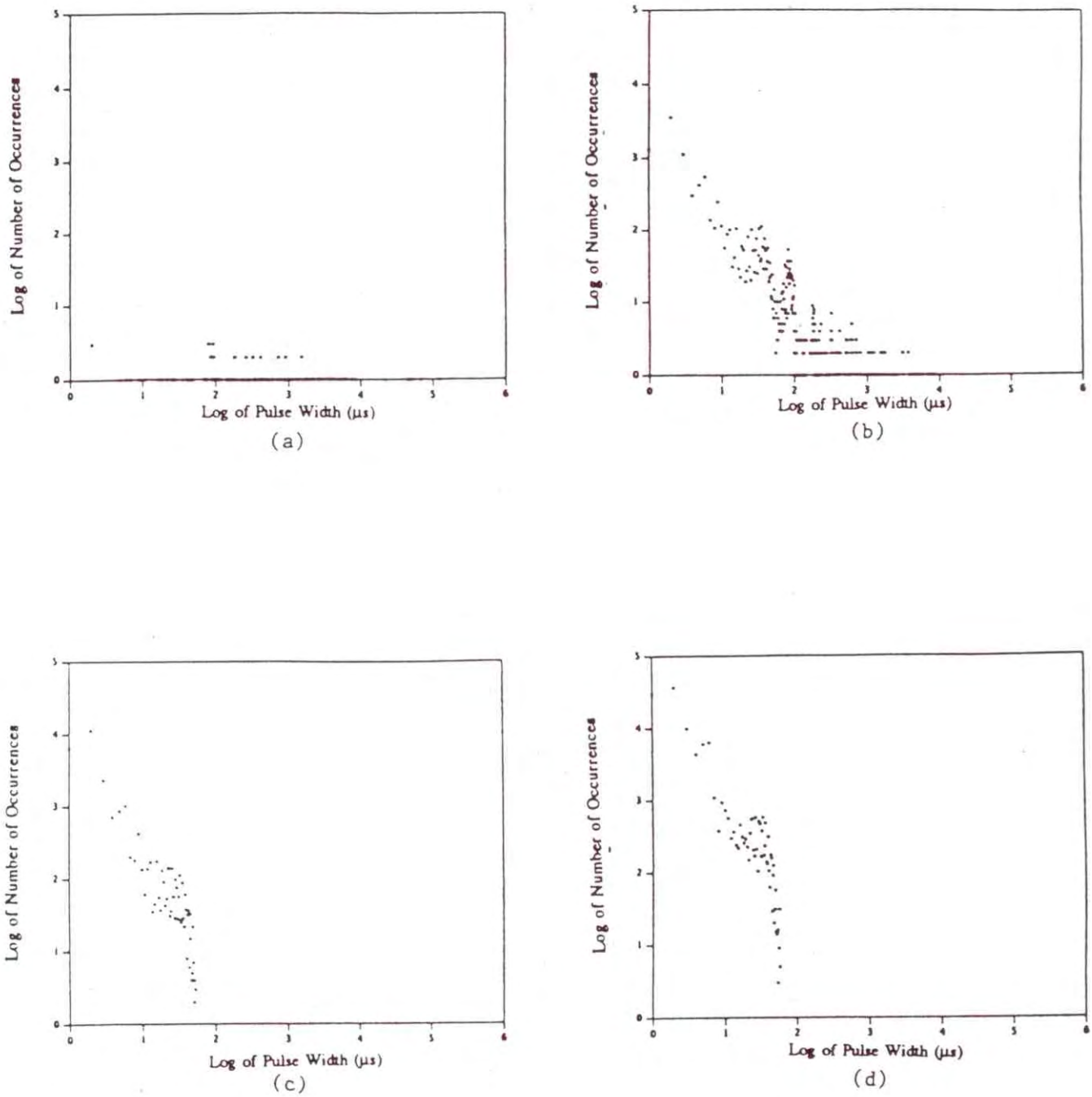

Figure 33. Pulse width distributions of measured noise/interference at thresholds of (a) 0, (b) 5, (c) 10, (d) 20, (e) 30, and (f) 40 (case study 4).

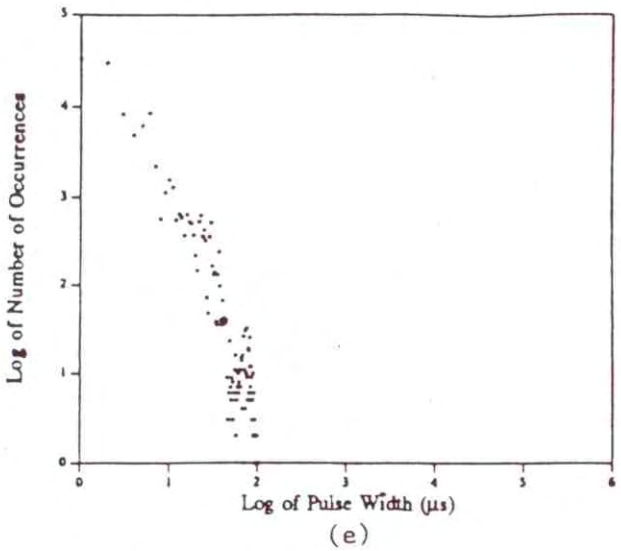

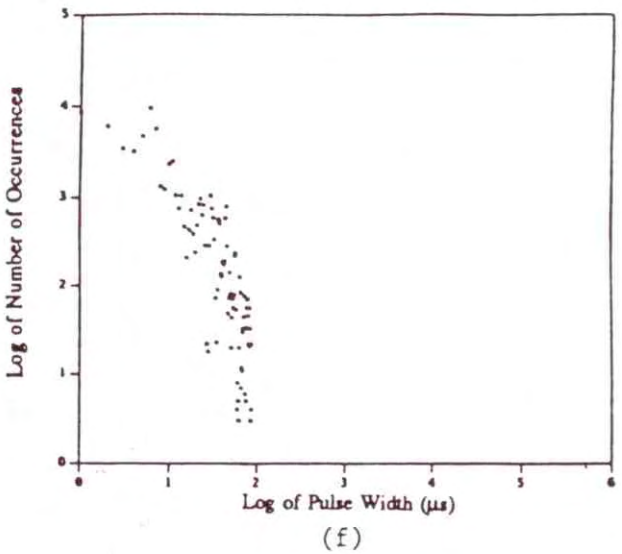

Figure 33 (cont.). Pulse width distributions of measured noise/interference at thresholds of (a) 0, (b) 5, (c) 10, (d) 20, (e) 30, and (f) 40 (case study 4).

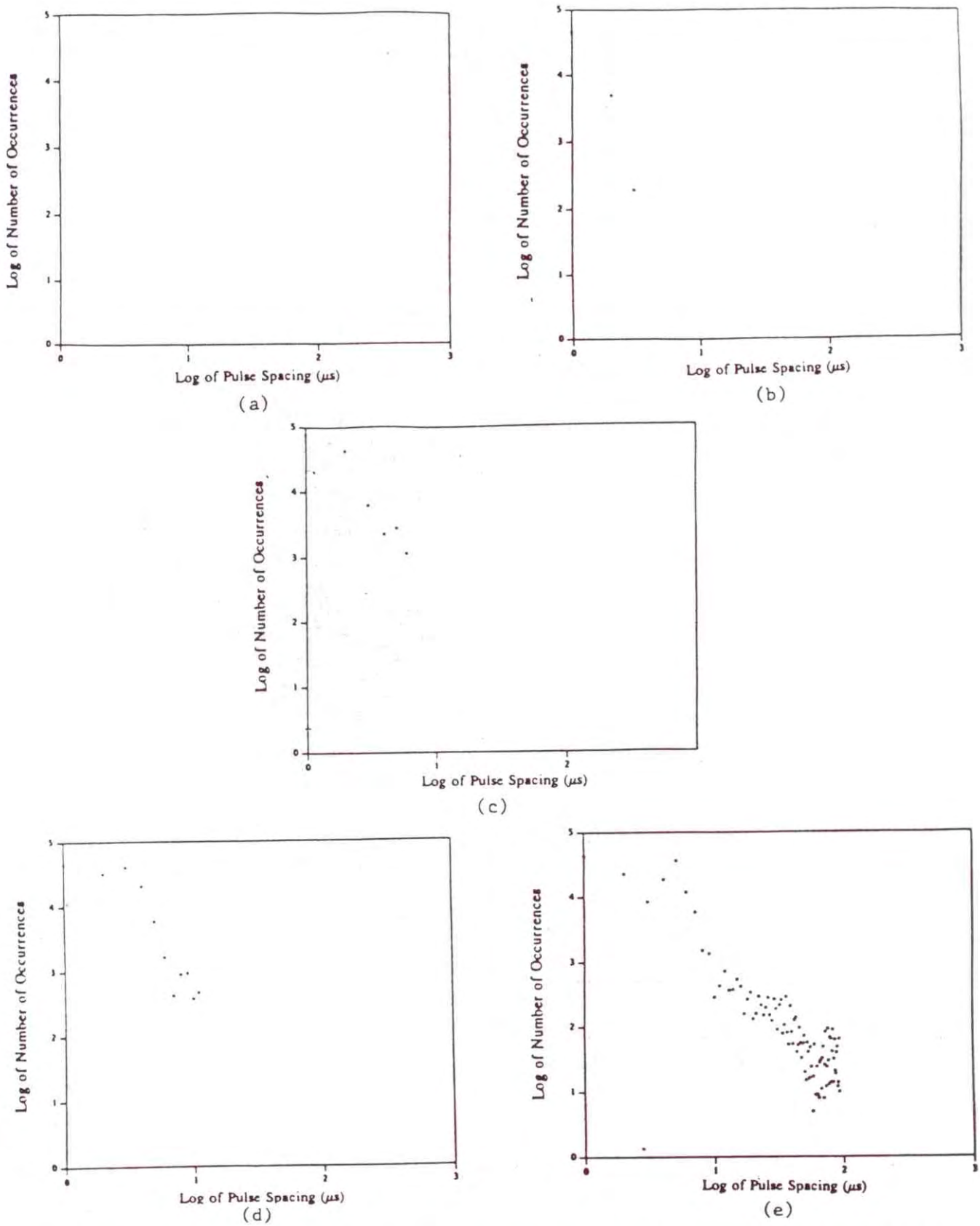

Figure 34. Pulse spacing distributions of measured noise/interference at thresholds of (a) 0, (b) 5, (c) 10, (d) 20, and (e) 30 (case study 4).

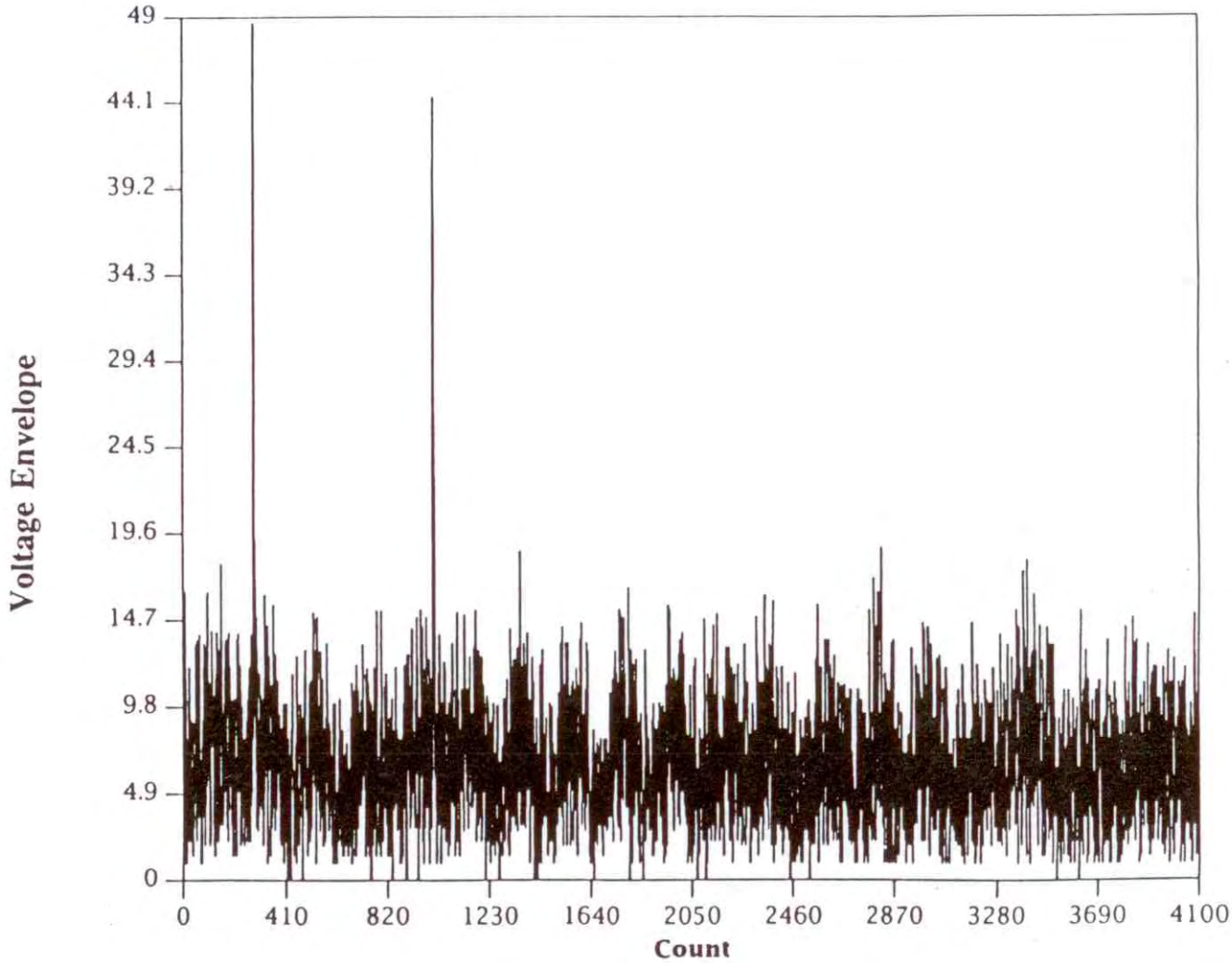

Figure 35. Voltage envelope of measured noise/interference (case study 5).

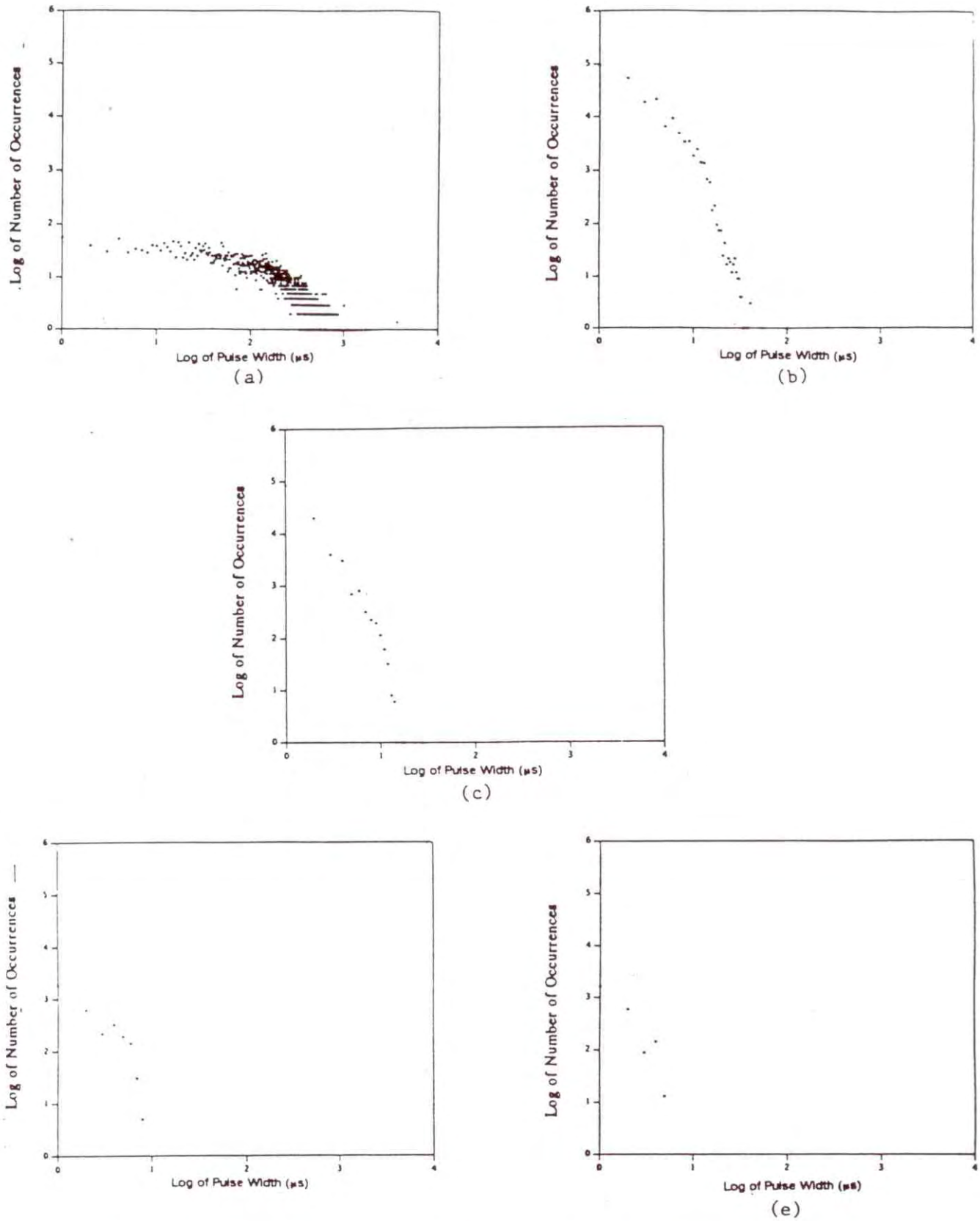

Figure 36. Pulse width distributions of measured noise/interference at thresholds of (a) 0, (b) 5, (c) 10, (d) 25, and (e) 30 (case study 5).

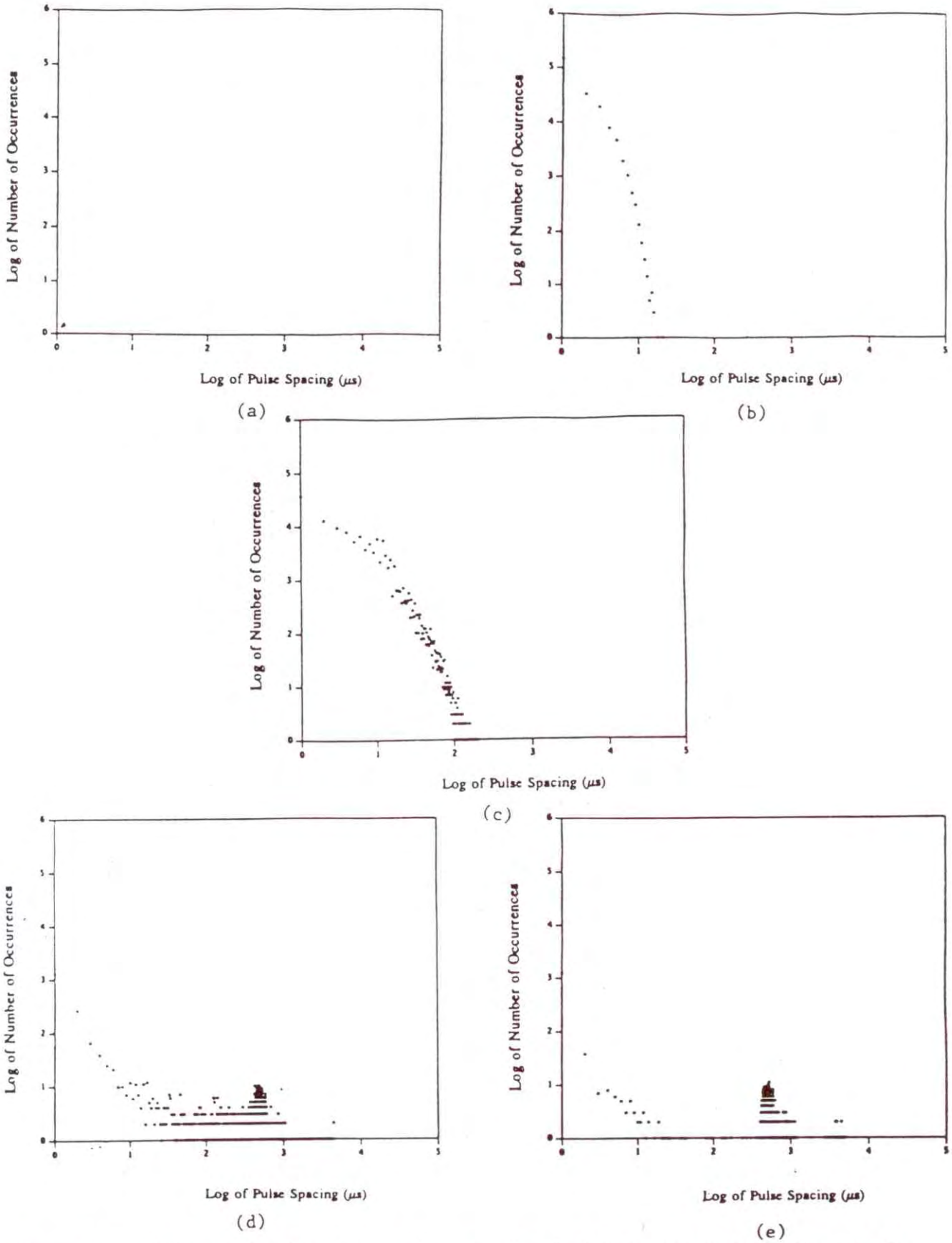

Figure 37. Pulse spacing distributions of measured noise/interference at thresholds of (a) 0, (b) 5, (c) 10, (d) 20, and (e) 30 (case study 5).

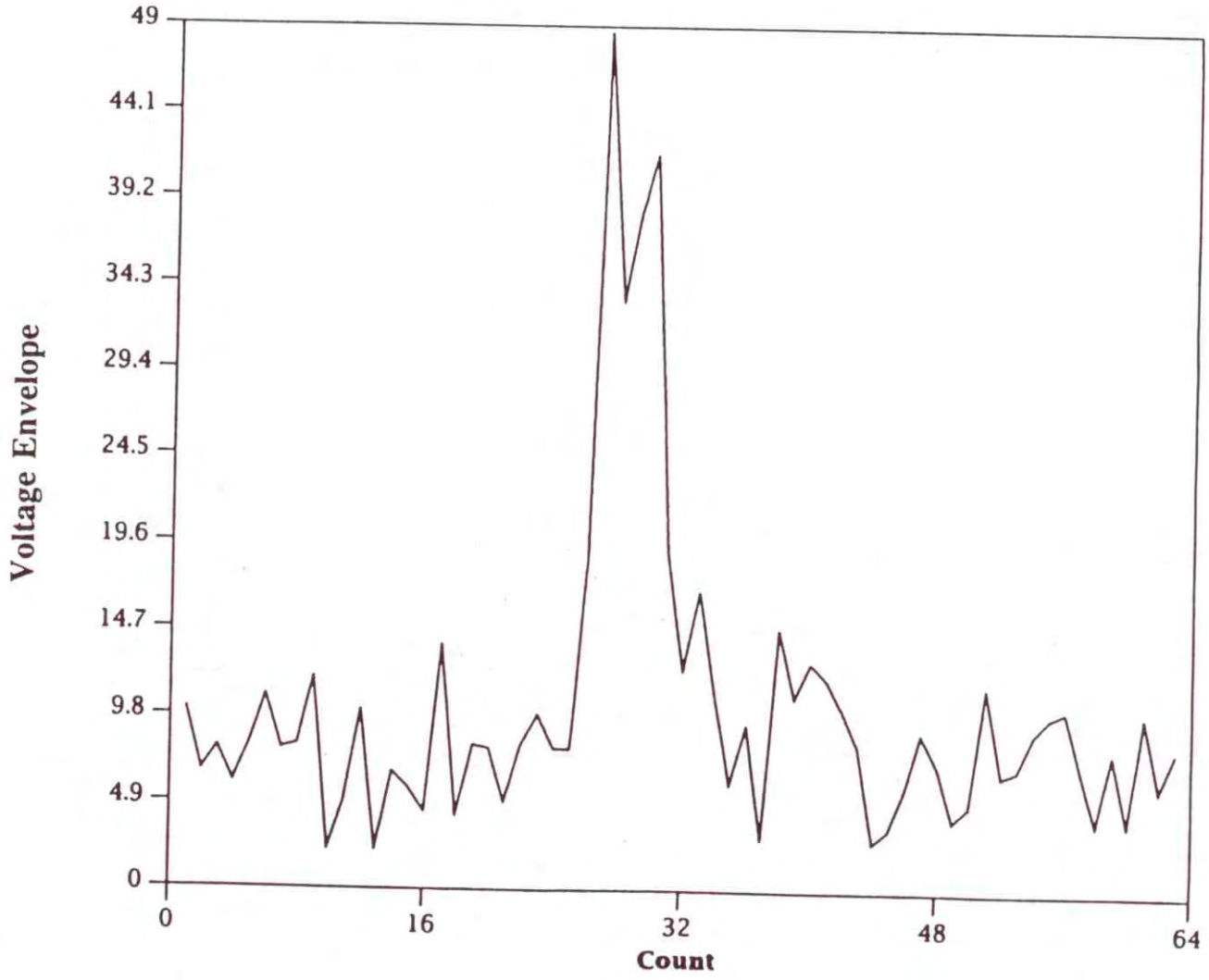

Figure 38. Voltage envelope of measured noise/interference on a scale from 0 to 64ms. (case study 5).

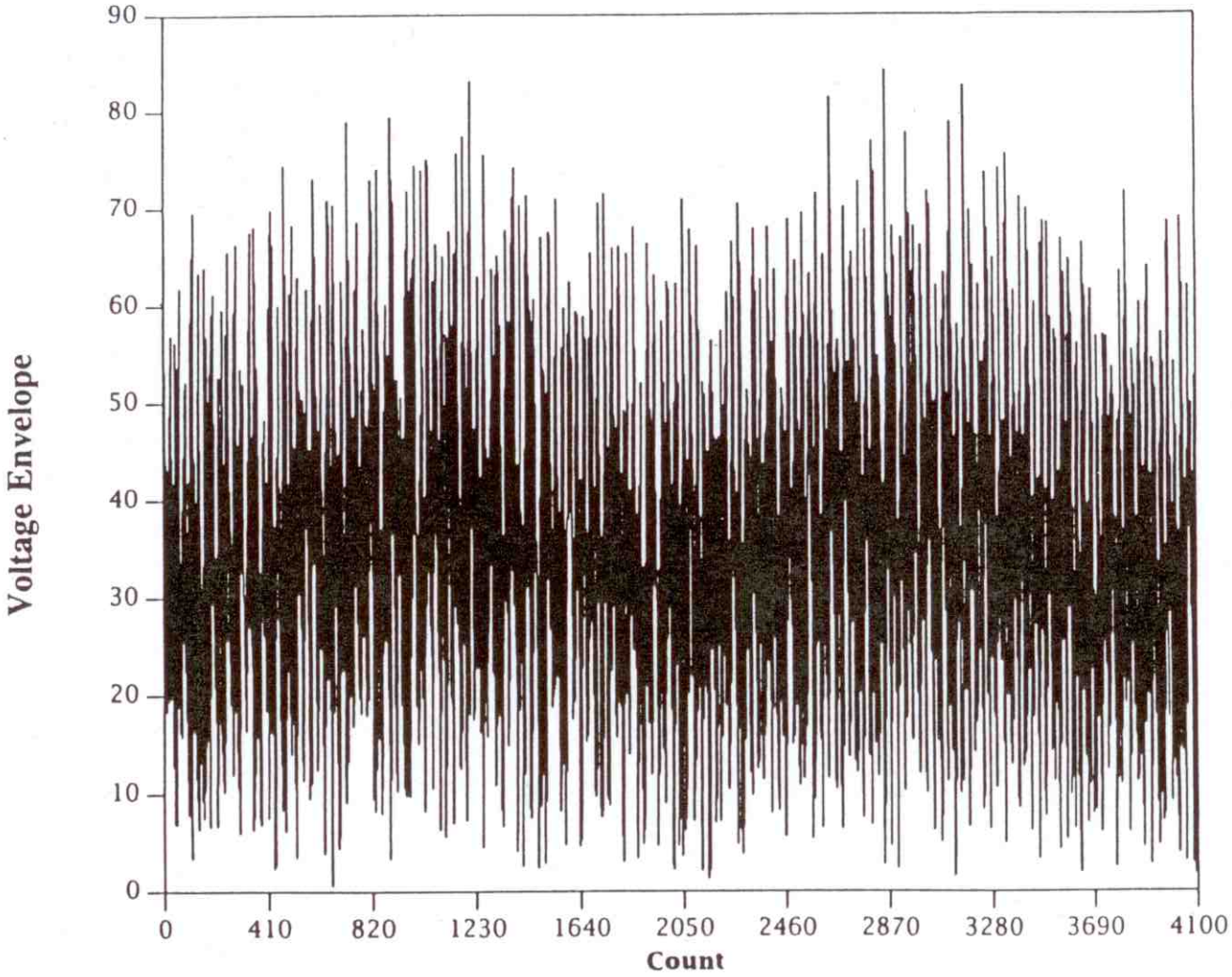

Figure 39. Voltage envelope of simulated noise/interference.

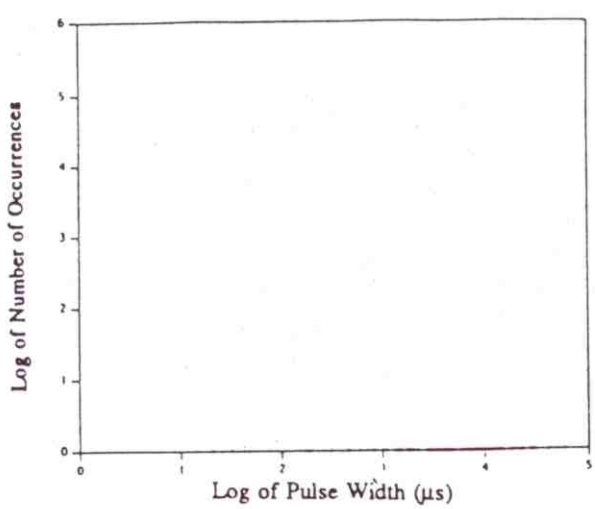

(a)

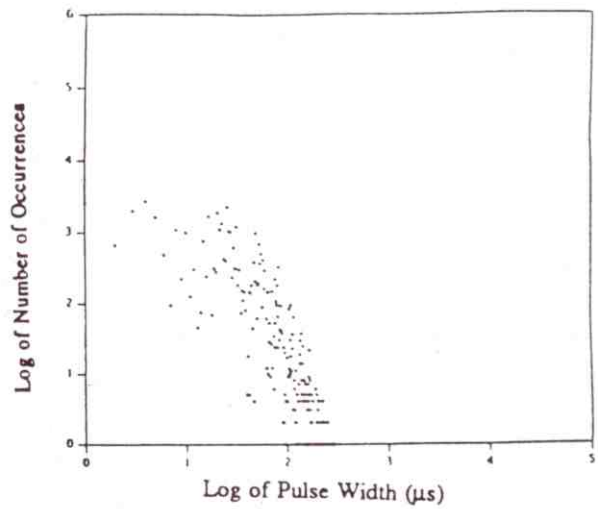

(b)

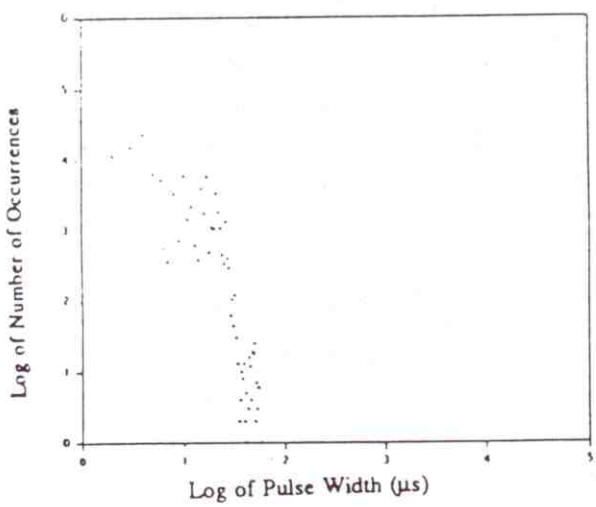

(c)

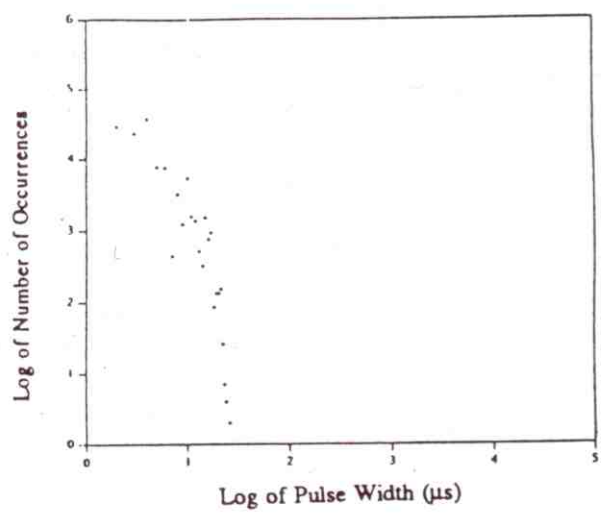

(d)

Figure 40. Pulse width distributions of simulated noise/interference at thresholds of (a) 0.5, (b) 10, (c) 20, (d) 30, (e) 40, (f) 50, (g) 70, and (h) 80.

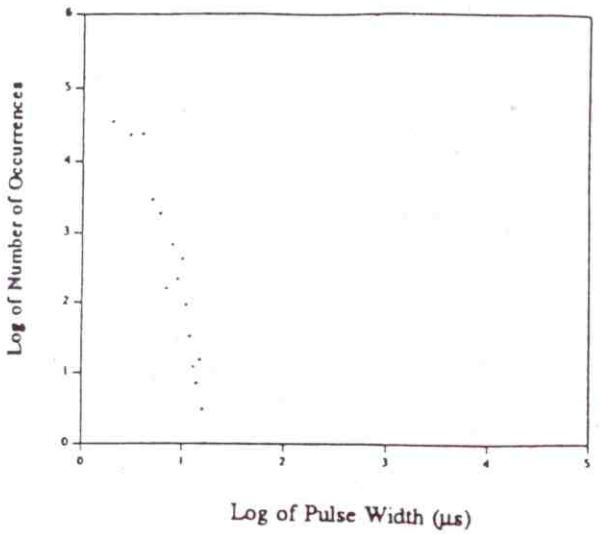

(e)

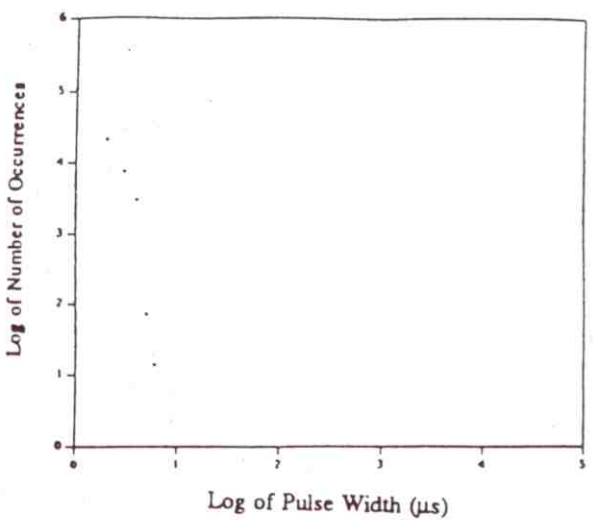

(f)

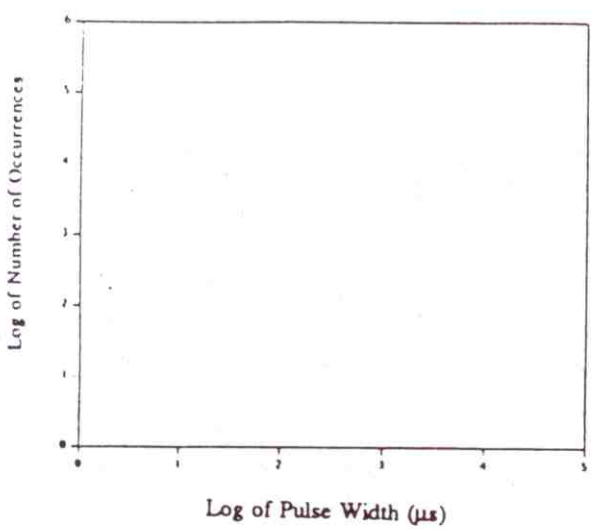

(g)

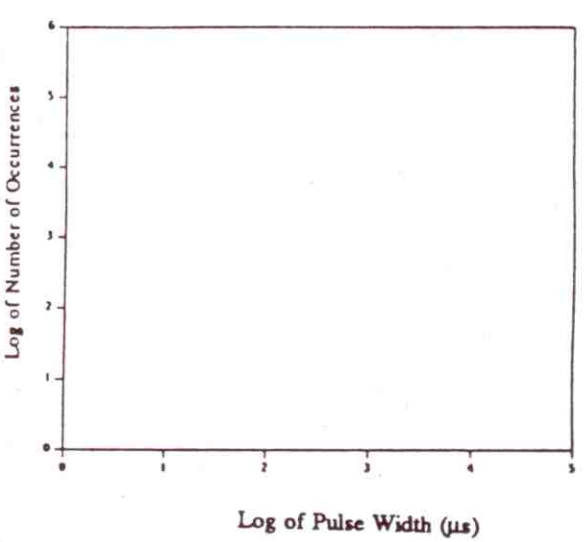

(h)

Figure 40 (cont.). Pulse width distributions of simulated noise/interference at thresholds of (a) 0.5, (b) 10, (c) 20, (d) 30, (e) 40, (f) 50, (g) 70, and (h) 80.

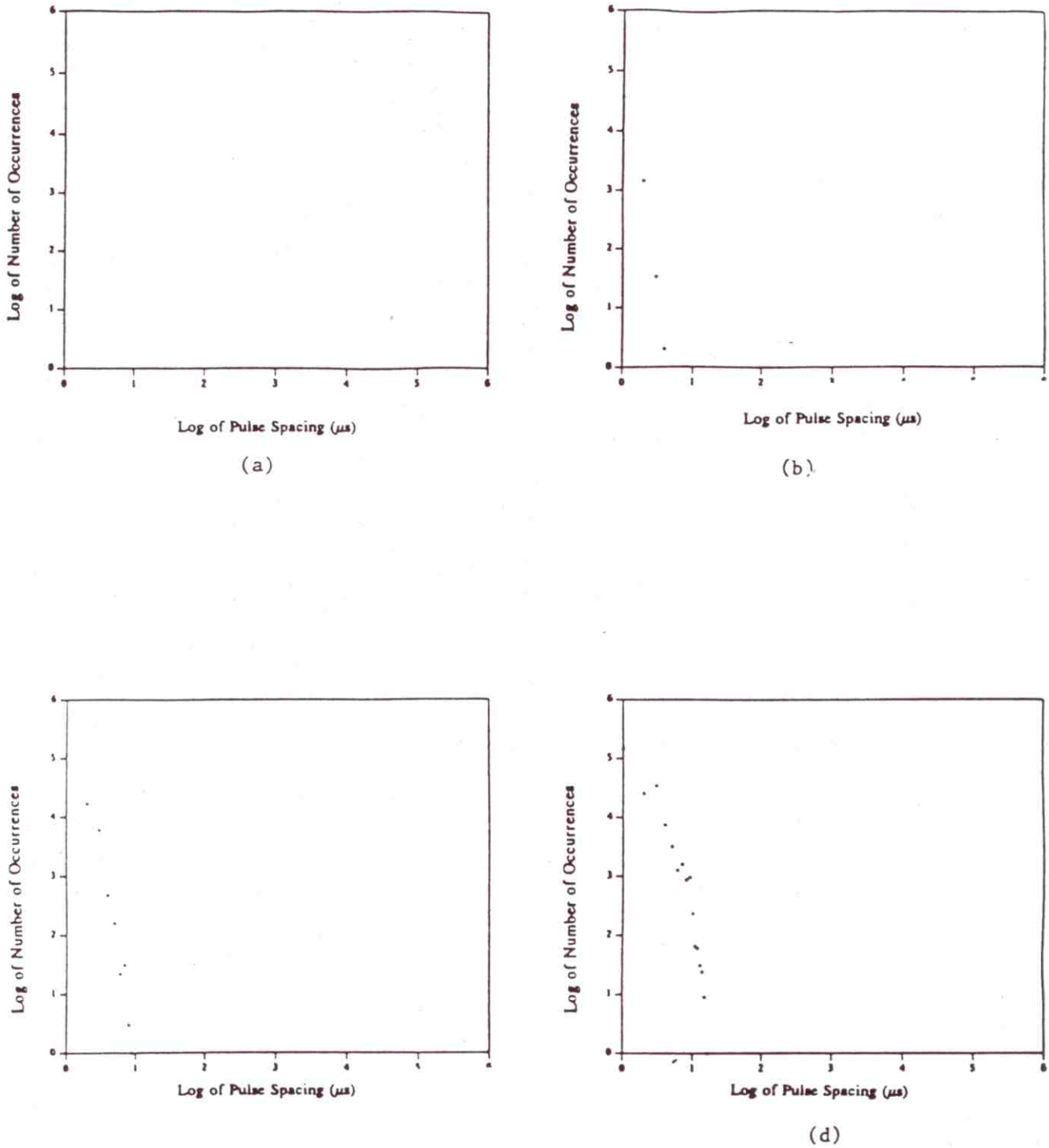

Figure 41. Pulse spacing distributions of simulated noise/interference at thresholds of (a) 0, (b) 10, (c) 20, (d) 30, (e) 40, (f) 50, (g) 70, and (h) 80.

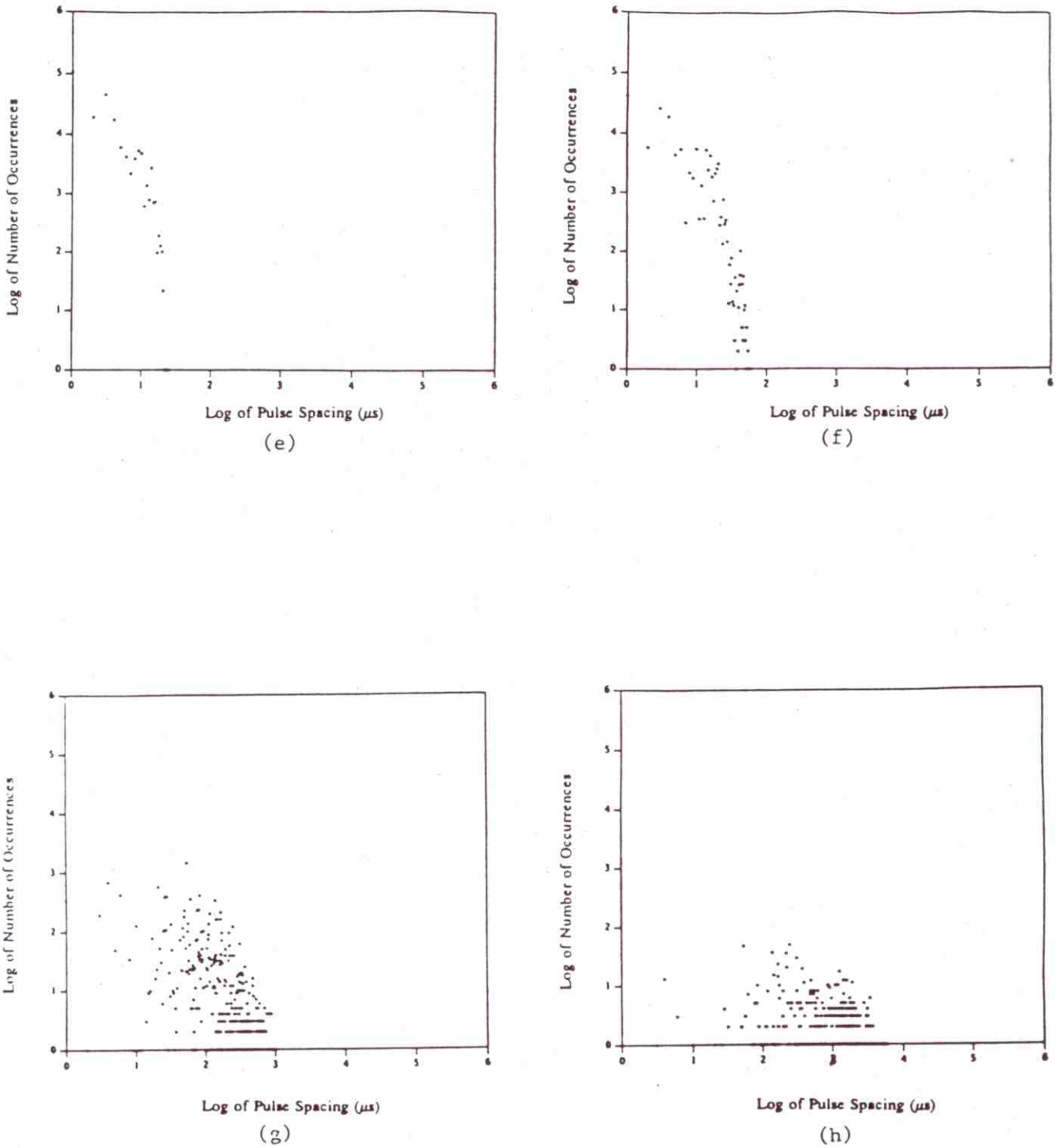

Figure 41 (cont.). Pulse spacing distributions of simulated noise/interference at thresholds of (a) 0, (b) 10, (c) 20, (d) 30, (e) 40, (f) 50, (g) 70, and (h) 80.

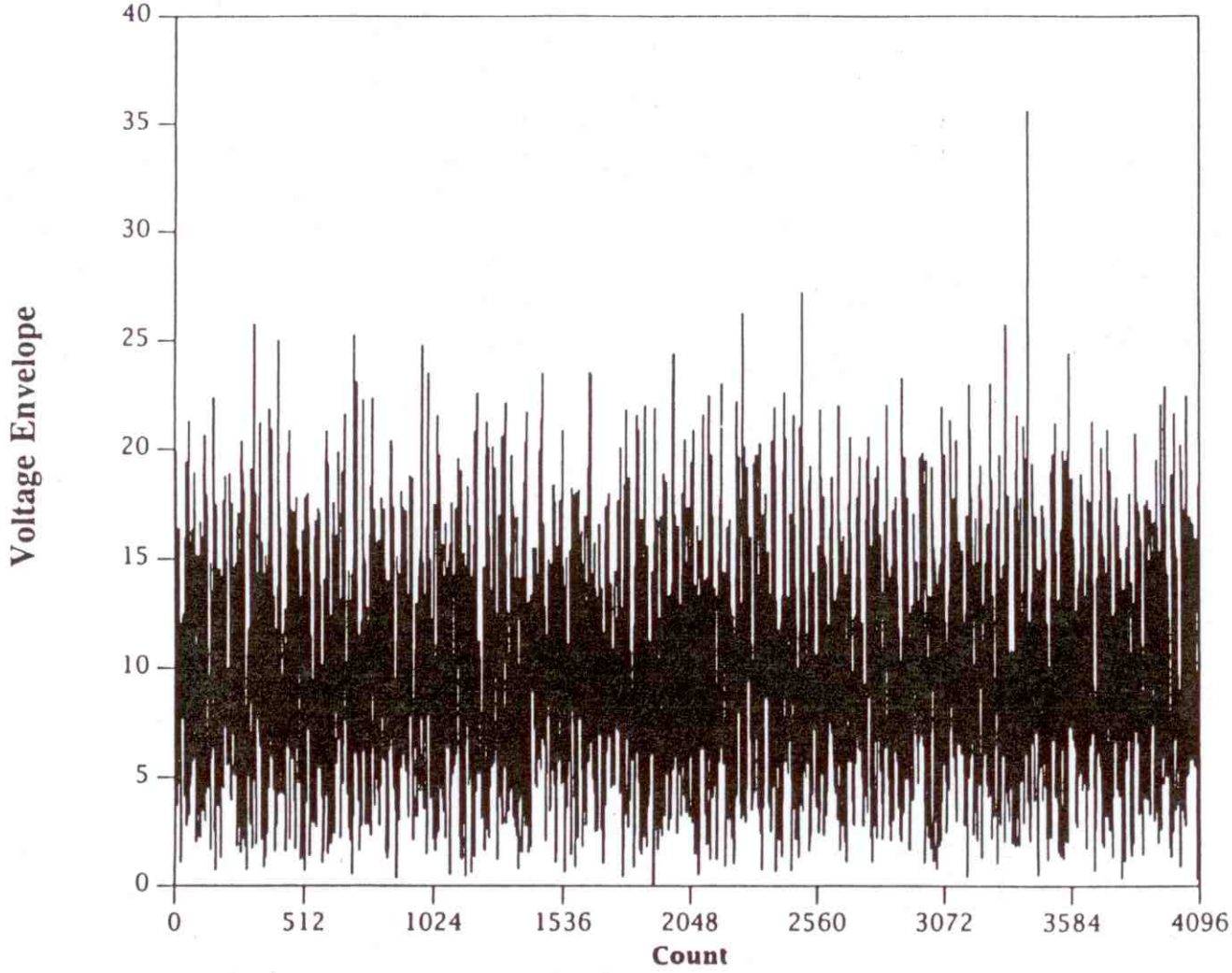

Figure 42. Voltage envelope of simulated noise/interference.

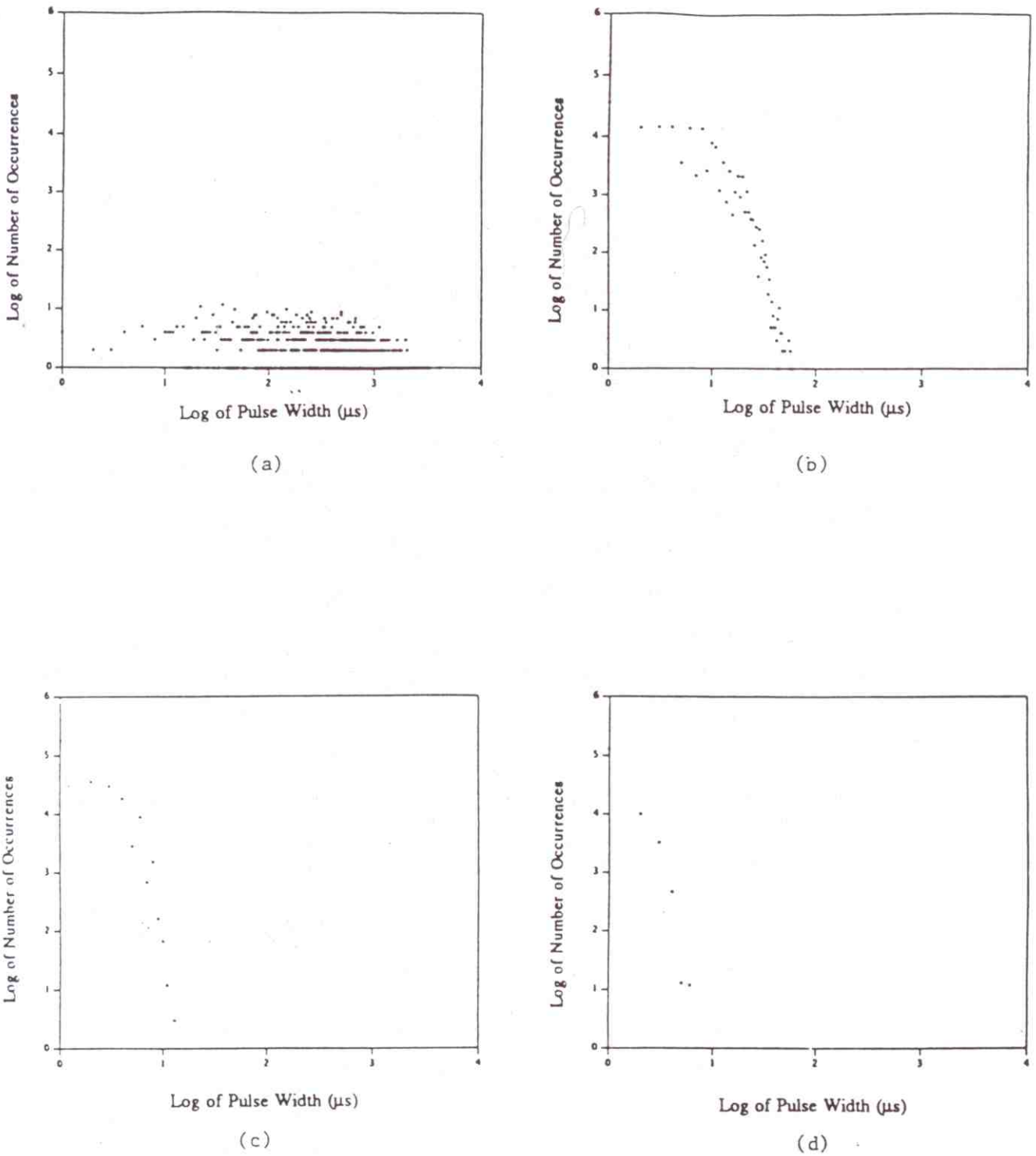

Figure 43. Pulse width distributions of simulated noise/interference at thresholds of (a) 0.5, (b) 5, (c) 10, (d) 15, (e) 20, (f) 25, (g) 30, and (h) 40.

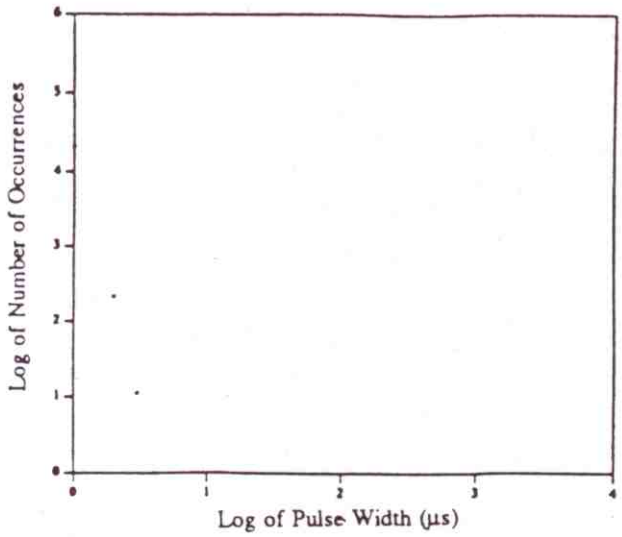

(e)

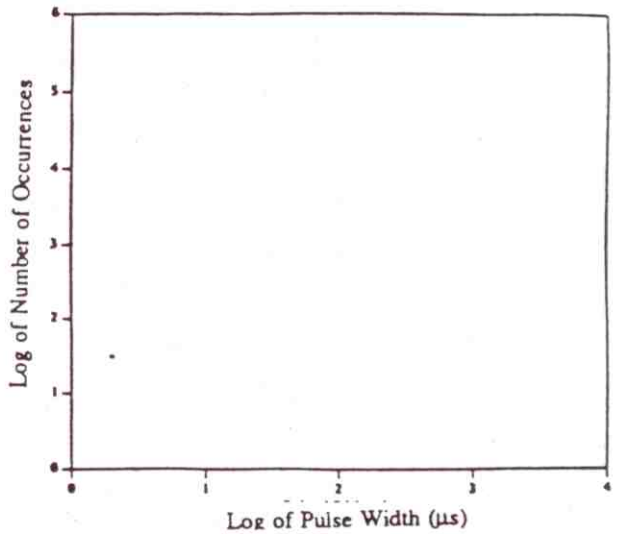

(f)

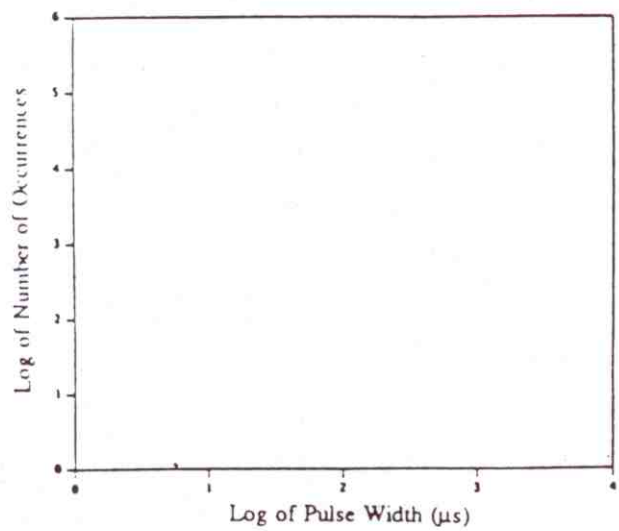

(g)

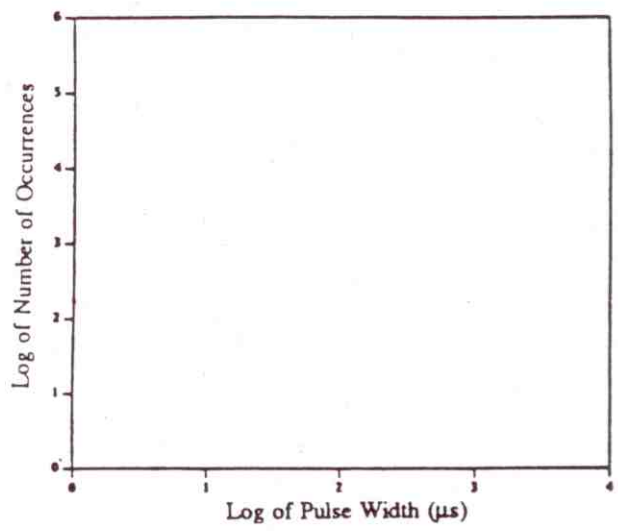

(h)

Figure 43 (cont.) Pulse width distributions of simulated noise/interference at thresholds of (a) 0.5, (b) 5, (c) 10, (d) 15, (e) 20, (f) 25, (g) 30, and (h) 40.

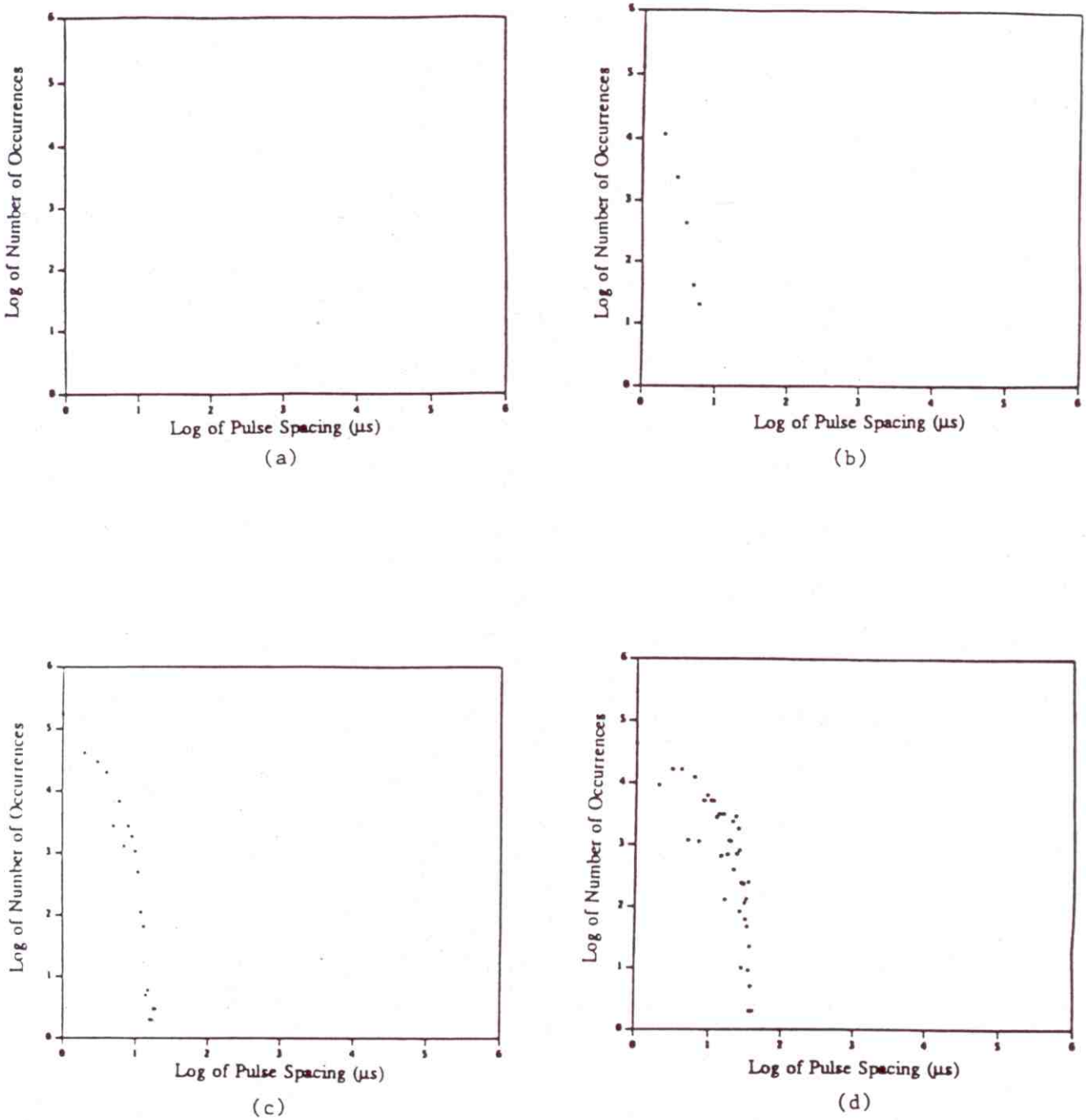

Figure 44. Pulse spacing distributions of simulated noise/interference at thresholds of (a) 0, (b) 5, (c) 10, (d) 15, (e) 20, (f) 25, (g) 30, and (h) 40.

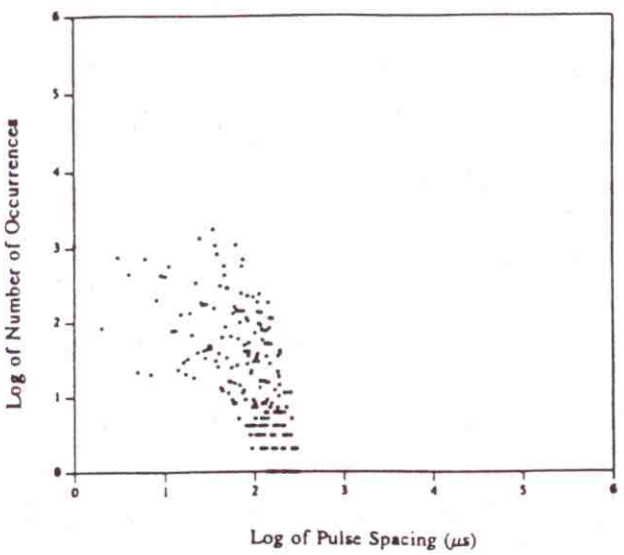

(e)

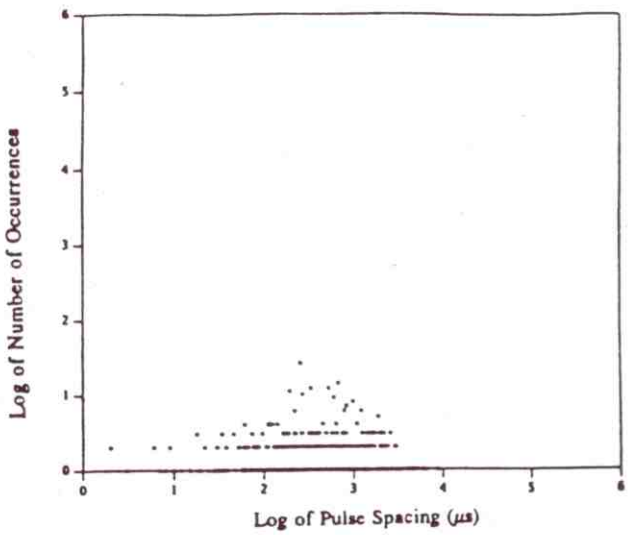

(f)

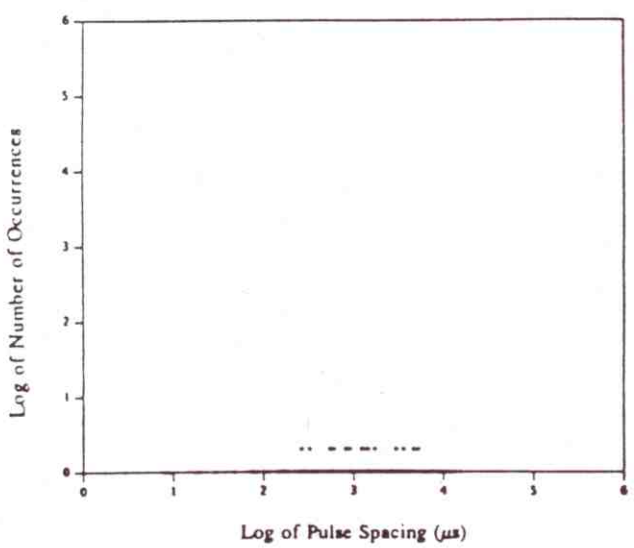

(g)

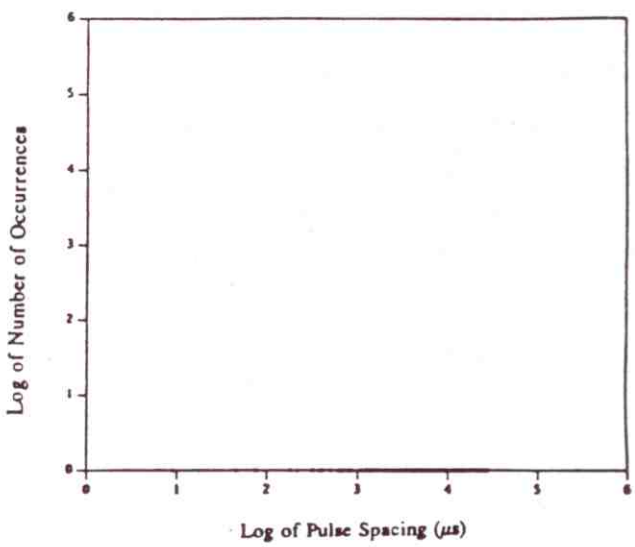

(h)

Figure 44 (cont.). Pulse spacing distributions of simulated noise/interference at thresholds of (a) 0, (b) 5, (c) 10, (d) 15, (e) 20, (f) 25, (g) 30, and (h) 40.

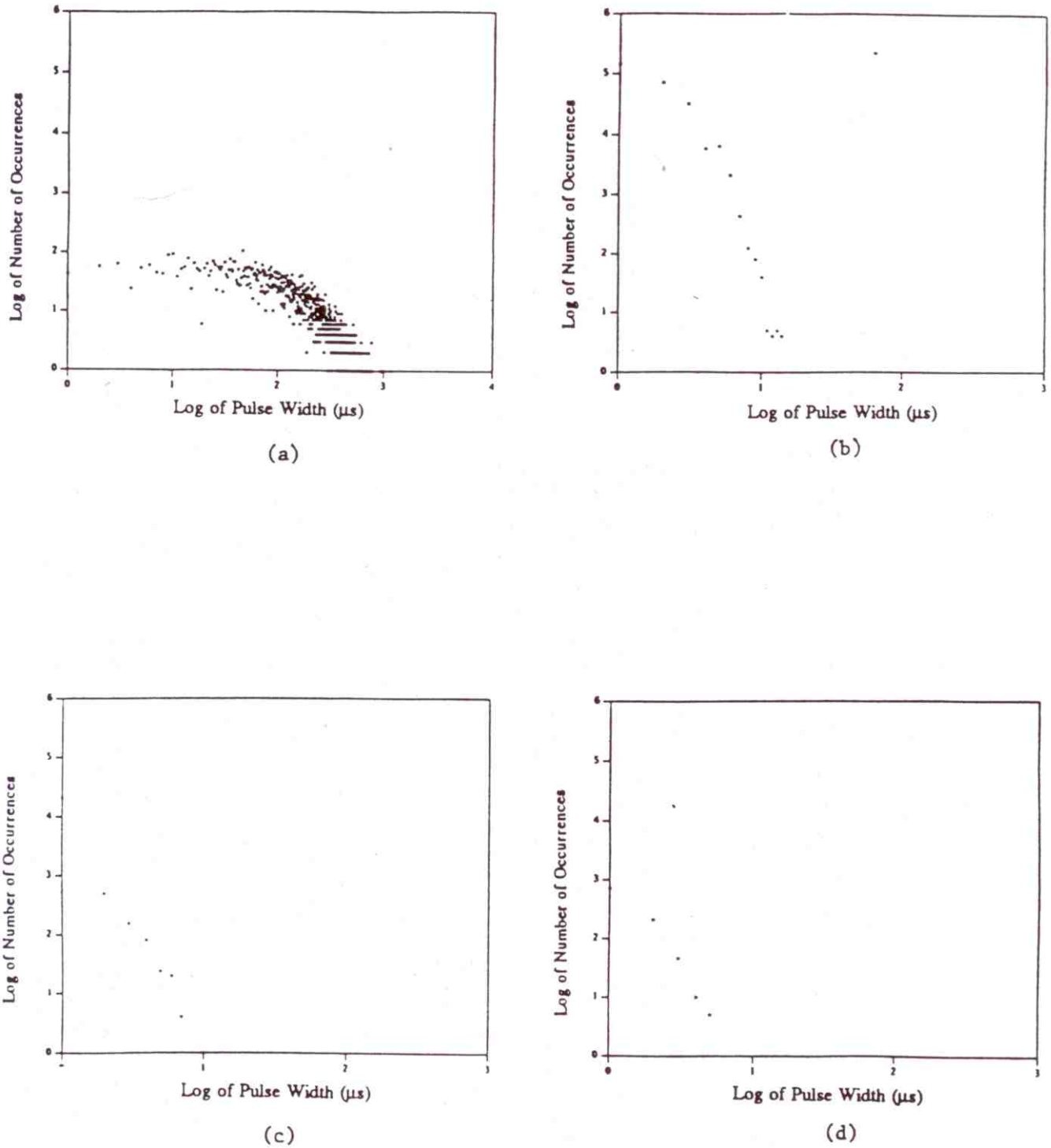

Figure 45. Pulse width distributions of simulated noise/interference at thresholds of (a) 0.5, (b) 5, (c) 10, (d) 15, (e) 20, (f) 25, (g) 30, and (h) 40.

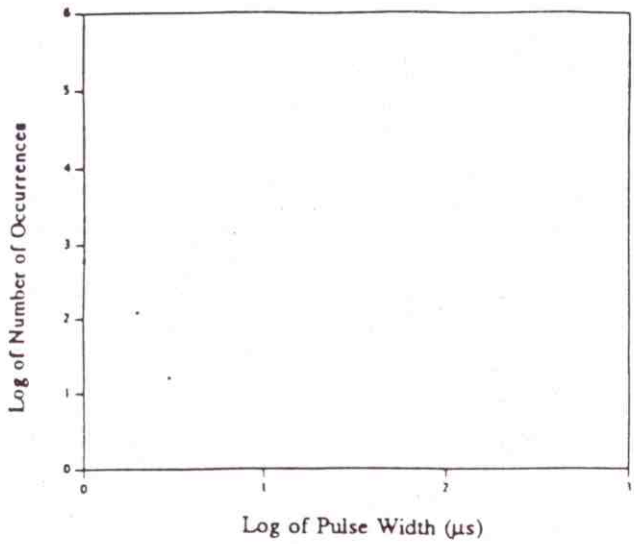

(e)

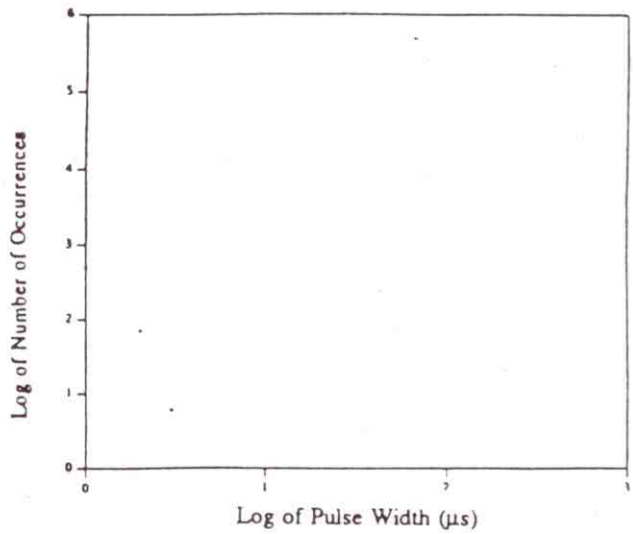

(f)

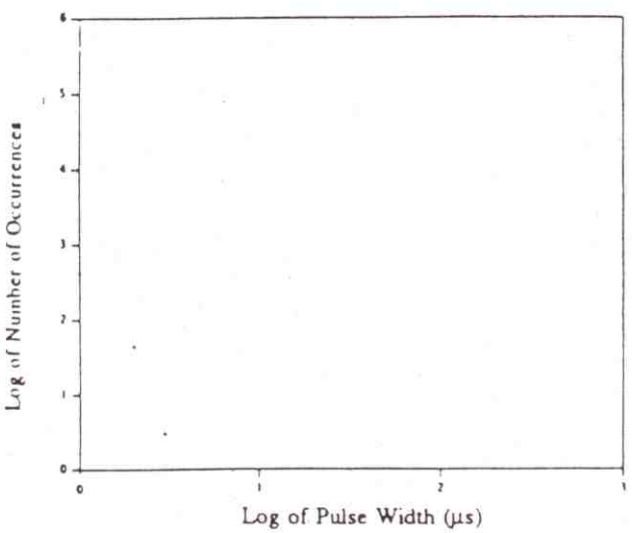

(g)

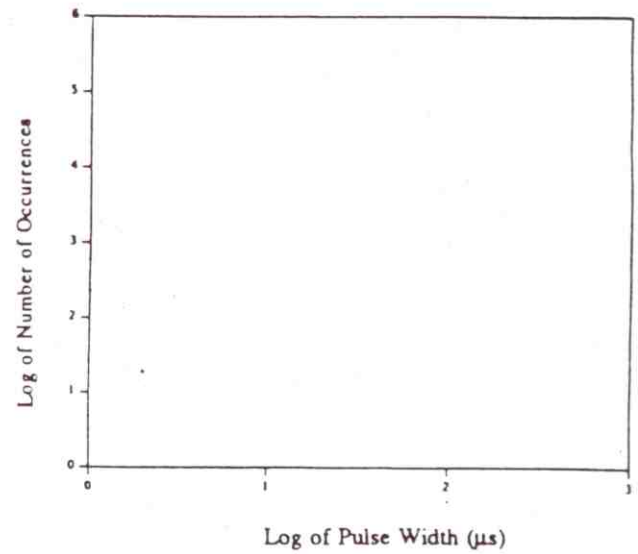

(h)

Figure 45 (cont.). Pulse width distributions of simulated noise/interference at thresholds of (a) 0.5, (b) 5, (c) 10, (d) 15, (e) 20, (f) 25, (g) 30, and (h) 40.

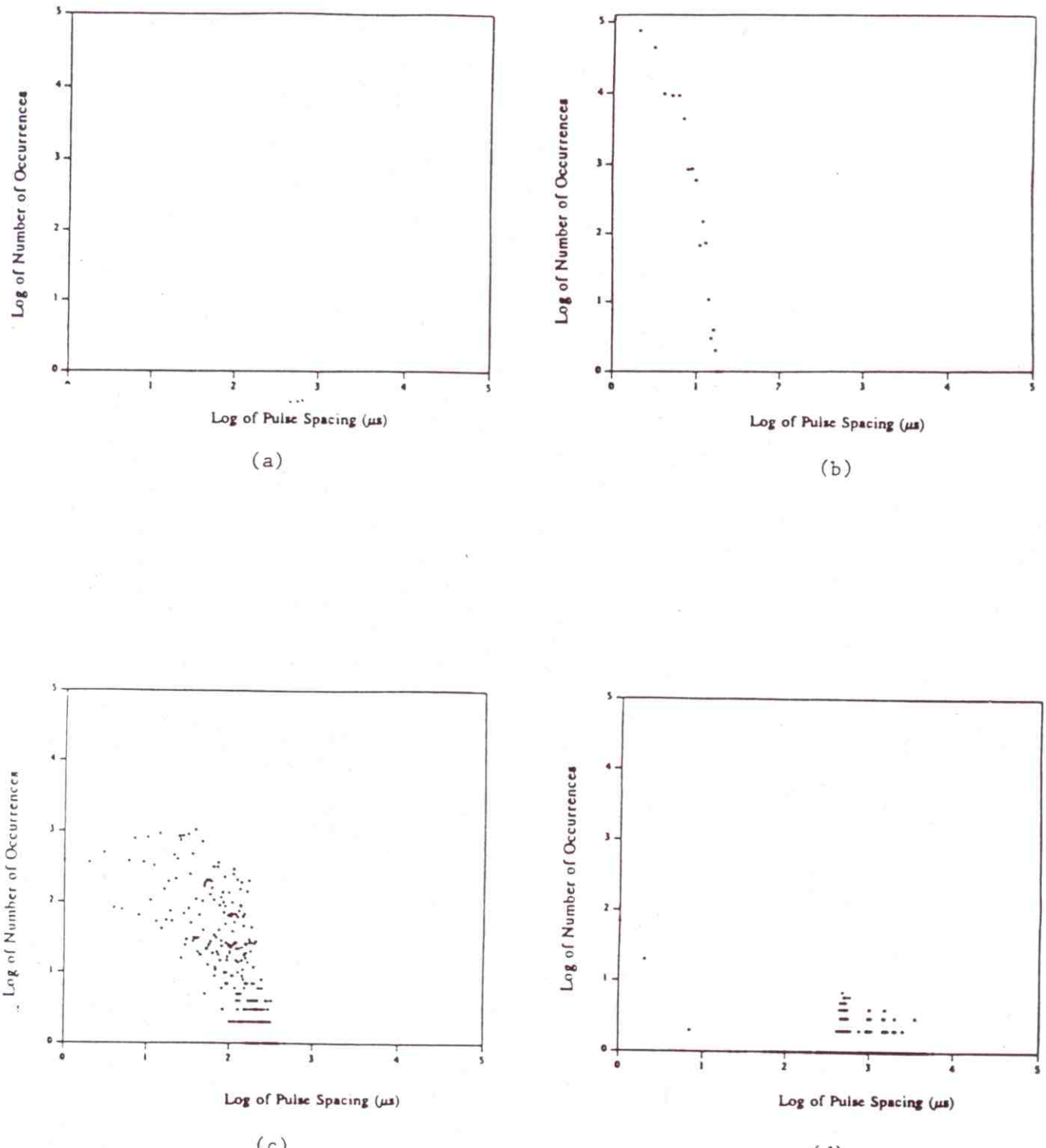

Figure 46. Pulse spacing distributions of simulated noise/interference at thresholds of (a) 0, (b) 5, (c) 10, (d) 15, (e) 20, (f) 25, (g) 30, and (h) 40.

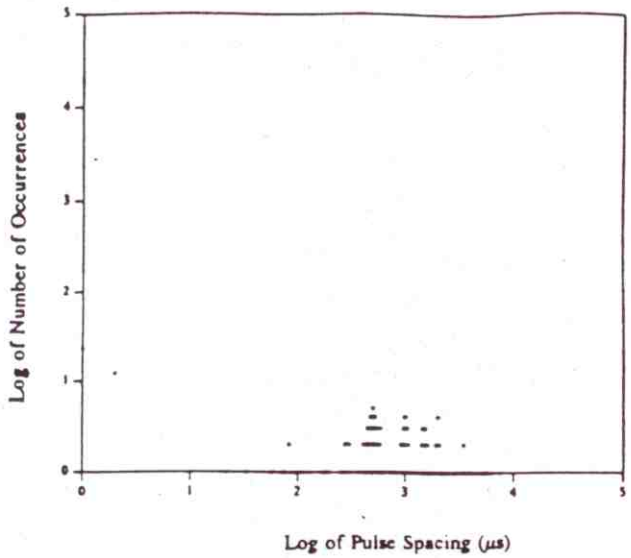

(e)

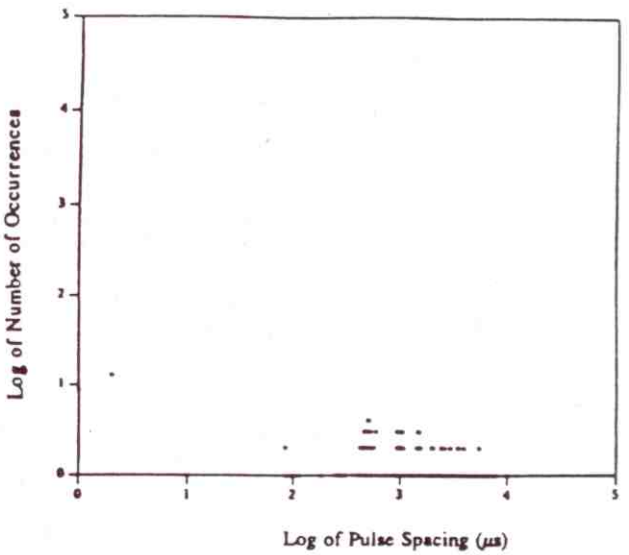

(f)

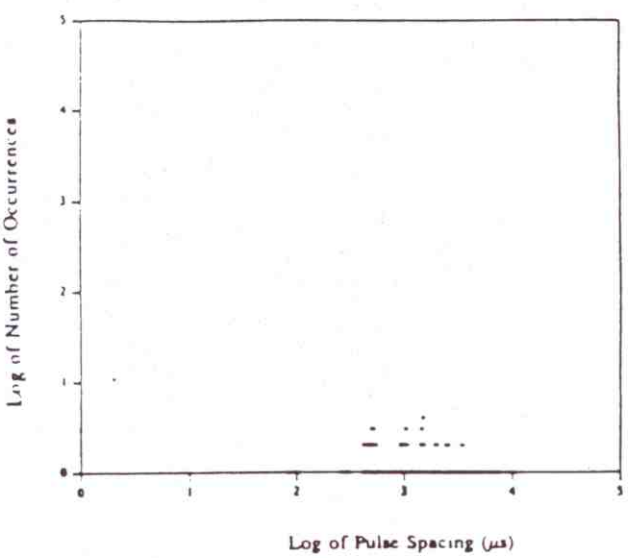

(g)

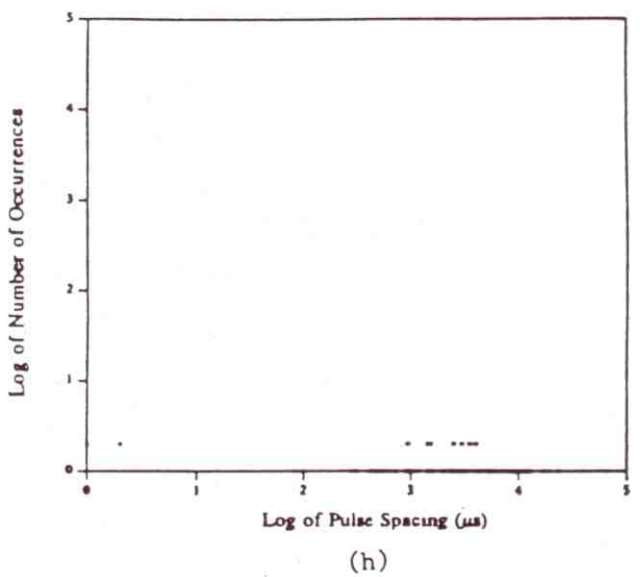

(h)

Figure 46 (cont.). Pulse spacing distributions of simulated noise/interference at thresholds of (a) 0, (b) 5, (c) 10, (d) 15, (e) 20, (f) 25, (g) 30, and (h) 40.

threshold one expects the pulse width distribution to have relatively few events, with those events occurring at relatively large widths. One also expects the pulse spacing distribution to have extremely few, if any, events, with such events occurring at the minimum spacing (1 μs).

As the threshold is gradually increased from zero, one expects to encounter upgoing and downgoing crossings more frequently, so that one expects the pulse width distribution to have relatively more events, with these events occurring at relatively smaller widths. Similarly, one expects the pulse spacing distribution to have numerous events (more than 0 or 1), with many of these events occurring at spacings greater than the minimum spacing (1 μs), because the probability that the envelope exceeds the threshold begins to decrease.

As the threshold is increased further and approaches the upper edge of the envelope, the probability that the envelope exceeds the threshold continues to decrease, and the number of envelope crossings is also decreasing. One therefore expects the pulse width distribution to have fewer events, with these events occurring at smaller widths. One also expects the pulse spacing distribution to have fewer events, with these events occurring at larger spacings.

Finally, to the extent that the upper and lower halves of the envelope are symmetric about the mean value of the envelope, one expects the pulse width and spacing distributions to exhibit complementary behavior in the following sense. Consider two values of the threshold which are symmetric about the mean value of the envelope; that is, the larger threshold exceeds the mean value of the envelope by the same amount that the smaller threshold is less than the mean value of the envelope. If the envelope is symmetric about its mean, one expects the distribution of upgoing crossings at the upper threshold to be identical to the distribution of downgoing crossings at the lower threshold, and vice versa. Thus, one expects the pulse spacing distribution at the upper threshold to be identical to the pulse width distribution at the lower threshold, and vice versa.

To varying degrees, all of these features are present in Figures 23 through 37. However, the pulse width and spacing distributions are especially helpful for modeling the impulsive noise in the fifth case study. For example, the pulse width distributions in Figure 36 at thresholds of 20 and 30 reveal numerous pulse widths between 2 and 10 μs, whereas the base width of the central lobe of an impulse filtered with a 400 kHz lowpass filter is 2.5 μs. A pulse width greater than 2.5 μs can be achieved either by passing an impulse through a filter with a bandpass less

of 2.5 μs, but whose times of arrival differ by less than 2.5 μs. However, the pulse spacing distributions in Figure 37 at thresholds of 20 and 30 reveal numerous pulse spacings on the order of or less than 10 μs, which is indicative of fine structure in the pulses, suggesting that the pulses consist of superpositions of individual impulses. That this is the case can be seen in Figure 38, which shows the voltage envelope for the fifth case study, plotted on an expanded scale between 0 and 64 μs. The pulse in the center of the plot consists of a superposition of two or more filtered impulses.

The pulse spacing distributions in Figure 37 at thresholds of 20 and 30 also exhibit bumps in the vicinity of 500 μs, which indicate that the pulses tend to occur periodically in time. However, the fact that the bumps have finite widths and are not delta functions indicates that the pulses are not precisely periodic, as discussed above. Thus, the level crossing distributions reveal both fine structure and time correlations associated with impulsive noise, which should be taken into account in the noise/interference model.

The level crossing distributions also indicate that the impulsive noise in the fifth case study is not atmospheric noise. Lightning flashes contain one or more strokes whose pulse widths are on the order of 100 microseconds, with spacings between strokes on the order of tens of milliseconds (Uman, 1987). On the other hand, the level crossing distributions for the fifth case study reveal pulse widths on the order of several microseconds and pulse spacings on the order of half a millisecond.

3.2 Comparisons of Model with Measurements

To investigate the level crossing properties of the noise/intterference model, simulations of one-second duration were performed, with and without impulsive noise. The noise/interference in the first simulation, to be compared with the first case study, consists of Gaussian noise and narrowband interferers, using the parameter values listed in Table 2. The first 4 ms of the voltage envelope are plotted in Figure 39, and the pulse width and pulse spacing distributions computed from the entire one-second record are shown in Figures 40 and 41, respectively.

The pulse width distribution at zero threshold has not been displayed in Figure 40 because there are no occurrences of pulse widths at this threshold; as explained above, the occurrence

of one or more events would require the I- and Q-channel voltages to simultaneously vanish at two or more sample times, which is extremely unlikely. On the other hand, the pulse width distributions of the measured data at zero threshold show numerous occurrences. This is because the data were obtained using A/D converters with a finite resolution (finite number of bits). Thus, values of the voltage envelope which are finite, but less than the resolution of the A/D converters, are recorded as zero. Therefore, to make a meaningful comparison between the measured and simulated distributions at small values of the threshold, the simulated distribution has been computed for a small, but finite (0.5) value of the threshold. Aside from this caveat, the general characteristics of the distributions computed from the measured data in the first case study (Figures 24 and 25) and the simulated data appear very similar to one another.

The noise/interference in the second simulation, to be compared with the fifth case study, consists of Gaussian noise, narrowband interferers, and impulsive noise using the parameter values listed in Table 3. The impulses are uniformly distributed in time; that is, 50 impulses are uniformly distributed in time within each 4 ms block of the simulation, resulting in a total of 12,500 impulses in the entire one-second simulation. The first 4 ms of the voltage envelope are plotted in Figure 42, and the pulse width and pulse spacing distributions computed from the entire one-second record are shown in Figures 43 and 44, respectively. At the lower values of the threshold (less than 20), the measured (Figures 36 and 37) and simulated distributions are qualitatively similar. However, at the higher thresholds the pulse widths of the simulated data are narrower than those of the measured data. The simulated pulse spacing distributions also fail to reproduce the features of the measured distributions. For example, at a threshold of 30 the simulated distribution does not have the pronounced tail that the measured distribution has at small pulse spacings, and the bump in the simulated distribution in the vicinity of 500-1000 μs is much broader than it is in the measured distribution. This is not unexpected, since no attempt was made to model the fine structure of the pulses by superimposing filtered impulses, and the impulses were not correlated in time, but were uniformly distributed in time (within each 4 ms block).

To rectify these deficiencies, noise/interference was simulated using the same parameter values that were used in the previous example, but with the impulses correlated in time using the following procedure. First, the impulses are distributed only within windows of 4 μs duration.

The window that each impulse is placed within is chosen randomly from the total set of windows, and within each window the distribution of arrival times is uniform. Second, the spacing between the centers of the windows is a random variable uniformly distributed between 450 μs and 550 μs. Thus, the impulses occur in bursts which exhibit fine structure (with an average of 6.25 impulses per burst), and the arrival times of the bursts are approximately (but not precisely) periodic. As in the previous simulation, 50 impulses are distributed within each 4 ms block, resulting in a total of 12,500 impulses in the entire one-second simulation.

The resulting pulse width and pulse spacing distributions are shown in Figures 45 and 46, respectively. The distributions in Figure 45 indicate that, relative to the previous example, the pulse widths at high thresholds have been broadened (due to the superposition of filtered impulses within the bursts). Also, the pulse spacing distributions at high thresholds in Figure 46 have a tail at small values of pulse spacing (due to the fine structure within the bursts), and the bump in the vicinity of 500-1000 μs is narrower than in the previous example (due to the time correlations of the bursts). Although the simulated distributions typically have fewer occurrences associated with these features than do the measured distributions, these differences in the number of occurrences could be removed by simulating the impulsive noise with a greater number of impulses. One could also envisage a more sophisticated modeling of the arrival time distribution of the impulses to more accurately reproduce the shapes of these features. However, the examples demonstrate that the qualitative features in the measured distributions that cannot be simulated using uniformly distributed times of arrival of the impulses can be simulated by appropriately distributing the impulses in time.

4. SUMMARY AND CONCLUSIONS

A simple model of wideband HF noise/interference has been developed, based on analyses of measured data. In contrast to previously developed models, which provide descriptions of the statistical characteristics of the noise/interference (for example, the amplitude probability distribution), the present model describes the noise/interference waveform itself, and can therefore be used to simulate the noise/interference process. The statistical characteristics of the process have been investigated to guide the model development and to check the validity of the model.

In Part I of this series, the first-order statistics of the noise/interference were examined, and it was shown that the quantities generated from the simulated data closely resemble the corresponding measured quantities for a variety of measured data. Thus, the time-averaged behavior of the amplitude and phase of the simulated noise/interference was shown to be consistent with that of the measured data.

In the present report, certain higher-order statistics of the noise/interference have been analyzed. These analyses are necessary to investigate the relationships between the noise/interference process at different instants in time. In particular, the autocorrelation function and the pulse width and spacing distributions of the voltage envelope have been investigated.

An analytic expression for the autocorrelation function of the simulated noise/interference was derived, and, using this expression for guidance, it was shown that the wide variety of autocorrelation functions of the measured data can be simulated using the proposed model with appropriate choices for the amplitudes and frequencies of the dominant narrowband interferers. However, the nonstationarity of the noise/interference, which is evident in some of the measured data, has not yet been incorporated into the model.

Pulse width and pulse spacing distributions were computed for both measured and simulated noise/interference, and it was shown that, in the absence of impulsive noise, the measured and simulated distributions are qualitatively similar. However, it was found that, in the presence of impulsive noise, the model as previously formulated (with a uniform distribution for the times of arrival of the impulses) does not generate all the observed features in the measured distributions. Accordingly, the model was refined by developing a "bursty" distribution for the times of arrival of the impulses, whereby the impulses are correlated in time. It was

shown that the refined model does indeed generate features in the distributions that are similar to those in the measured distributions.

The comparisons of measured and simulated statistical quantities in this work (as well as in Part I) are of a qualitative nature. Quantitative comparisons are difficult because one is dealing with an infinite variety of waveforms generated by random processes. Ultimately, the validity of any model for the simulation of noise/interference can only be established by quantitative comparisons of radio performance using simulated and measured waveforms.

Conspicuously absent from the model development is the incorporation of a waveform for wideband HF atmospheric noise. The development of such a waveform requires the analysis of additional data containing atmospheric noise. However, the fact that the impulsive noise investigated thus far can be modeled as a train of filtered impulses using an appropriate time of arrival distribution suggests that atmospheric noise, as well as other manmade impulsive noise, can also be modeled as a train of filtered impulses, appropriately distributed in time. The pulse width and spacing distributions should enable one to model the distributions of times of arrival in a manner analogous to the modeling of the impulsive noise discussed in the present work. These investigations are currently under way and will be reported elsewhere.

5. ACKNOWLEDGMENTS

The authors wish to thank Mr. Marc N. Richard of the Mitre Corporation for providing noise/interference data collected with the Mitre WBHF test facility. The authors also thank Messrs. J. McEvoy and W. Bonser of the U.S. Air Force Rome Laboratory, Messrs. D. Bodson and G. Rekstad of the National Communications System, and LTC Robert Oldham of the U.S. Army Communications/Electronics Command for their funding support of the work reported herein.

6. REFERENCES

Abraham, L.G., M.I. Clune, D.C. Rogers, and B.G. Thornton (1989), Stationarity of wideband HF noise after interference excision, IEEE 1989 Military Commun. Conf., Boston, MA, Paper No. 48.3.

CCIR (1974), HF ionospheric channel simulators, XIIIth Plenary Assembly, ITU, Geneva, Switzerland, Vol. III, Report 549, pp. 66-72.

Cox, D.R. and H.D. Miller (1965), The Theory of Stochastic Processes (Chapman and Hall, New York, NY).

Ehrman, L., L.B. Bates, J.F. Eschle, and J.M. Kates (1982), Real-time software simulation of the HF radio channel, IEEE Trans. Commun. Com-30, No. 8, pp. 1809-1817, Aug.

Girault, R., J. Thibault, and B. Durand (1988), Software ionospheric channel simulator, IEE Fourth Intl. Conf. on HF Radio Systems and Techniques, London, UK, IEE Pub. 284, pp. 321-325.

Hall, H.M. (1966), A new model of "impulsive" phenomena: application to atmospheric noise communications channels, Electron. Lab., Stanford Univ., Stanford, CA, Tech. Rep. 3412-8 and 7050-7, SU-SEL-66-052, Aug.

Hoffmeyer, J.A. and L.E. Vogler (1987), Measurement, modeling, and simulation of LOS microwave channels, NATO AGARD Conf. Proc., No. 419, Scattering and Propagation in Random Media, Rome, Italy, May, Paper No. 31.

Hoffmeyer, J.A. and L.E. Vogler (1990), A new approach to HF channel modeling and simulation, IEEE 1990 Military Commun. Conf., Monterey, CA, Paper No. 60.2.

Hoffmeyer, J.A., L.E. Vogler, J.F. Mastrangelo, L.E. Pratt, and C.J. Behm (1991), A new HF channel model and its implementation in a real-time simulator, IEE Fifth Intl. Conf. on HF Radio Systems and Techniques, Edinburgh, UK, IEE Pub. 339, pp. 173-177.

Lemmon, J.J. and C.J. Behm (1991), Wideband HF noise/interference modeling, Part I: First-order statistics, NTIA Report 91-277, May (NTIS Order No PB 91-208454).

Le Roux, Y.M., G. Savidan, G. DuChaffaut, P. Gourvez, and J.P. Jolivet (1987), A combined evaluation and simulation system of the HF channel, IEE Fifth Intl. Conf. on Ant. and Prop., York, UK, IEE Pub. 274, pp. 171-175.

Longuet-Higgins, M.S. (1962), The distribution of intervals between zeros of a stationary random function, Phil. Trans. Roy. Soc., London, 254, p. 557.

Mastrangelo, J., J. Hoffmeyer, C. Behm, and L. Pratt (1991), A new wideband HF simulation system for testing HF radios, IEEE 1991 Military Commun. Conf., McLean, VA, Paper No. 49.5.

McFadden, J.A. (1956), The axis crossing intervals of random functions, IRE Trans. Information Theory, IT-2, pp. 146-150.

McRae, D.D. and F.A. Perkins (1988), Digital HF modem performance measurements using HF link simulators, IEE Fourth Intl. Conf. on HF Radio Systems and Techniques, London, UK, IEE Pub. 284, pp. 314-317.

Mooney, O.J. (1985), Implementation of an HF ionospheric channel simulator using a digital signal processor, IEE Third Intl. Conf. on HF Commun. Systems and Techniques, London, UK, pp. 27-31.

Perry, B.D. and R. Rifkin (1989), Measured wideband HF mid-latitude channel characteristics, IEEE 1989 Military Commun. Conf., Boston, MA, Paper No. 48.1.

Rice, S.O. (1944 and 1945), Mathematical analysis of random noise, Bell System Tech. J., 23, pp. 282-332, July 1944; 24, pp. 46-156, January 1945.

Uman, M.A. (1987), The Lightning Discharge (Academic Press, Orlando, FL).

Vogler, L.E. and J.A. Hoffmeyer (1988), A new approach to HF channel modeling and simulation, Part I: Deterministic model, NTIA Report 88-240, Dec. (NTIS Order No. PB 89-203962/AS).

Vogler, L.E. and J.A. Hoffmeyer (1990), A new approach to HF channel modeling and simulation, Part II: Stochastic model, NTIA Report 90-255, Feb. (NTIS Order No. PB 90-200338/AS).

Vogler, L.E., J.A. Hoffmeyer, J.J. Lemmon, and M. Nesenbergs (1988), Progress and remaining issues in the development of a wideband HF channel model and simulator, NATO AGARD Conf. Proc., Propagation Effects and Circuit Performance of Modern Military Radio Systems with Particular Emphasis on those Employing Bandspreading, Paris, France, Oct., Paper No. 6.

Watterson, C.C. (1981), HF channel-simulator measurements on the KY-870/P FSK burst-communication modem - set 1, NTIA Contractor Report CR-81-13 (NTIS Order No. PB 82-118944).

Watterson, C.C. (1982), HF channel-simulator measurements on the KY-879/P FSK burst-communication modem - set 2, NTIA Contractor Report CR-82-20, Dec. (NTIS Order No. PB 83-194738).

Watterson, C.C. and R.M. Coon (1969), Recommended specifications for ionospheric noise simulators, ESSA Tech. Report ERL-127-ITS-89.

Watterson, C.C., J.R. Juroshek, and W.D. Bensema (1969), Experimental verification of an ionospheric channel model, ESSA Tech. Report ERL-112-ITS-80.

Watterson, C.C., J.R. Juroshek, and W.D. Bensema (1970), Experimental confirmation of an HF channel model, IEEE Trans. Commun. Technol. COM-18, pp. 792-803.

APPENDIX

Table 1 displays the measurement parameters that were used to obtain the noise/interference records discussed in this report. Listed are the times, dates, center frequencies, and values of the variable attenuation that were used to record these data. Each record is identified by a record number. The following plots display the power (I^2+Q^2) versus time for each of the records. Each plot shows the power averaged over 1,024 consecutive samples (i.e., over 1 ms) and plotted (in dB) versus time for the entire one-second record.

Table A-1. Measurement Characteristics of Wideband HF Noise/Interference Records

Record Number	Date (1989)	Time (UT)	Center Frequency (MHz)	Variable Attenuation (dB)
1	15 March	04:01:22	9.244	24
2	15 March	05:50:42	7.844	21
3	15 March	06:22:00	10.662	16
4	15 March	07:48:05	7.844	29
5	15 March	09:46:34	5.936	22
6	15 March	11:57:02	7.844	21
7	15 March	15:15:59	19.29	6
8	15 March	19:22:32	23.862	6
9	15 March	20:06:49	15.848	26
10	22 March	22:21:16	19.29	27
11	15 March	22:34:52	19.29	6
12	10 March	00:29:22	19.29	6
13	10 March	00:39:19	18.718	24
14	17 March	00:57:51	15.848	29
15	17 March	03:20:34	10.662	11
16	10 March	03:41:19	13.666	12
17	10 March	03:48:17	13.666	18
18	17 March	04:45:19	9.244	28

Table A-1. (Cont.)

Record Number	Date (1989)	Time (UT)	Center Frequency (MHz)	Variable Attenuation (dB)
19	10 March	06:25:57	10.662	18
20	10 March	06:32:43	9.244	30
21	17 March	07:08:11	10.662	11
22	17 March	08:47:51	5.936	21
23	10 March	09:51:21	7.844	31
24	10 March	09:58:11	5.936	27
25	10 March	17:37:32	23.862	6
26	27 March	23:37:48	19.29	12
27	28 March	02:05:34	15.848	25
28	28 March	03:27:56	13.666	25
29	28 March	05:59:35	15.848	6
30	28 March	08:13:01	15.848	29
31	28 March	10:26:48	13.666	20
32	28 March	12:07:27	18.718	17
33	28 March	19:04:31	19.29	16
34	28 March	22:10:40	19.29	17
35	28 March	23:39:48	15.848	26
36	29 March	02:31:34	13.666	27
37	29 March	03:28:33	10.662	27
38	29 March	14:53:31	25.885	6
39	29 March	16:27:07	23.862	6
40	29 March	18:51:19	25.885	6
41	29 March	20:37:32	19.29	16
42	29 March	20:45:25	19.29	16

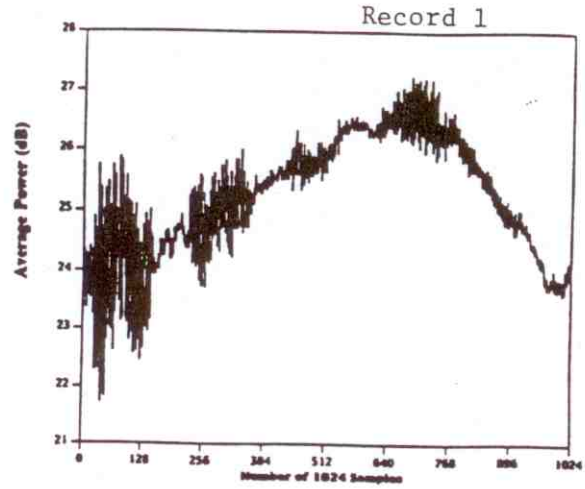
Record 1
Average Power (dB)
Number of 1024 Samples

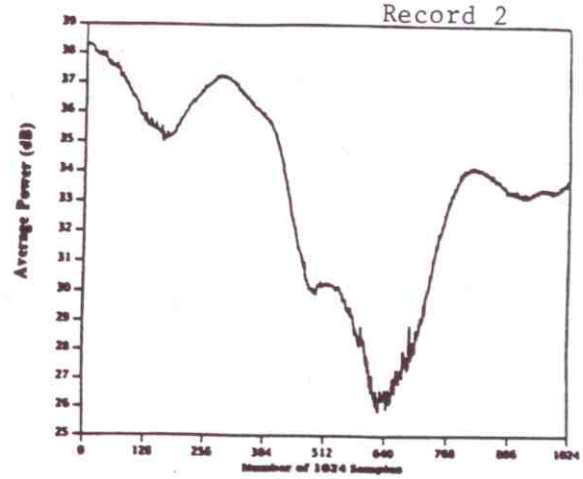
Record 2
Average Power (dB)
Number of 1024 Samples

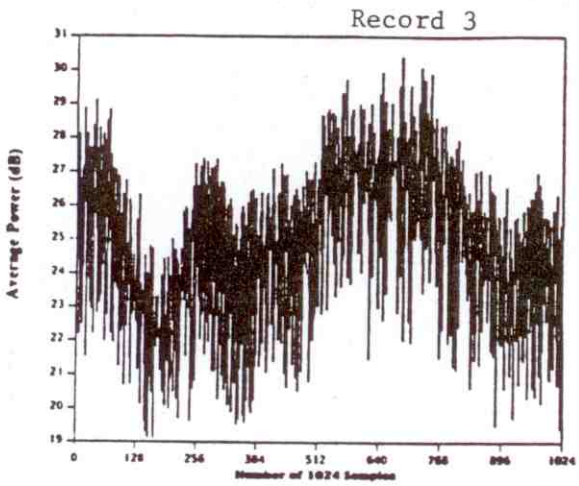
Record 3
Average Power (dB)
Number of 1024 Samples

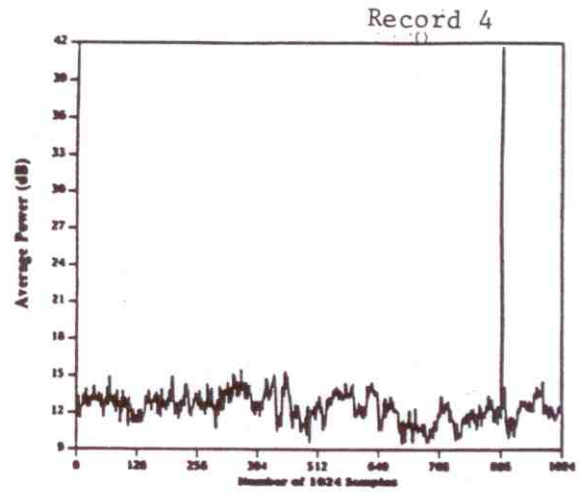
Record 4
Average Power (dB)
Number of 1024 Samples

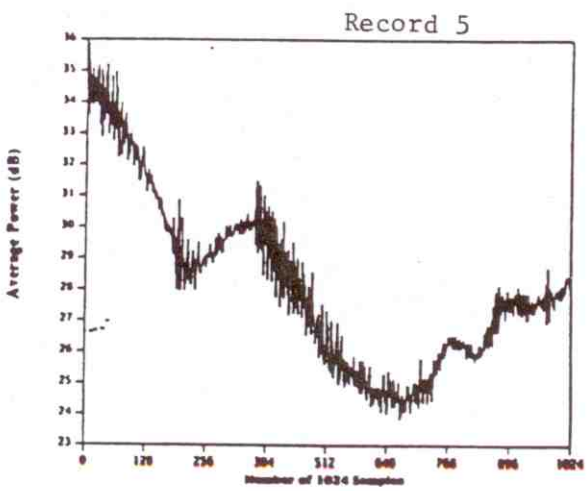
Record 5
Average Power (dB)
Number of 1024 Samples

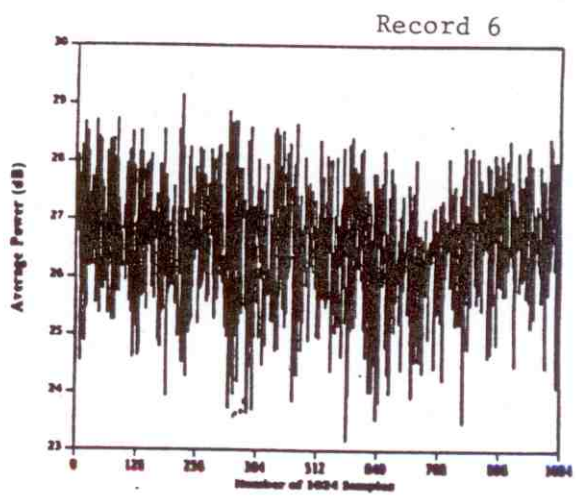
Record 6
Average Power (dB)
Number of 1024 Samples

Record 7

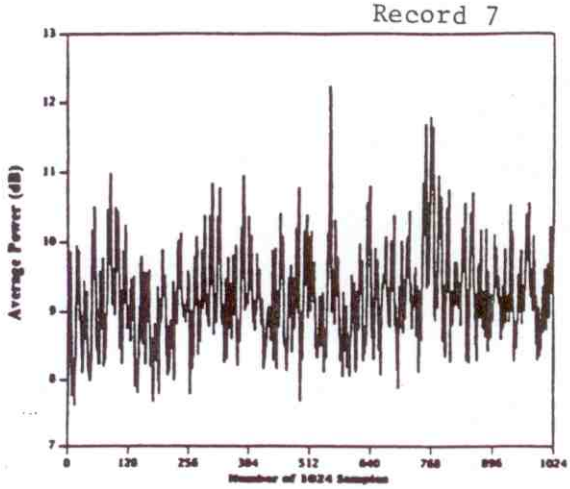

Record 8

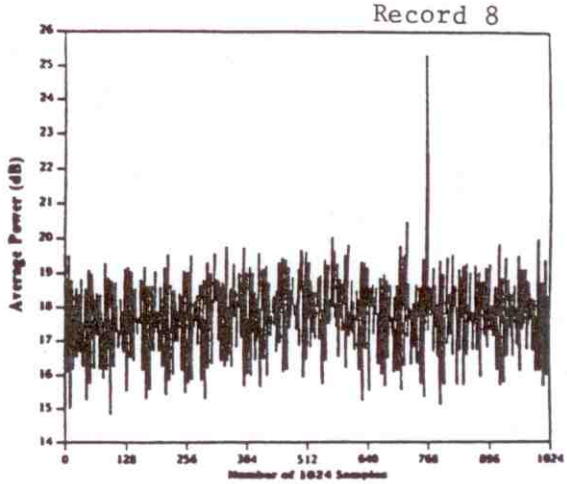

Record 9

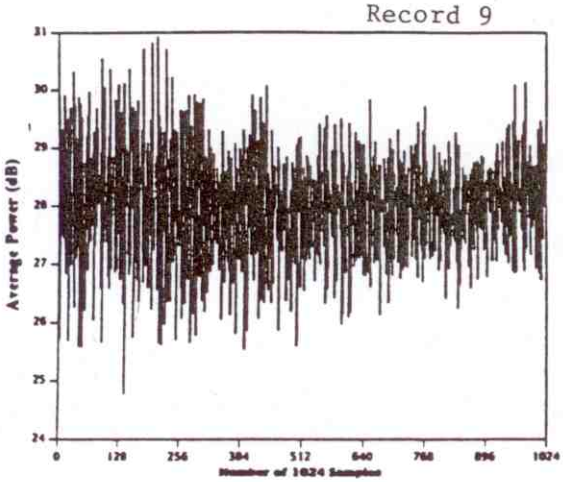

Record 10

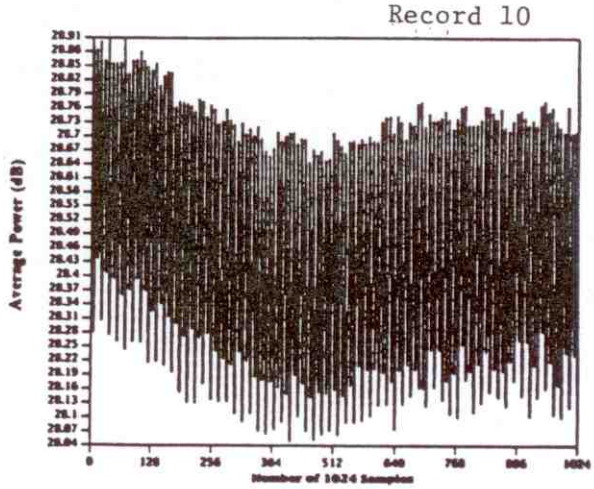

Record 11

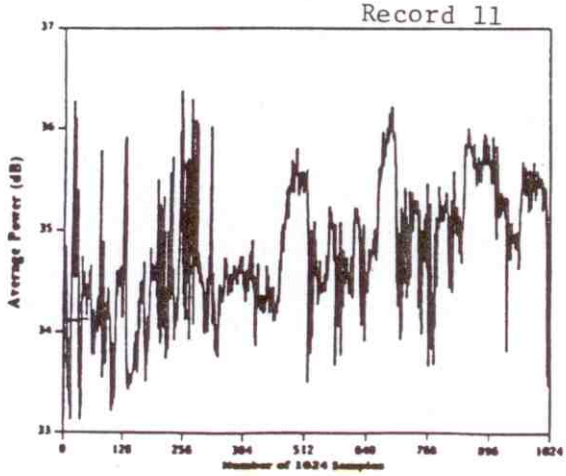

Record 12

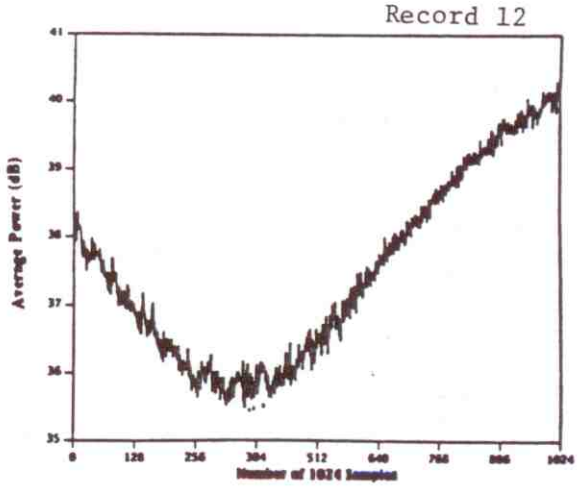

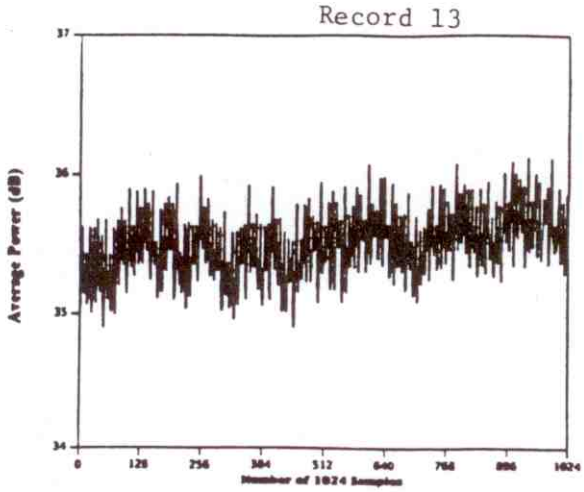
Record 13
Average Power (dB)
Number of 1024 Samples

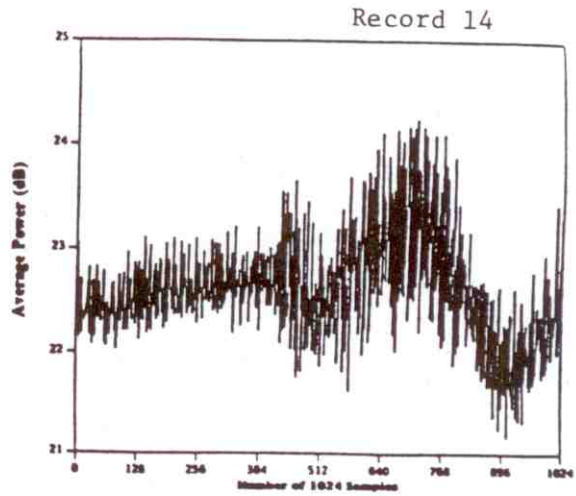
Record 14
Average Power (dB)
Number of 1024 Samples

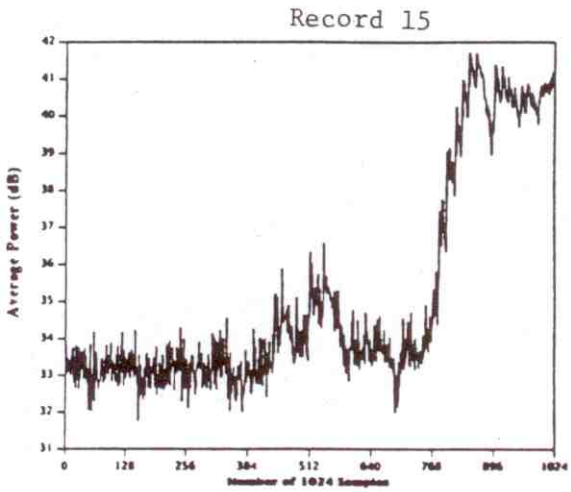
Record 15
Average Power (dB)
Number of 1024 Samples

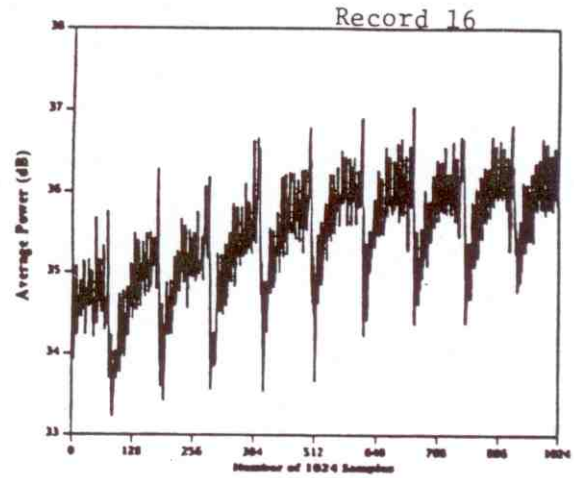
Record 16
Average Power (dB)
Number of 1024 Samples

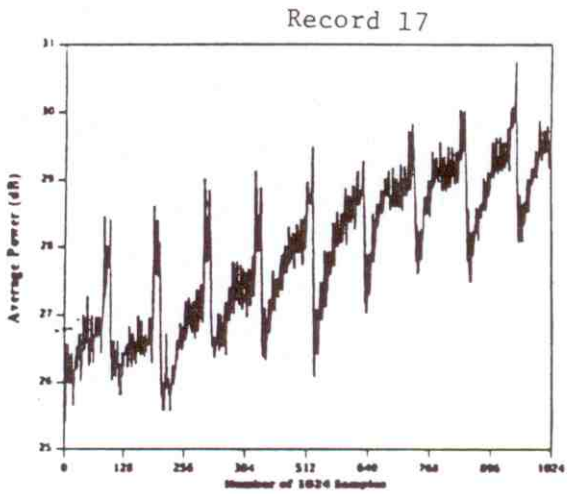
Record 17
Average Power (dB)
Number of 1024 Samples

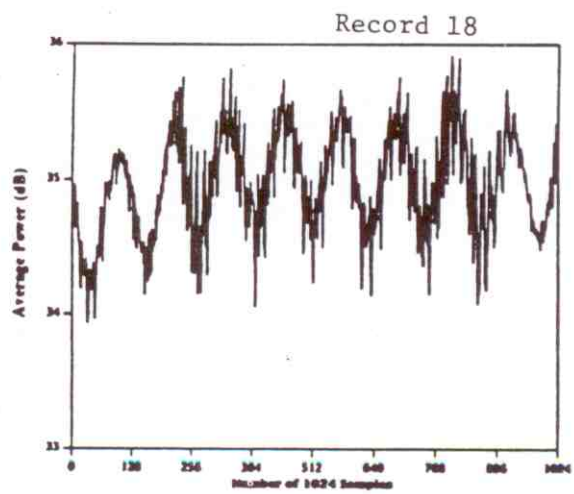
Record 18
Average Power (dB)

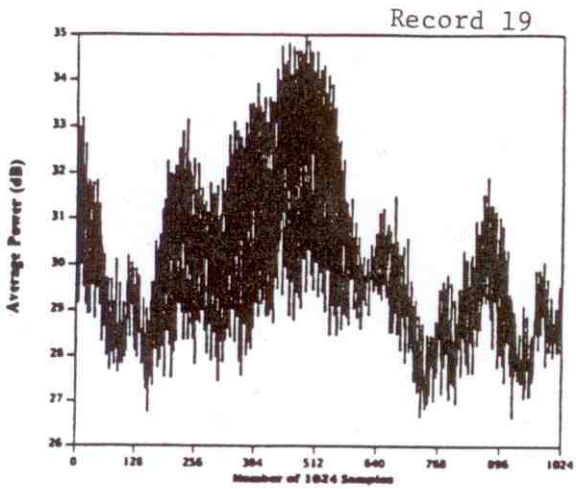
Record 19
Average Power (dB)
Number of 1024 Samples

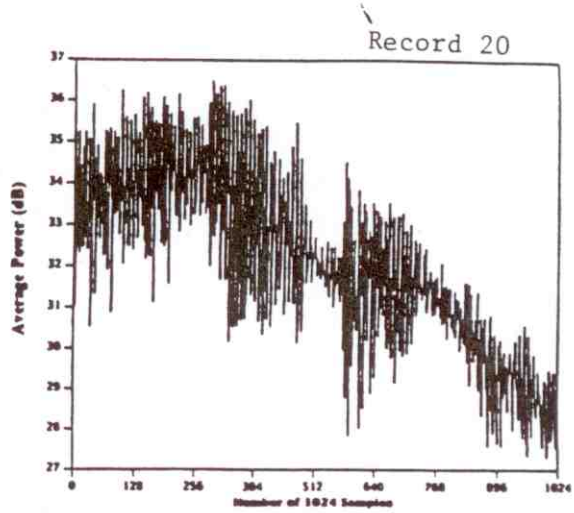
Record 20
Average Power (dB)
Number of 1024 Samples

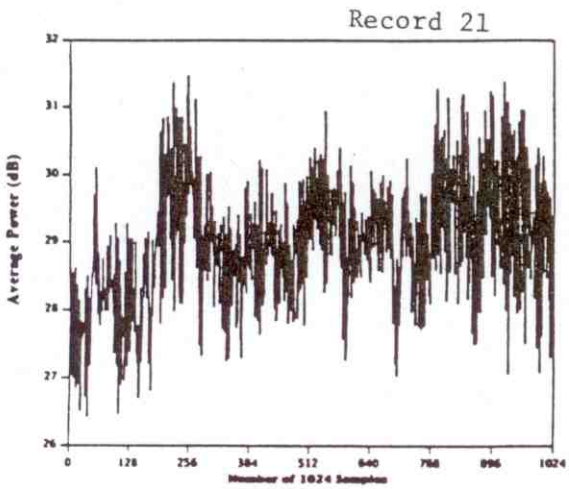
Record 21
Average Power (dB)
Number of 1024 Samples

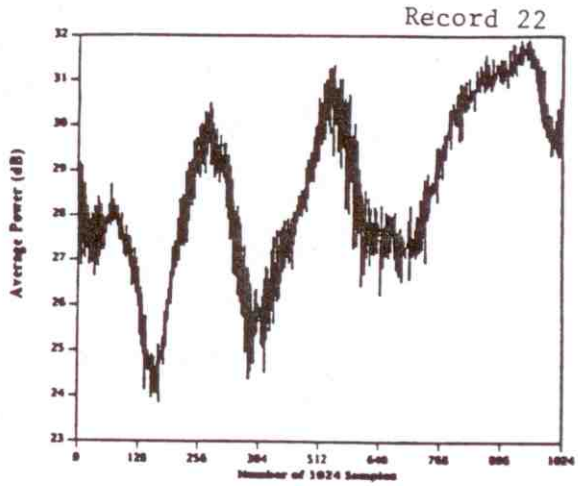
Record 22
Average Power (dB)
Number of 1024 Samples

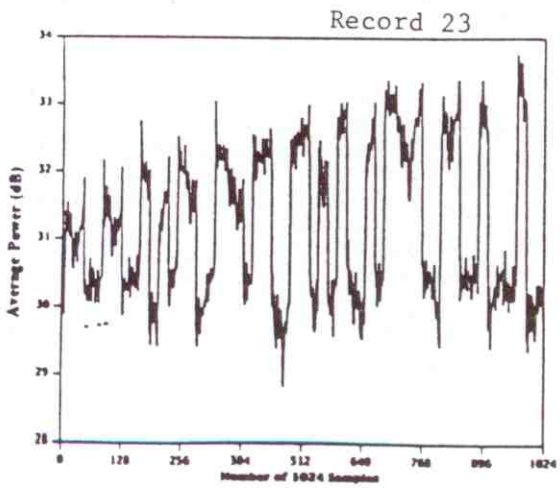
Record 23
Average Power (dB)
Number of 1024 Samples

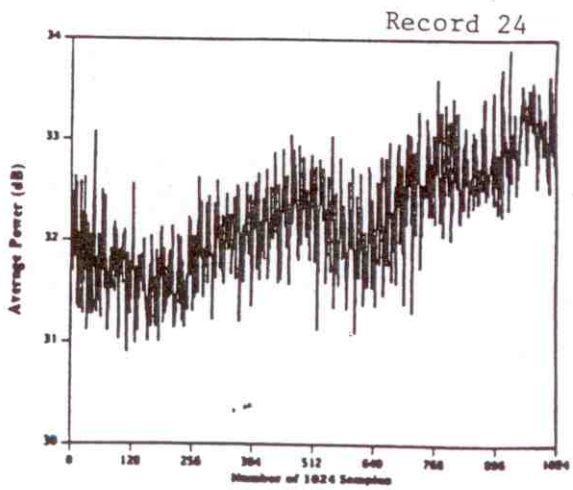
Record 24
Average Power (dB)
Number of 1024 Samples

Record 25

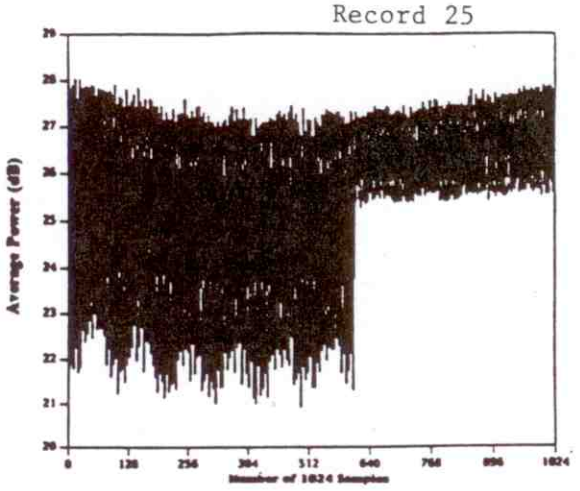

Record 26

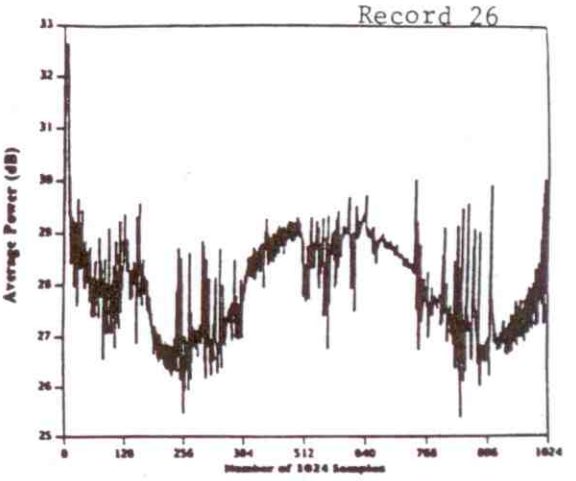

Record 27

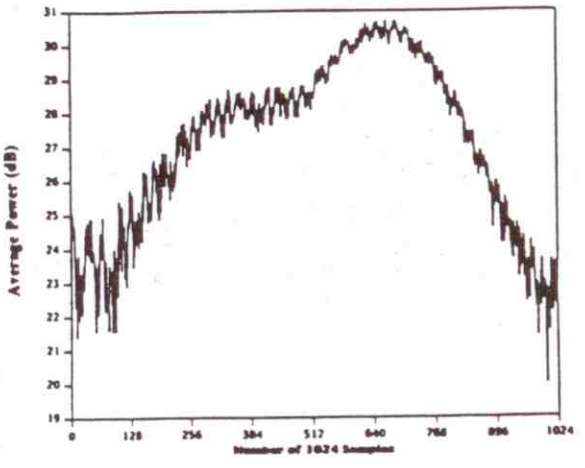

Record 28

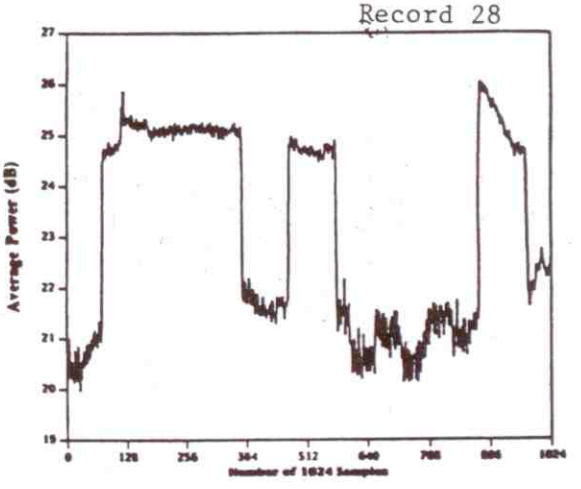

Record 29

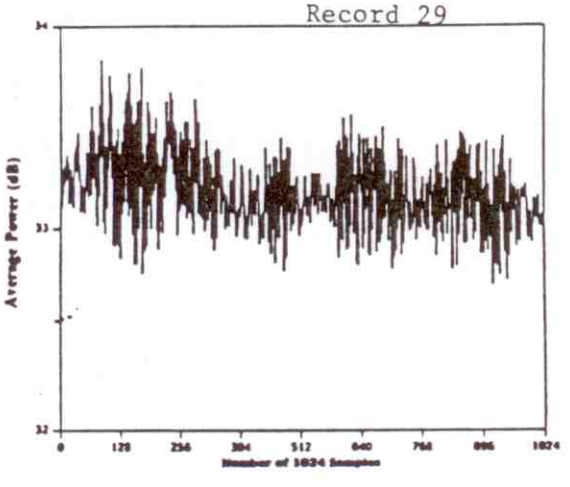

Record 30

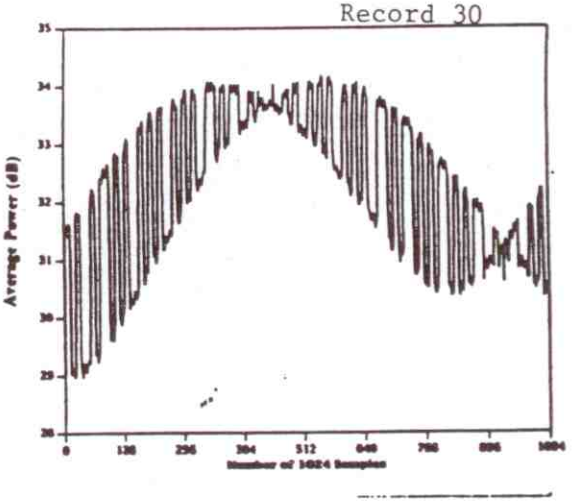

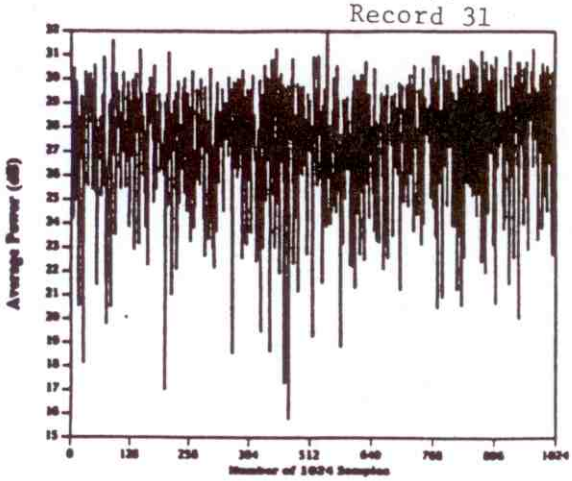
Record 31
Average Power (dB)
Number of 1024 Samples

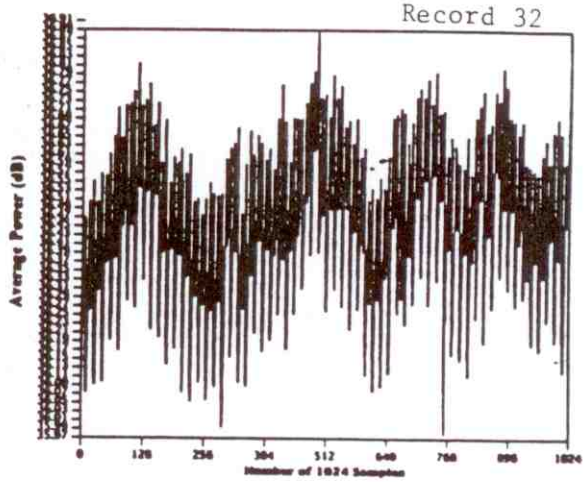
Record 32
Average Power (dB)
Number of 1024 Samples

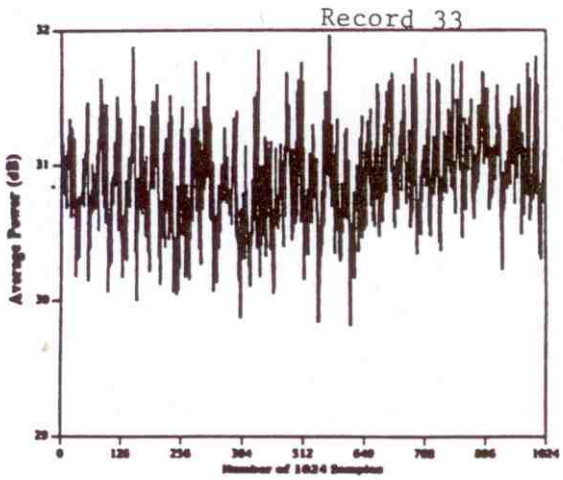
Record 33
Average Power (dB)
Number of 1024 Samples

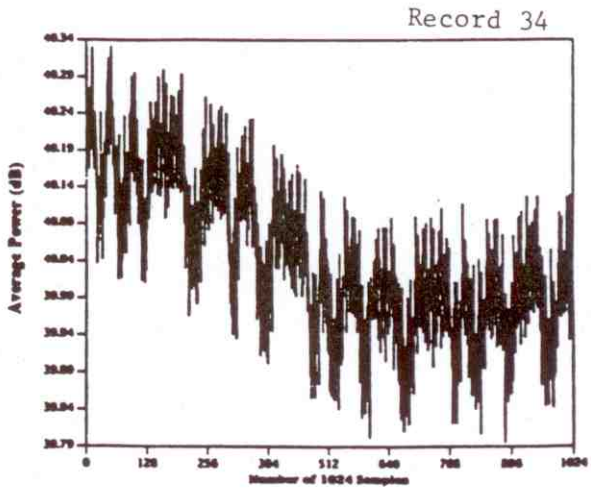
Record 34
Average Power (dB)
Number of 1024 Samples

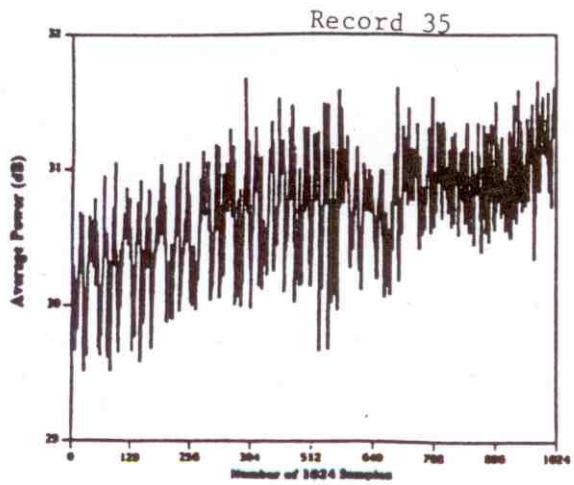
Record 35
Average Power (dB)
Number of 1024 Samples

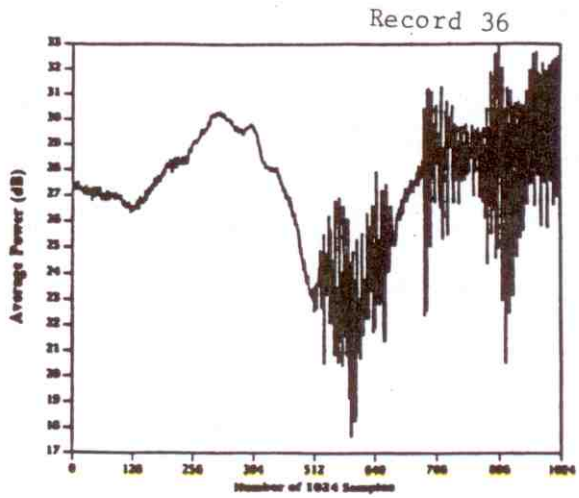
Record 36
Average Power (dB)
Number of 1024 Samples

Record 37

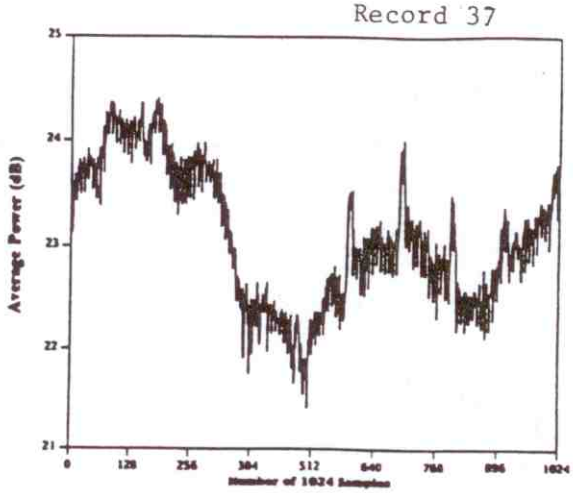

Record 38

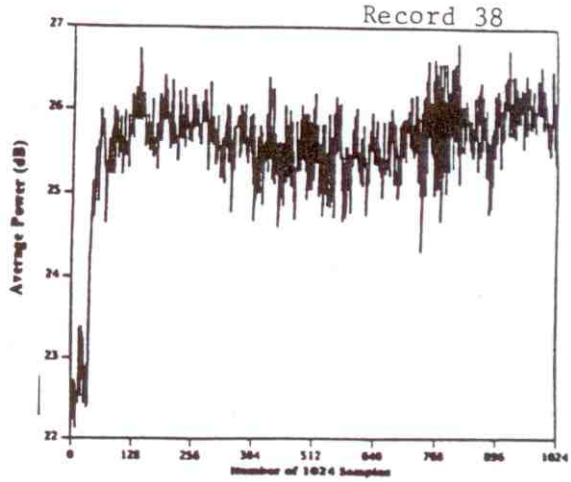

Record 39

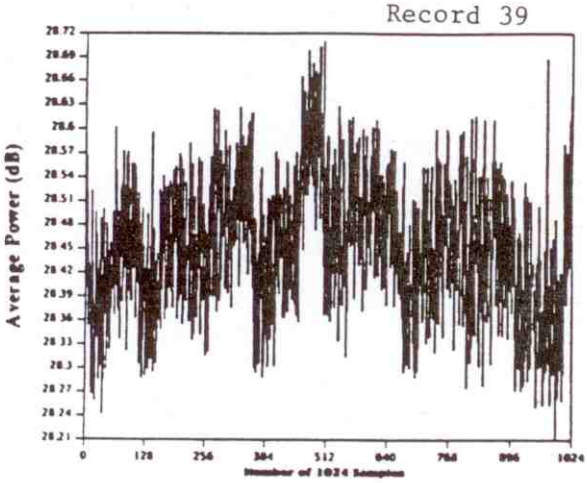

Record 40

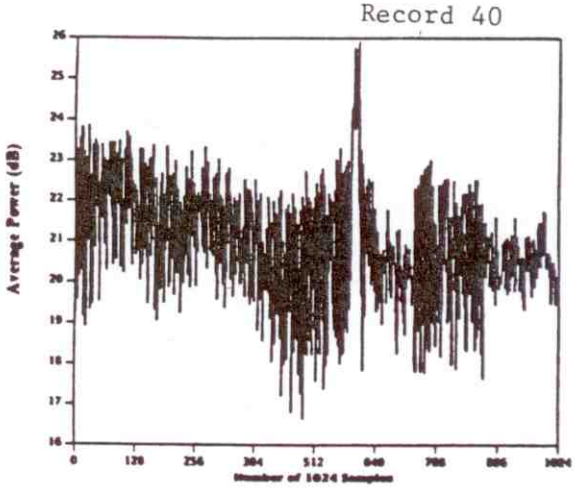

Record 41

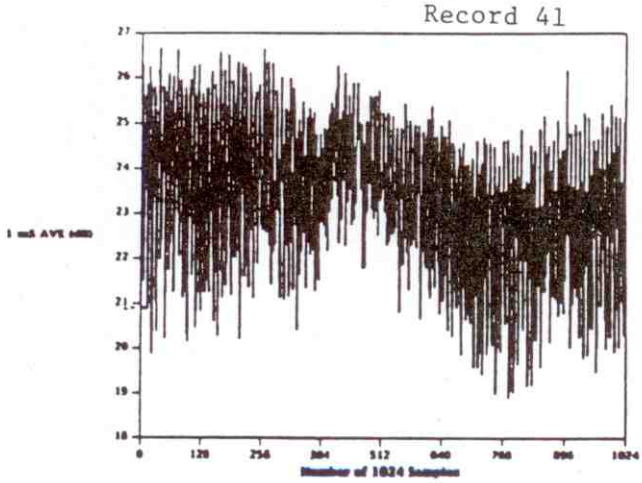

Record 42